HELDA
HELSINGIN YLIOPISTO
HELSINGFORS UNIVERSITET
UNIVERSITY OF HELSINKI

UNIVERSITY OF HELSINKI

https://helda.helsinki.fi

Structure-antitumor activity relationships of tripodal imidazolium-amino acid based salts : effect of the nature of the amino acid, amide substitution and anion

Valls, Adriana

2021-12-15

Valls , A , Altava , B , Aseyev , V , Carreira-Barral , I , Conesa , L , Falomir , E , Garcia-Verdugo , E , Luis , S V & Quesada , R 2021 , ' Structure-antitumor activity relationships of tripodal imidazolium-amino acid based salts : effect of the nature of the amino acid, amide substitution and anion ' , Organic & Biomolecular Chemistry , vol. 19 , no. 48 , pp. 10575-10586 . https://doi.org/10.1039/d1ob01825f

http://hdl.handle.net/10138/351862
https://doi.org/10.1039/d1ob01825f

unspecified
acceptedVersion

Downloaded from Helda, University of Helsinki institutional repository.

This is an electronic reprint of the original article.

This reprint may differ from the original in pagination and typographic detail.

Please cite the original version.

Please do not adjust margins

ARTICLE

Structure–Antitumor Activity Relationships of Tripodal Imidazolium- Amino Acid Based Salts. Effect of the Nature of the Amino Acid, Amide Substitution and Anion

Received 00th January 20xx,
Accepted 00th January 20xx

DOI: 10.1039/x0xx00000x

Adriana Valls,[a] Belén Altava,*[a] Vladimir Aseyev,[b] Israel Carreira-Barral,[c] Laura Conesa,[a] Eva Falomir,[a] Eduardo García-Verdugo,[a] Santiago Vicente Luis,*[a] Roberto Quesada.[c]

The antitumor activity of imidazolium salts is highly dependent upon their lipophilicity that can be tuned by the introduction of different hydrophobic substituents on the nitrogen atoms of the imidazolium ring of the molecule. Taking this in consideration, we have synthesized and characterized a series of tripodal imidazolium salts derived from L-valine and L-phenylalanine containing different hydrophobic groups and tested them against four cancer cell lines at physiologic and acidic pH. At acidic pH (6.2) the anticancer activity of some of the tripodal compounds changes dramatically, being this parameter crucial to control their cytotoxicity and selectivity. Moreover, several of these compounds displayed selectivity against the control healthy cell line higher than four. The transmembrane anion transport studies revealed moderate transport abilities suggesting that the observed biological activity is likely not the result of just their transport activity. The observed trends in biological activity at acidic pH agree well with the results for the CF leakage assay. These results strongly suggest that this class of compounds can serve as potent chemotherapeutic agents.

Introduction

Cancer disease kills yearly millions of people, being the second-leading cause of death in the world;[1,2] therefore, the development of potential therapeutic agents to fight against this illness using chemotherapy is of great interest.[3-6] In this regard, one important issue is the selectivity of the drugs used in chemotherapy, since most of them show severe toxicities to normal cells. Moreover, the solubility, bioavailability and polymorphism associated to active pharmaceutical ingredients is another problem, restricting their use and application in chemotherapy.[7,8] In the last decade, ionic liquids have been considered of great interest in pharmaceutical and medical applications due to their biological activity,[9-13] and considerable efforts have been made towards the development of derivatives of these salts with antimicrobial and anticancer properties.[14-20] In this context, imidazolium based-ionic liquids have been found to be a promising type of compounds showing intriguing anticancer activities against different cancer cells.[21-25] Some of the first imidazolium salts displaying high activity against a wide panel of cancer cell lines were tested by Malhotra *et. al.* showing that the length of the 3-alkyl substituent is one of the main vectors controlling cytotoxicity.[26] Later, 4,5-dichloro-1,3-bis(naphthalen-2-ylmethyl)imidazolium bromide was described as a potential anticancer drug, being its activity associated to the presence of the imidazolium cation and the naphthylmethyl substituent. This compound, however, had extremely poor water solubility, which would impair its distribution upon systemic administration. The balance between water solubility and high anticancer activity has represented a major obstacle for the potential clinical use of lipophilic imidazolium salts.[27] More recently, a series of tripodal imidazolium salts have been evaluated as antibacterial and anticancer agents providing a new and interesting approach for new bioactive systems.[28,29]

In this context, our research group has been involved in the preparation of imidazolium based compounds derived from amino acids.[30-34] Therefore, continuing with our previous work related with L-valine imidazolium tripodal salts,[34] and the evaluation of ditopic and monotopic imidazolium salts derived from amino acids as antibacterial agents,[35] we present here the synthesis of different tripodal imidazolium salts derived from amino acids and the evaluation of the synergetic effects between their lipophobicity and anticancer activity. In order to tune their physicochemical and potential antitumor properties, we considered different natural amino acids (*L*-phenylalanine and *L*-valine) as well as different amide substitutions (aliphatic and aromatic) and different anions. Furthermore, for the amphiphilic tripodal compounds, self-aggregation studies in aqueous media have been carried out to determine their critical aggregation concentration. In addition, these salts were evaluated as transmembrane transporters of anions with the aim of deciphering their mechanism of action.[36-40] The

[a] *Department of Inorganic and Organic Chemistry, ESTCE, University Jaume I, Av. Sos Baynat, s/n, 12004, Castellón, Spain. E-mail: altava@uji.es, luiss@uji.es*
[b] *Department of Chemistry, University of Helsinki, P.O. Box 55 (A413, A. I. Virtasen aukio 1), FIN-00014 HY Helsinki, Finland*
[c] *Department of Chemistry, Faculty of Science, Universidad de Burgos, 09001 Burgos, Spain*

† Footnotes relating to the title and/or authors should appear here.
Electronic Supplementary Information (ESI) available: [details of any supplementary information available should be included here]. See DOI: 10.1039/x0xx00000x

Please do not adjust margins

Please do not adjust margins

microenvironment around tumor cells is unusually acidic as compared to healthy cells as a result of the altered cancer cell metabolism. This acidic microenvironment provides cancer cells with adaptative advantages. Moreover, the intracellular pH is slightly alkaline, contributing to drug resistance.[41-43] Accordingly, anticancer, self-assembly and anion transport studies were performed under physiologic and slightly acidic pH condition.[44-47]

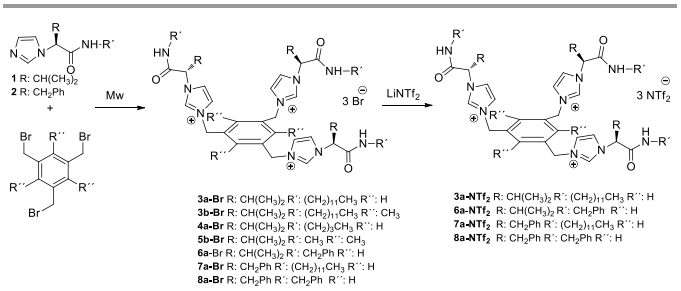

Scheme 1. Synthesis of the tripodal imidazolium salts

Results and discussion

Synthesis

The imidazole based compounds **1** and **2** were obtained from the corresponding α-amino amides as described previously.[33] Tripodal imidazolium salts **2-Br** to **8-Br** were obtained in >70% yield by treatment of the imidazole **1** or **2** with the corresponding (tris-bromomethyl)aryl compound under Mw at 70°C.[34] The anion exchange was carried out by reaction of the bromide imidazolium salts with $LiNTf_2$ in CH_3CN leading to the corresponding NTf_2 salts in good yields (> 80%) (Scheme 1). The corresponding bromide salts were solid at room temperature, while the analogous bis(trifluoromethylsulfonyl)amide salts were waxy or liquid compounds.

Anticancer and toxicity studies

The *in vitro* anticancer activities of the synthesized compounds were examined against four human cancer cell lines, characterizing tumors of different origins. The human lung adenocarcinoma cell line A549, the human cervix tumor cell line HeLa, the human colon adenocarcinoma cell line HT-29 and the human breast cancer cell line MCF-7. Furthermore, human embryonic kidney cell HEK-293 was used as control to evaluate the selectivity of the compounds to carcinoma cells. All the cells were incubated in culture media with varying concentrations of the examined compound and the impact of treatment was measured using the MTT assay (Figure S1).[49] The experiments were performed at different pH values using a standard DMEM medium for pH 7.5 and a PIPES buffer to fix the pH to 6.2. The IC_{50} values obtained for the cells under investigation, correspond to the average from three experiments and are summarized in Tables 1 and 2.

Table 1. IC_{50} and selectivity values for A549, HeLa, HT-29, MCF-7 and HEK-293 cell lines in the presence of tripodal compounds **3**-**8** at physiological pH.

Entry	Compound	H_2O Solubility (0.5 mM)	IC_{50} (μM)[a]					α[b]	β[c]
			A549	HeLa	HT-29	MCF-7	HEK-293		
1	**3a-Br**	S	15.0 ± 0.5	12.9 ± 0.2	16.8 ± 1.2	19.4 ± 1.3	13.0 ± 0.9	0.9	1.0
2	**3b-Br**	S	18.9 ± 1.4	14.2 ± 0.6	16 ± 3	13 ± 3	13.5 ± 0.9	0.7	1
3	**4a-Br**	S	90 ± 9	93 ± 6	>200	>200	>200	>2.2	>2.1
4	**5b-Br**	S	>200	>200	>100	>200	>200	-	-
5	**6a-Br**	S	>100	84 ± 17	>200	>200	>200	-	>2.4
6	**7a-Br**	I	23.5 ± 0.7	2.09 ± 0.03	34.4 ± 1.3	21 ± 3	2.7 ± 0.4	0.1	1.3
7	**8a-Br**	I	23.6 ± 1.3	11.7 ± 0.8	57 ± 2	27 ± 2	15 ± 3	0.6	1.3
8	**3a-NTf_2**	I	17.1 ± 0.6	7.3 ± 0.3	99 ± 3	89 ± 3	9.7 ± 1.1	0.6	1.3
9	**6a-NTf_2**	I	93 ± 5	96 ± 12	>200	>200	42 ± 7	0.5	0.4
10	**7a-NTf_2**	I	21 ± 4	5.0 ± 0.6	45.8 ± 1.1	22.2 ± 0.6	2.8 ± 0.2	0.1	0.6
11	**8a-NTf_2**	I	4.8 ± 0.6	13 ± 5	82 ± 7	44 ± 5	12.1 ± 1.9	2.5	0.9

[a] (IC_{50} (x ± sd) average from three experiments after 48h); [b] (**α** = IC_{50} (HEK-293) / IC_{50} (A549)); [c] (**β** = IC_{50} (HEK-293) / IC_{50} (HeLa)). S for soluble and I for insoluble

When experiments were run at pH 7.5 (Table 1), the results indicate that compounds **3a-Br**, **3b-Br**, **7a-Br**, **8a-Br**, **3a-NTf_2**, **7a-NTf_2** and **8a-NTf_2** exhibited considerable cancer cell growth inhibition against the examined cancer types with IC_{50} values in the 20 μM range or lower on the four cell lines (entries 1, 2, 6, 7, 8, 10 and 11, Table 1). This activity can be related to the nature of the substituents. Thus, compounds **8a-Br** and **8a-NTf_2** present six benzyl groups, and the aromaticity and planarity of these groups are features shared by several other anticancer agents. The intercalation of such groups into the base pairs of DNA can introduce structural distortions that inhibit transcription and replication.[50,51] On the other hand, compounds **3a-Br**, **3b-Br**, **7a-Br**, **3a-NTf_2** and **7a-NTf_2** present long alkyl chains

 This journal is © The Royal Society of Chemistry 20xx

Please do not adjust margins

Please do not adjust margins

facilitating their interaction with the lipidic membrane. In those cases, the observed toxicity could be related to their transmembrane transport ability or to their alteration of membrane viscoelasticity as will be discussed later.[52,53] Compounds **4a-Br**, **5b-Br**, **6a-Br** and **6a-NTf$_2$**, the less active ones, fail in the presence of such substituents.

For the tumoral cell lines HT-29 and MCF-7, none of the studied compounds offers good selectivity when comparing with the healthy cell line HEK-293 (β <1). Nevertheless, for the cell lines A549 and HeLa compounds **4a-Br**, **6a-Br** and **8a-NTf$_2$** presented a selectivity higher than 2, having the compound **8a-NTf$_2$** the best antitumor properties for the cell line A549 with an IC_{50} of 4.8 μM and α = 2.5 (entry 11, Table 1).

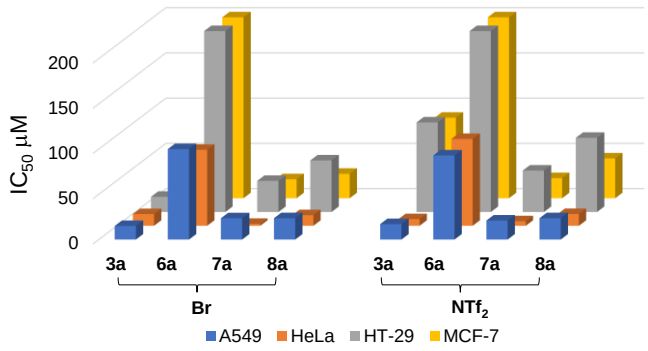

Figure 1. Plot of IC_{50} values for A549, HeLa, HT-29, MCF-7 and HEK-293 cell lines for tripodal compounds **3a, 6a, 7a, 8a** at pH 7.2.

Regarding the anion nature, as can be observed in Figure 1, the anion effect is significantly important for the four cell lines studied specially for HT-29 and MCF-7. In general, the bromide anion confers better antitumor activities than the analogous compound with NTf_2 anion.[54]

Table 2 shows the cytotoxicity of the different tripodal compounds for the cell line A549 using two different pH values: normal (7.2) and acidic (6.2). In general, for bromide salts, the IC_{50} obtained at an acidic pH is not significantly affected by non-active compounds **4a-Br, 5b-Br** and **6a-Br** (IC_{50} >100), and lowered for active ones **3a-Br**, **3b-Br**, **7a-Br** and **8a-Br** (entries 1, 2, 6, 7, Table 2), with IC_{50} one order of magnitude lower at pH 6.2 (entry 6). Similar trends have been described in the literature.[42¡Error! Marcador no definido.] It has to be emphasized the increase of the selectivity index at acidic pH for compounds **3b-Br** and **8a-Br** (from S.I. 0.7 and 0.6 to S.I. 4.8 and 3.5 respectively (entries 2, 7, Table 2)). Moreover, the results obtained for **NTf$_2$** salts were especially significant, since the cytotoxicity to A549 of receptors **3a-NTf$_2$** and **8a-NTf$_2$** decreased dramatically as the pH decreased, more than two orders of magnitude for **8a-NTf$_2$** (entries 8 and 10, Table 2), while the bromide analogous salts presented increase of antitumor activity at acidic pH, underscoring the role of the anion.

Optical microscopy images for A549 cell line after 48 h incubation with compound **7a-Br** at pH 7.2, reveal clear signs of morphological changes appearing as irregularities or, even, disruption of the cell membrane, swelling and formation of some blebs (Figure 2). These are signs of cell death provoked by our compounds. Taking in consideration the results obtained, the aggregation and anion transport properties of these compounds were studied at different pH values to investigate the possible mechanism of action and the dependence of their mode of action on aggregation.

Table 2. IC_{50} and selectivity values for A549 cell line in the presence of tripodal compounds **3-8** at different pH values

Entry	Compound	IC_{50} (μM) [a]			α [b]	γ [c]
		A549 (pH 7.2)	A549 (pH 6.2)	HEK-293 (pH 7.2)	A549 (pH 7.2)	A549 (pH 6.2)
1	**3a-Br**	15.0 ± 0.5	5.3 ± 0.4	13.0 ± 0.9	0.9	2.5
2	**3b-Br**	18.9 ± 1.4	2.8 ± 0.5	13.5 ± 0.9	0.7	4.8
3	**4a-Br**	90 ± 9	>100	>200	>2.2	-
4	**5b-Br**	>200	>100	>200	-	-
5	**6a-Br**	>100	>100	>200	-	-
6	**7a-Br**	23.5 ± 0.7	1.4 ± 0.3	2.7 ± 0.4	0.1	1.9
7	**8a-Br**	23.6 ± 1.3	4.2 ± 0.3	15 ± 3	0.6	3.5
8	**3a-NTf$_2$**	17.1 ± 0.6	>100	9.7 ± 1.1	0.6	<1
9	**7a-NTf$_2$**	21 ± 4	3.1 ± 0.6	2.8 ± 0.2	0.1	1
10	**8a-NTf$_2$**	4.8 ± 0.6	>100	12.1 ± 1.9	2.5	< 1

[a] IC_{50} (x ± sd) average from three experiments; [b] α = IC_{50} (HEK-293) / IC_{50} (A549); [c] γ = IC_{50} (HEK-293) / IC_{50} (A549) at pH 6.2.

This journal is © The Royal Society of Chemistry 20xx

Please do not adjust margins

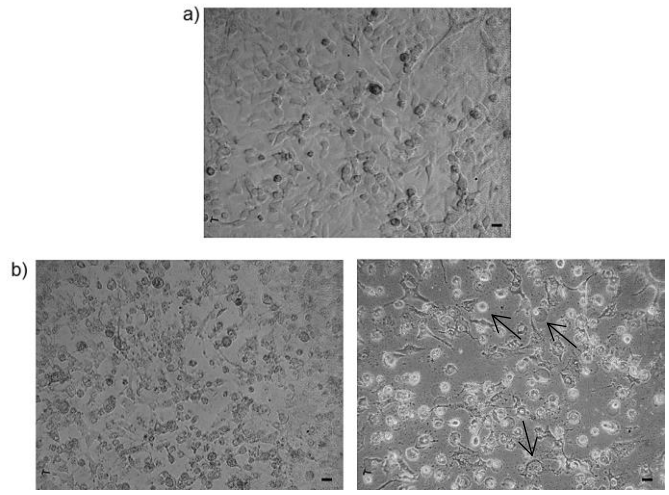

Figure 2. Microscopic appearance of A549 cell line in DMEM medium: a) control; b) incubated with **7a-Br** (5 μM) at physiologic pH, after 2 days under white and phase contrast (scale bar: 10 μm).

Aggregation behavior

The self-assembly behavior of the tripodal compounds in aqueous media, including the analysis of the size distributions and the morphologies of the aggregates formed, was investigated by ^{1}H-NMR, light scattering (LS), fluorescence, optical microscopy and SEM.

Fluorescence: To investigate the microenvironment of the self-assembly in water by fluorescence the pyrene 1:3 ratio method was used.[55,56] The plots of the pyrene I_1/I_3 ratio as a function of the total surfactant concentration shows, at the region where self-assembly starts to occur, a typical sigmoidal decrease. This allows defining the critical aggregation concentration (CAC) at the breaking point of the curve. Below the CAC the pyrene I_1/I_3 ratio value indicates a polar environment and as the surfactant concentration increases the pyrene I_1/I_3 ratio decreases rapidly, indicating that the pyrene is sensing a more hydrophobic environment. Above the CAC, the pyrene I_1/I_3 ratio reaches a roughly constant value because of the incorporation of the probe into the hydrophobic region of the aggregates. Different approaches have been used to estimate CAC values from I_1/I_3 ratios.[57,58] The most common approach is the use of the break points, either directly or by extrapolating the values from the intersection of the two straight lines defined at the constant and variable regions of the I_1/I_3 sigmoidal curve.[59,60] As CAC represents the threshold of concentration at which self-aggregation starts, the corresponding value can be estimated from the break point at lower concentration.[61-64]The corresponding CACs obtained by fluorescence in water are shown in Table 3. All the compounds presented CAC values in the μM range, only for compound **4a-Br** the CAC was in the mM range, being the lower CAC value for compound **3a-Br** (entry 1, Table 3).

Table 3. Estimated CACs obtained in aqueous media using fluorescence studies at 25ºC.

Entry	Amphiphilic compound	Solvent	CACs [a] (μM)	
1	**3a-Br**	H_2O	0.6	4.2
2	**3a-Br**	Buffer pH 7.2	7.1	
3	**3a-Br**	Buffer pH 6.2	16.2	
4	**3b-Br**	H_2O	10.5	
5	**4a-Br**	H_2O	1387	
6	**4a-Br**	Buffer pH 7.2	1747	
7	**4a-Br**	Buffer pH 6.2	1792	
8	**5b-Br**	H_2O	120	
9	**6a-Br**	H_2O	41.6	

[a] values at the break points.

The plot of the I_1/I_3 ratio for the corresponding emission spectra *vs* concentrations showed for compounds **3b-Br**, **4a-Br**, **5b-Br** and **6a-Br** one single break point reaching in all cases values of $I_1/I_3 \approx 1.1$ or lower after the break point (Figure S1 and S2). However, for compound **3a-Br**, the plot of the I_1/I_3 ratios for the corresponding emission spectra *vs* concentration presented two single break point suggesting the presence of two different aggregates (Figure 2). The first break point was at 0.6 μM with values of $I_1/I_3 \approx 1.6$, affording aggregates with an appreciable pyrene solvent exposed, while the second break point was located at higher concentrations (4.2 μM) reaching I_1/I_3 values ≈ 1.1 and leading to aggregates with a low polarity microenvironment for pyrene.

Moreover, it has been described that pyrene can show a broad excimer emission band around 470 nm in dilute surfactant water solutions containing vesicles or bilayer structures.[65-67] In this regard, compounds **3a-Br** and **3b-Br** presented a broad emission band (I_e) around 470 nm suggesting the formation of vesicles or bilayers. The I_e/I_1 ratio increased as concentration increased, reaching two maxima and decreasing sharply until concentrations where no further change in the I_1/I_3 ratio is observed (Figure 3 and S1). The two maxima observed are within the sigmoidal decrease of the I_1/I_3 ratio.

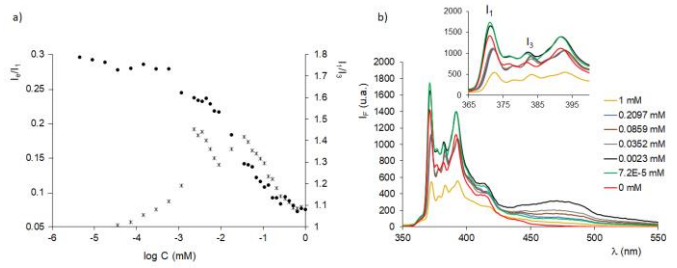

Figure 3. a) Plot of the I_1/I_3 (circles, right axes) and Ie/I_1 (stars, left axes) ratios *v* log C for **3a-Br** in H_2O at 25ºC. b) Emission spectra of pyrene in H_2O in the presence of different amounts of **3a-Br**.

To study the role of the pH in the aggregation behavior, fluorescence studies for **3a-Br** and **4a-Br** were measured in water and at acidic pH using the corresponding phosphate buffer solution (10 mM) (Figure S3). For the tripodal compound **3a-Br,** the acidic pH increased the CAC reducing the formation of aggregates (entries 2 and 3, Table 3). However, for compound **4a-Br** the CAC did not increase significantly from pH 7.2 to pH 6.2 (entries 6 and 7, Table 3). It must be mentioned that the CAC values increase from water to buffer pH 7.2 for both **4a-Br** and **3a-Br** (entries 1-2 and entries 5-6, Table 3).

Comparing the CAC values in water and the IC_{50} for the cell line A549 in the case of the tripodal compounds **3a-Br, 4a-Br, 6a-Br, 3b-Br** and **5b-Br**, the IC_{50} is above the CAC for **3a-Br**, **3b-Br**, **5b-Br** and **6a-Br**, implying that the compounds are aggregated to some extend at the antitumoral response concentration. However, for compounds **4a-Br**, the IC_{50} is 15 times below the CAC, indicating that the compound is not aggregated at the concentration of elicitin antitumoral response and that the monomeric species is mainly the responsible of its moderate cytotoxicity.[68]

Interestingly, for **3a-Br** at acidic pH, the CAC value is above the IC_{50}, implying that the compound is not aggregated at the antitumoral response concentration. This is in accordance with the decrease of the IC_{50} at pH 6.2 (entry 1, Table 2). Thus, the monomeric species seems to be the main responsible of the cytotoxic activity, with higher concentrations of the monomeric bioactive species available at concentrations below the CAC, suggesting higher activities for increased values of CAC.

Proton NMR experiments: Due to the low solubility of some of the tripodal compounds in water (< 0.5 mM, see Table 1), ^{1}H-NMR aggregation studies were run in D_2O/CD_3OD (1/1 v/v) for **3a-Br, 3b-Br**, **4a-Br, 5b-Br** and **6a-Br** from *ca.* 0.1 to 4 mM, precluding an accurate analysis for compounds **7a-Br**, **8a-Br** and **3**, **7**, **8** NTf_2 derivatives due solubility problems in aqueous media.

Figure 4 shows the partial ^{1}H NMR spectra of the compound **3a-Br** in D_2O/CD_3OD solvent mixture (1/1, v/v) at concentrations ranging from 0.1 to 4 mM at 30 ºC. When the concentration was increased, the imidazolium signals Hb and Hc, and that of one for the aromatic protons (Ha), shifted downfield ($\Delta\delta$= 0.06-0.08), indicating that these groups become slightly more involved in hydrogen bonding upon concentration. while minor changes were detected for the signals of the hydrophobic chains ($\Delta\delta \approx 0.01$). However, one of the methylene protons of the alkyl chains (NH-CH_2) and the methyl protons of the valine side chain shifted upfield upon aggregation ($\Delta\delta \approx 0.05$ and 0.03 respectively) (Figure 4b). Similar trend was observed for the corresponding protons of **3b-Br** (see ESI, Figure S4). However, for the tripodal **4a-Br** when the concentration increased from 0.2 to 4 mM, the imidazolium and aromatic protons signals shifted slightly downfield ($\Delta\delta$ = 0.01-0.02) while no significant chemical shift variation was observed for signals of the hydrophobic chain and the methyl protons of the valine side chain (ESI, Figure S5). Moreover, for the tripodal compounds **5b-Br** and **6a-Br,** when the concentration increased from 0.2 to 4 mM, no significant chemical shift variation was observed for any of the proton signals, suggesting that probably they were strongly aggregated at the lowest concentration.

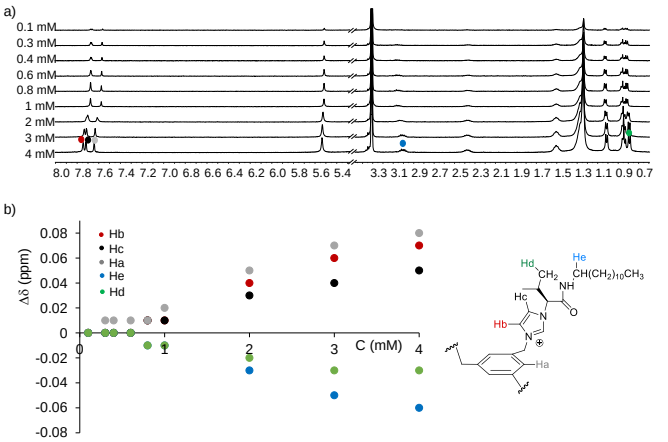

Figure 4. a) Partial ^{1}H NMR (400 MHz at 30ºC) of the compound **3a-Br** in CD_3OD/D_2O (1/1, v/v) obtained for various concentrations. b) $\Delta\delta$ *vs*. concentration plot for several signals.

Light scattering (LS) measurements: LS intensity measurements were also used to study the aggregates. The hydrodynamic size distributions of the aggregates were investigated by means of dynamic light scattering (DLS) deducing the apparent hydrodynamic diameters D_h from the diffusion coefficients. Experiments could not be performed in pure water for the 0.01 to 0.5 mM concentration range as at such low concentrations no reproducible results could be achieved. Thus, the experiments were performed on compounds **3a-Br, 3b-Br**, **5b-Br** and **6a-Br** in CH_3OH/H_2O within the 0.1 - 6 mM concentration range at 25 ºC. For **4a-Br** the experiment could not be properly achieved in CH_3OH/H_2O.

For compounds **3a-Br**/**3b-Br** and **5b-Br**/**6a-Br** the total intensity of scattered light as a function of the total surfactant concentration, increased almost linearly with concentration, suggesting that the aggregates increase in number when concentration increases, keeping their average size constant (Figure S6). For **3a-Br** the hydrodynamic diameter is around 300 nm while it increases to 500 nm for **3b-Br** and **6a-Br**, reaching 800 nm for **5b-Br**.

Optical microscopy and SEM: The formation of aggregates in H_2O and H_2O/CH_3OH (1/1 v/v) for **3a-Br, 3b-Br**, **4a-Br, 5b-Br** and **6a-Br** was studied by optical microscopy and SEM. For compounds **3a-Br,**

Please do not adjust margins

3b-Br, 4a-Br and **6a-Br**, optical microscopy in H_2O/CH_3OH (1/1, v/v), allowed to observe the formation of spherical aggregates at 6 mM concentrations with sizes between 0.5-5 μm (Figure S7). However, for tripodal compound **5b-Br** only a homogeneous solution was observed. Furthermore, in the case of compound **4a-Br** dendritic structures from spherical aggregates were observed. Moreover, SEM images in H_2O for **3a-Br** (0.1 mM) and **6a-Br** (0.4 mM) allowed to observe the formation of distorted spherical aggregates with sizes lower than 2 μm and 0.5 μm size respectively (Figure 5).

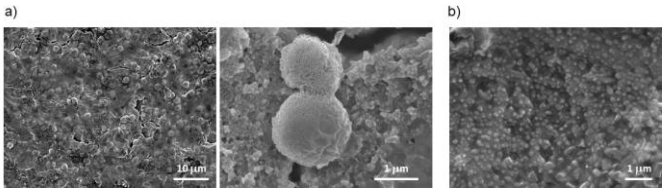

Figure 5. SEM images for some tripodal compounds in H_2O/CH_3OH (1/1 v/v): a) **3a-Br** and b) **6a-Br**

Anion transport studies: In order to investigate the origin of the cytotoxicity of these compounds, their transmembrane transport activity and their potential to disturb the membrane integrity were explored in model POPC liposomes. First, the ability of these compounds to facilitate chloride efflux from chloride-loaded vesicles was monitored using a chloride-selective electrode (ISE). The liposome suspension was placed in an isotonic, chloride-free medium and the studied tripodal imidazolium salts were added as aliquots of stock DMSO solutions. Release of all encapsulated chloride by addition of a detergent allowed the normalization of the chloride leakage and facilitated chloride efflux was monitored over time for each compound. For these experiments, NTf_2 salts were employed, and different external anions tested (Table 4, ESI Figure S8-S19).

Table 4. Chloride affinity in CD_3CN/D_2O (8/2 v/v) (log K 1:1 , BC_{50}), chloride-efflux rates in model liposomes (% Cl s^{-1}, at pHi/pHe 7.2) using different external anions.

Entry	Compound	log β[a][b]	Chloride efflux rate (%Cl·s^{-1})[c]		
			NO_3^-	HCO_3^- /SO_4^{2-}	SO_4^{2-}
1	**3a-NTf₂**	1.76 ± 0.04	13.6±1.2	11.7±1.4	12.8
2	**6a-NTf₂**	1.43 ± 0.03	16.4±1.1	21.2±1.4	21.7
3	**7a-NTf₂**	1.74 ± 0.02	17.0±1.9	11.0±0.6	15.5
4	**8a-NTf₂**	1.62 ± 0.02	25.1±1.4	22.7±2.5	23.4

[a] Obtained by simultaneous non-linear regression fitting of all the available ^1H NMR signals, [b] log β is defined as the formation constant for the 1:1 receptor/substrate complex in M^{-1}; [c] 10% imidazolium salt to POPC molar ratio. Each value represents the average of at least three trials, carried out with three batches of vesicles, except those obtained with sulfate, which correspond to one experiment.

To provide the appropriate basic data for chloride transport studies, ^1H NMR anion-binding studies were also conducted for the NTf_2 salts in aqueous acetonitrile (Table 4, ESI Figures S20-S23). The corresponding stability constants, K_a, were determined, by following the shift of the ^1H NMR signals of five protons of the receptor and fitting the data to 1:1 and 1:2 receptor:anion binding isotherms using HypNMR (ESI, Figures S24-27). Interestingly, as shown in Table 4, we observed their ability to bind only one chloride anion with very different binding constants for the corresponding 1:1 complex (entries 1-4, Table 4). The highest binding constants were obtained for compounds **3a-NTf₂** and **7a-NTf₂** both containing dodecyl alkyl chains (entries 1 and 3).

The NTf_2 salts showed moderate chloride-transport abilities, being compounds **6a-NTf₂** and **8a-NTf₂** the most active ones (Table 4, entries 2 and 4). Little differences were observed in the chloride efflux activity when different anions such as nitrate or bicarbonate/sulfate were used as the external anions (Table 4 and ESI Figures S8-S19). These results suggested the possibility of these compounds promoting an unspecific transmembrane transport and acting as membrane-disrupting agents. To check this possibility, carboxyfluorescein (CF) release assays were carried out. In this assay, CF is loaded at high concentration inside the liposomes. At this concentration, CF is non-emissive because of self-quenching processes. Leakage from the interior of the vesicles result in an immediate dilution and recovering of the CF fluorescence. Addition of detergent at the end of the experiment lyse the vesicles and allows normalization of the data for comparison purposes. The results at pH = 7.2 and pH = 6.2 are shown in Table 5 (ESI Figures S28-S49, where the normalized intensity at λ = 520 nm is represented over time).

Table 5. Carboxyfluorescein leakage observed upon addition of the studied compounds to POPC vesicles (0.05 mM) at different external pH.

Entry	Compound	CF efflux rate[a] (%CF·s^{-1}), pH_i/pH_e	
		7.2/7.2	7.2/6.2
1	**3a-Br**	1.7 ± 0.6	6.5 ± 3.3
2	**3b-Br**	2.8 ± 1.0	6.8 ± 3.6
3	**4a-Br**	21.6 ± 2.1	8.6 ± 3.5
4	**5b-Br**	3.1 ± 0.6	0
5	**6a-Br**	12.3 ± 0.3	15.1 ± 1.8
6	**7a-Br**	1.7 ± 0.7	0
7	**8a-Br**	24.6 ± 0.7	32.0 ± 4.0
8	**3a-NTf₂**	4.7 ± 0.6	--
9	**6a-NTf₂**	28.1 ± 3.1	--
10	**7a-NTf₂**	6.9 ± 0.9	--
11	**8a-NTf₂**	35.7 ± 0.2	--

a)10% imidazolium salt to POPC molar ratio. Each value represents the average of at least three individual experiments, carried out with different batches of vesicles.

The most active derivative in all assays was compound **8a-Br/NTf₂**. Compounds **4a-Br** and **6a-Br/NTf₂** were also found to form large non-selective pores in the lipid membrane. The maximum leakage detected for these compounds was 25%/36%, 22% and 12%/28% respectively, being NTf_2 salts more active in these assays. When these experiments were carried out at pH = 6.2 using the bromide salts, the main difference was the lack of activity showed by compound **4a-Br** under these conditions, whereas the leakage of CF promoted by **8a-Br** increased to 32% in the time frame of these experiments.

These assays suggested that the observed biological activity is likely not the result of just their transport activity. For instance,

This journal is © The Royal Society of Chemistry 20xx

Please do not adjust margins

Please do not adjust margins

compounds **3a-Br/NTf$_2$**, **3b-Br, 7a-Br/NTf$_2$** and **5b-Br** did not act as detergents although **3a-Br/NTf$_2$**, **3b-Br**, **7a-Br/NTf$_2$** presented high cytotoxic activities (Table 1). On the other hand, compound **8a-Br/NTf$_2$**, the most active in liposomes, displays a significant cytotoxicity which is enhanced at acidic pH. This behavior agrees with the results of **8a-Br** in the CF leakage assay. Loss of activity of **4a-Br** at acidic pH is also in agreement with the results discussed in cytotoxicity studies.

Conclusions

A series of novel tripodal pseudopeptides derived from *L*-valine and *L*-phenylalanine containing different hydrophobic groups have been synthetized, showing good cancer cell growth inhibition against different cancer cell lines, with IC_{50} values in the 20 μM range or lower. Results demonstrate that an optimum lipophilicity of the tail is needed for an efficient cytotoxicity, being compound **3a-Br** the most bioactive. Moreover, when the anticancer activity is studied at pH 6.2 the cell growth inhibition and selectivity against HEK-293 changes dramatically, increasing the inhibition in some cases more than one order of magnitude. Interestingly, compounds **3a-NTf$_2$** and **8a-NTf$_2$** presented loss of antitumor activity at acidic pH, decreasing the cell growth inhibition more than two orders of magnitude for **8a-NTf$_2$**. The transmembrane anion transport studies at physiologic pH revealed compound **8a-NTf$_2$** as the most active for chloride and carboxyfluorescein (CF) release assays with a leakage of 25% and 36% respectively. When carboxyfluorescein (CF) release assays were carried out at external pHe = 6.2 using the bromide salts, the main difference is the lack of activity showed by compound **4a-Br** which is in agreement with the decrease in its cytotoxic activity at this acidic pH.

Finally, aggregation studies have been carried out using different techniques and the results have revealed that spherical aggregates are formed in aqueous media. Furthermore, compounds with long alkyl chains have CAC values in the μM range being aggregated to some extent at their cytotoxicity concentration. The observed increase of the CAC at acidic pH suggests the presence of a higher amount of active monomeric species, which is in accordance with the increase of the antitumoral activity at acidic pH for **3a-Br**, suggesting that the monomeric species is mainly the responsible for the antitumoral activity.

Experimental

Materials and methods

Reagents and solvents, including NMR solvents, were purchased from commercial suppliers, and were used without further purification. Deionized water was obtained from a MilliQ® equipment. Imidazoles **1** and **2** were obtained as previously described.[33] Tripodal compounds were prepared through a slight modification of the procedure reported elsewhere.[34]

Anticancer and toxicity studies

A549, HeLa, HT-29, MCF-7 and HEK-293 cell lines were provided by ATCC®. Cell culture media were purchased from Gibco (Grand Island, NY). Fetal bovine serum (FBS) was obtained from HyClone (Utah, USA). Supplements and other chemicals not listed in this section were obtained from Sigma Chemical Co. (St. Louis, MO). Plastics for cell culture were supplied by Thermo Scientific BioLite (Madrid, Spain). All tested compounds were dissolved in DMSO at a concentration of 10 mM and stored at −20 °C until use.

A549, HeLa, HT-29, MCF-7 and HEK-293 cell lines were maintained in Dulbecco's modified Eagle's medium (DMEM) containing glucose (1 g/L), glutamine (2 mM), penicillin (50 μg/mL), streptomycin (50 μg/mL), and amphotericin B (1.25 μg/mL), supplemented with 10% FBS. All pH 6.2 media were prepared replacing the carbonate by PIPES buffer (10 mM) and adjusting the pH with 1M HCl or 1M NaOH.

Cell proliferation assay

In 96-well plates, 3×10^3 (A549, HeLa, HT-29, MCF-7 and HEK-293) cells per well were incubated with serial dilutions of the tested compounds (from 200 μM to 0,2 μM) in a total volume of 100 μL of their growth media. The 3-(4,5-dimethylthiazol-2-yl)-2,5-diphenyltetrazolium bromide (MTT; Sigma Chemical Co.) dye reduction assay in 96-well microplates was used as previously described.[48] After 2 days of incubation (37 °C, 5% CO_2 in a humid atmosphere), 10 μL of MTT (5 mg/mL in phosphate-buffered saline, PBS) was added to each well, and the plate was incubated for a further 3 h (37 °C). The supernatant was discarded and replaced by 100 μL of DMSO to dissolve formazan crystals. The absorbance was then read at 540 nm by Multiskan™ FC microplate reader. For all concentrations of compound, cell viability was expressed as the percentage of the ratio between the mean absorbance of treated cells and the mean absorbance of untreated cells. Three independent experiments were performed, and the IC_{50} values (i.e., concentration half inhibiting cell proliferation) were graphically determined using GraphPad Prism 4 software.

Statistical analysis: GraphPad Prism v4.0 software (GraphPad Software Inc., La Jolla, USA) was used for statistical analysis. For all experiments, the obtained results of the triplicates were represented as means with standard deviation (SD).

^{1}H NMR studies

The NMR experiments were carried out on a Varian INOVA 500 spectrometer (500 MHz for ^{1}H and 125 MHz for ^{13}C), on a Bruker Avance III HD 400 spectrometer (400 MHz for ^{1}H and 100 MHz for ^{13}C) or on a Bruker Avance III HD 300 spectrometer (300 MHz for ^{1}H and 75 MHz for ^{13}C). Chemical shifts are reported in ppm using TMS as the reference. Titration experiments followed by ^{1}H NMR spectroscopy were performed in CD_3CN/D_2O 8/2 v/v at 303 K and data fitting was carried out with the HypNMR 2008 version 4.0.71 software. For each ^{1}H NMR titration, the signals of the protons H_a, H_b, H_f, H_g, NH, were monitored for changes in chemical shift, which provided several data sets that were employed in the determination of the association constants K_a. Data for chloride anion were fitted satisfactorily to the 1:1 binding model. For CAC determination,

Please do not adjust margins

Please do not adjust margins

different solutions of the compounds with concentrations ranging from 0.1 to 4 mM in CD_3OD/D_2O were introduced in NMR tubes and the spectra taken at 30 ºC. CAC values were estimated at the cross point of the two straight lines extrapolated from the changes in chemical shifts as a function of the inverse of the concentration.

Fluorescence spectroscopy measurements

Fluorescence measurements were performed with a Spex Fluorolog 3-11 instrument equipped with a 450 W xenon lamp (right angle mode). Pyrene was used as a fluorescence probe to determine the CAC of the bromide salts of **3a**, **3b**, **4a**, **5b** and **6a** in aqueous media at 25±1 °C. Firstly, a stock pyrene solution (1.98×10^{-4} mol/L) was prepared in ultrapure methanol. Then, different solutions of the bromide salts (ranging from 1×10^{-3} to 1×10^{-6} mol/L) were prepared in different vials (1 mL) and 5 µL of the pyrene solution were added to each vial, achieving a final pyrene concentration of 9.89×10^{-7} mol/L. The fluorescence spectra of pyrene were recorded for all the samples from 350 to 550 nm after excitation at 337 nm. The slit width was set at 5 nm for both excitation and emission. The peak intensities at 373 and 383 nm were determined as I_1 and I_3, respectively. The ratios of the peak intensities at 373 and 383 nm (I_1/I_3) of the emission spectra were recorded as a function of the logarithm of concentration. The CAC values were taken from the break point using the intersection of the best fit straight lines. The CAC was obtained from the average of three measurements for each compound.

Light scattering (LS) measurements

Light scattering measurements were performed using a Brookhaven Instruments BI-200SM goniometer, a BI-9000AT digital correlator, and a red laser operating at wavelength of 633 nm. Scattering angle was 45°. The round measurement cell was thermostated at 25 °C. A 0.6 mM solution of the compounds **3a-Br** and **3b-Br** was prepared in Milli-Q water. The solvent was filtered through a Millipore Millex syringe filter (0.22 µm). Before each measurement, the scattering cell was rinsed several times with the solution. The LS measurements started 5-10 min after the sample solutions were placed in the LS optical system to allow the sample to equilibrate. The data acquisition was carried out for 10 min and each experiment was repeated three times. The data were analyzed with the cumulant method using the software provided by the manufacturer.

Optical images

Images were recorded with a OLYMPUS COVER-018 microscope, BX51TF model, at 25 ºC.

SEM images

Scanning Electron Microscopy was performed in a JEOL 7001F microscope with a digital camera. Samples were obtained by slow evaporation of a solution of the compounds (1 to 2 mg/mL) directly onto the sample aluminum holder, and were conventionally coated before the measurement, using the sputtering technique in which microscopic particles of platinum are rejected from the surface after the material is itself bombarded by energetic particles of a plasma or gas.

Membrane transport assays

Preparation of Phospholipid Vesicles: A chloroform solution of 1-palmitoyl-2-oleoyl-sn-glycero-3-phosphocoline (POPC) (20 mg/mL) (Sigma Aldrich) was evaporated to dryness using a rotary evaporator and the resulting film was dried under high vacuum for, at least, two hours. A sodium chloride aqueous solution (489 mM and 5 mM phosphate buffer, pH 7.2, or 451 mM and 20 mM phosphate buffer, pH 7.2) was added to rehydrate the lipid film. The resulting suspension was vortexed and subjected to nine freeze-thaw cycles; subsequently, it was extruded twenty-nine times through a polycarbonate membrane (200 nm) employing a LiposoFast basic extruder (Avestin, Inc.). The resulting unilamellar vesicles were dialysed against a sodium nitrate (489 mM and 5 mM phosphate buffer, pH 7.2) or a sodium sulphate (150 mM and 20 mM phosphate buffer, pH 7.2) aqueous solutions, to remove unencapsulated chloride.

Ion selective electrode (ISE) transport assays. Chloride/Nitrate Transport Assays: Unilamellar vesicles (average diameter: 200 nm) made of POPC and containing a sodium chloride aqueous solution (489 mM and 5 mM phosphate buffer, pH 7.2, for chloride/nitrate exchange assays, or 451 mM and 20 mM phosphate buffer, pH 7.2, for chloride/bicarbonate exchange assays) were suspended in a sodium nitrate (489 mM and 5 mM phosphate buffer, pH 7.2) or a sodium sulphate (150 mM and 20 mM phosphate buffer, pH 7.2) aqueous solution, respectively, the final lipid concentration being 0.5 mM and the final volume 5 mL. A solution of the carrier in DMSO, usually 5 µL to avoid the influence of the organic solvent during the experiments, was added, and the chloride released was monitored employing a chloride-selective electrode (HACH 9652C). Once the experiment was finished, a surfactant (Triton-X, 10% dispersion in water, 20 µL) was added to lyse the vesicles and release all the encapsulated chloride. This value was regarded as 100% release and used as such. For the chloride/bicarbonate exchange assays, a sodium bicarbonate aqueous solution was added to the vesicles suspended in the sodium sulphate one (150 mM and 20 mM phosphate buffer, pH 7.2), the final bicarbonate concentration during the experiment being 40 mM. The chloride efflux was monitored for another five minutes, until the vesicles were lysed with the surfactant. Replication experiments were performed with three batches of vesicles.

Carboxyfluorescein-based assays: POPC vesicles were loaded with a sodium chloride aqueous solution (451 mM NaCl and 20 mM phosphate buffer, 50 mM carboxyfluorescein, pH 7.2) and treated according to the procedure described above. After being subjected to extrusion, liposomes were suspended in a sodium sulphate aqueous solution (150 mM Na_2SO_4 and 20 mM phosphate buffer, pH 7.2). The unencapsulated carboxyfluorescein was removed by size-exclusion chromatography, using Sephadex G-25 as the stationary phase and the external solution as the mobile phase. The experiments were performed in 1-cm disposable cells, the final POPC concentration in the cuvette being 0.05 mM and the total volume 2.5 mL. For those experiments in which pHout = 6.2, the corresponding

 This journal is © The Royal Society of Chemistry 20xx

Please do not adjust margins

Please do not adjust margins

volume of the vesicles stock solution was suspended in a sodium sulphate aqueous solution at pH 6.2 immediately before starting the assay. At t = 60 s the anion carrier was added, and the emission changes were recorded during five minutes. At t = 360 s a pulse of the detergent Triton-X (10%) was added to lyse the vesicles and release all the entrapped carboxyfluorescein. This value was regarded as 100% release and used to normalize the data. Replication experiments were performed with three batches of vesicles

DSC measurements

Samples were placed in a 40 mL, hermetically sealed aluminum pan with a pinhole in the top. An empty aluminum pan was used as the reference. Samples were exposed to a flowing N_2 atmosphere. Before the DSC test, each sample was dried at 60 °C in a vacuum oven for 12 h. Transition temperatures were determined by using multiple cycles (typically three) involving heating the sample from –40 to 150-200 °C followed by cooling from 150-200 to –40 °C, both at a rate of 5 °C/min. Transition temperatures were determined at the second cycle.

Synthetic procedures

Synthesis of imidazolim salts: 4a-Br: (*S*)-N-butyl-2-(1H-imidazol-1-yl)-3-methylbutanamide (0.201 g, 0.914 mmol, 3.3 equiv) and 1,3,5-tris(bromomethyl)benzene (0.097 g, 0.273 mmol, 1 equiv) were dissolved in acetronitrile (2.65 mL) in a microwave vial. The conditions of this reaction in the microwave instrument were: 150 ºC, 1 h and 120 W. The resulting solution was vacuum evaporated, and the residue washed with diethyl ether and then with ethyl acetate. The solid obtained was vacuum dried to give a brown solid product (0.274 g, 97.7%): Tg 98 ºC; $[\alpha]_D^{25}$ = 10.8 deg cm^3 g^{-1} dm^{-1} (c = 0.011 g cm^{-3}, MeOH). ^{1}H NMR (400 MHz, methanol-*d*$_4$, δ ppm): 9.30 (s, 3H), 8.67 (s, NH), 7.74 (t, *J* = 1.8 Hz, 3H), 7.65 (t, *J* = 1.8 Hz, 3H), 7.60 (s, 3H), 5.55 (s, 6H), 4.69 (d, *J* = 10.0 Hz, 3H), 3.40-3.24 (m, 6H), 2.44 (m, *J* = 9.7, 6.5 Hz, 3H), 1.51 (m, 6H), 1.33 (m, 6H), 1.06 (m, 9H), 0.97-0.82 (m, 18H); ^{13}C NMR (101 MHz, methanol-*d*$_4$, δ ppm): 167.2, 167.1, 136.3, 129.7, 122.6, 122.5, 122.4, 68.9, 68.9, 52.1, 39.3, 39.1, 31.8, 31.8, 30.8, 30.8, 19.7, 17.9, 17.5, 12.6; IR (ATR): $\tilde{\upsilon}_{max}$ (cm^{-1}) = 3228, 3067, 2961, 2933, 2872, 1672, 1549, 1463, 1369, 1154. MS (TOF MS ES$^+$): m/z (%) = 433.75 (100) $[C_{45}H_{72}N_9O_3Br]^{2+}$, 946.42 (45) $[C_{45}H_{72}N_9O_3Br_2]^+$, 262.19 (70) $[C_{45}H_{72}N_9O_3]^{3+}$. Anal. calcd for $C_{45}H_{72}N_9O_3Br_3$: C 52.6, H 7.1, N 12.3 found C 52.8, H 7.0, N 12.5.

6a-Br. Prepared as described for compound **4a-Br** from 0.273 g of (*S*)-N-benzyl-2-(1H-imidazol-1-yl)-3-methylbutanamide (1.06 mmol, 4 equiv) and 0.977 g of 1,3,5-tris(bromomethyl)benzene (0.265 mmol, 1 equiv). The reaction gave a brown solid product (0.27 g, 98.9%): Tg 103 ºC; $[\alpha]_D^{25}$ = 26.5 deg cm^3 g^{-1} dm^{-1} (c = 0.011 g cm^{-3}, MeOH). ^{1}H NMR (500 MHz, $CDCl_3$, δ ppm):10.00 (s, 3H), 8.60 (s, 3H), 8.31 (s, 6H), 7.29 (s, 3H), 7.24-7.04 (m, 15H), 5.65 (d, *J* = 14.3 Hz, 3H), 5.28 (d, *J* = 14.1 Hz, 3H), 5.12 (d, *J* = 10.8 Hz, 3H), 4.44 (dd, *J*=15.0, 6.6 Hz, 3H), 4.07 (dd, *J*=15.0, 5.2 Hz, 3H), 2.48-2.29 (m, 3H), 0.97 (d, *J*=6.4 Hz, 9H), 0.70 (d, *J*=6.6 Hz, 9H); ^{13}C NMR (75 MHz, 30 °C, $CDCl_3$, δ ppm): 166.4, 137.3, 135.8, 135.5, 131.5, 128.5, 127.5, 127.3, 124.2, 119.4, 68.3, 52.0, 43.5, 30.8, 18.8, 18.3; IR (ATR): $\tilde{\upsilon}_{max}$ (cm^{-1}) = 3225, 3056, 2967, 1676, 1548. MS (ESI$^+$): m/z (%) = 296.4 (100) $[C_{54}H_{66}N_9O_3]^{3+}$, 484.9 (20) $[C_{54}H_{66}N_9O_3Br]^{2+}$. Anal. calcd for $C_{54}H_{66}N_9O_3Br_3$: C 57.5, H 5.9, N 11.2; found C 57.9, H 6.0, N 11.1.

7a-Br: Prepared as described for compound **4a-Br** from 0.245 g of (*S*)-N-dodecyl-2-(1H-imidazol-1-yl)-3-phenylpropanamide (0.639 mmol, 3.3 equiv) and 0.069 g of 1,3,5-tris(bromomethyl)benzene (0.193 mmol, 1 equiv). The reaction gave a brown solid product (0.253 g, 86.8%): Tg 106 ºC m.p. 173 °C; $[\alpha]_D^{25}$ = 2.3 deg cm^3 g^{-1} dm^{-1} (c = 0.011 g cm^{-3}, MeOH). ^{1}H NMR (400 MHz, $CDCl_3$, δ ppm): 9.35 (s, 3H), 8.35 (s, 3H), 8.10 (s, 3H), 8.09 (s, 3H), 7.43 (s, 3H), 7.23 – 6.97 (m, 30H), 5.74 (t, *J* = 8.2 Hz, 3H), 5.52 (d, *J* = 14.1 Hz, 3H), 4.98 (d, *J* = 13.9 Hz, 3H), 3.31 – 3.11 (m, 6H), 2.80 (d, *J* = 8.4 Hz, 3H), 1.60 (s, 6H),1.42–1.02 (m, 42H), 0.85 – 0.76 (m, 9H); ^{13}C NMR (101 MHz, $CDCl_3$, δ ppm): 165.8, 135.8, 135.2, 134.3, 131.4, 129.1, 128.9, 127.7, 124.1, 119.4, 63.1, 51.8, 39.9, 38.9, 31.9, 29.7, 29.4, 29.0, 26.9, 22.7, 14.1. IR (ATR): $\tilde{\upsilon}_{max}$ (cm^{-1})= 3398, 3289, 3063, 2955, 2922, 2852, 1656, 1556, 1466, 1156. MS (TOF MS ESI$^+$): m/z (%) = 673.93 (100) $[C_{81}H_{120}N_9O_3Br]^{2+}$, 422.31 (70) $[C_{81}H_{120}N_9O_3]^{3+}$, 1426.78 (80) $[C_{81}H_{120}N_9O_3Br_2]^+$. Anal. calcd for $C_{81}H_{120}N_9O_3Br_3{\cdot}2H_2O$: C 63.0, H 8.1, N 8.2 found C 63.2, H 8.4, N 8.0.

8a-Br. Prepared as described for compound **4a-Br** from (*S*)-N-benzyl-2-(1H-imidazol-1-yl)-3-phenylpropanamide (0.192 g, 0.63 mmol, 4 equiv) and 1,3,5-tris(bromomethyl)benzene (0.056 g, 0.157 mmol, 1 equiv) dissolved in acetronitrile (1.57 mL). The yellow liquid obtained was evaporated to dryness and washed with ethyl acetate to give a brown waxy product (0.141 g, 70.3%); m.p. 138 °C, $[\alpha]_D^{25}$ = 2.1 deg cm^3 g^{-1} dm^{-1} (c = 0.013 g cm^{-3}, MeOH). ^{1}H NMR (400 MHz, methanol-d$_4$/$CDCl_3$, δ ppm): 9.37 (s, 3H), 7.68-7.52 (m, 6H), 7.41 (s, 3H), 7.23-6.95 (m, 30H), 5.40-5.29 (m, 9H), 4.33 (d, *J* = 14.9 Hz, 3H), 4.15 (d, *J* = 14.9 Hz, 3H), 3.45 (dd, *J* = 13.7, 7.1 Hz, 3H), 3.38-3.24 (m, 3H); ^{13}C NMR (75 MHz, methanol-d$_4$/$CDCl_3$, δ ppm): 166.9, 135.7, 135.5, 134.0, 131.1, 128.9, 128.8, 127.6, 123.4, 120.6, 63.0, 51.9, 39.1, 26.1; IR (ATR): $\tilde{\upsilon}_{max}$ (cm^{-1}) = 3216, 3058, 2968, 1679, 1549. MS (ESI$^+$): m/z (%) = 344.5 (100) $[C_{66}H_{66}N_9O_3]^{3+}$, 556.8 (20) $[C_{66}H_{66}BrN_9O_3]^{2+}$. Anal. calcd for $C_{66}H_{66}N_9O_3Br_3{\cdot}4H_2O$: C 58.9, H 5.6, N 9.4; found C 58.5, H 5.7, N 9.0.

3a-NTf$_2$. 3,3',3''-(Benzene-1,3,5-triyltris(methylene))tris(1-((*S*)-1-(dodecylamino)-3-methyl-1-oxobutan-2-yl)-1H-imidazol-3-ium) bromide (0.091 g, $6.64{\cdot}10^{-2}$mmol, 1 equiv) and lithium bis((trifluoromethyl)sulfonyl)amide (0.0636 g, 0.221 mmol, 3.3 equiv) were dissolved in methanol in a round bottom flask (50 mL). The reaction mixture was stirred at room temperature for 24 h. The solvent was evaporated under reduced pressure and the resulting residue was extracted with CH_2Cl_2 (3x), dried with anhydrous $MgSO_4$, filtered, and vacuum concentrated. The reaction gave a yellow liquid product (0.086 g, 66%): Tg 7 ºC; $[\alpha]_D^{25}$ = 10.4 deg cm^3 g^{-1} dm^{-1} (c = 0.021 g cm^{-3}, MeOH). ^{1}H NMR (500 MHz, $CDCl_3$, δ ppm): 8.95 (s, 3H), 7.77 (s, 6H), 7.70 (s, 3H), 6.84-6.74 (m, NH), 5.48-5.30 (m, 6H), 4.53 (d, *J* = 10.3 Hz, 3H), 3.36 (m, 3H), 3.04 (m, 3H), 2.39 (m, 3H), 1.49 (m, 6H), 1.36-1.16 (m, 54H), 1.05 (d, *J* = 6.6 Hz, 9H), 0.88 (t, *J* = 6.9 Hz,

Please do not adjust margins

Please do not adjust margins

9H), 0.75 (d, *J* = 6.7 Hz, 9H);^{13}C NMR (126 MHz, $CDCl_3$, δ ppm): 166.1, 135.7, 135.0, 131.4, 123.4, 121.7, 120.9 (CF_3), 118.3 (CF_3), 69.0, 52.7, 40.0, 31.9, 29.6, 29.5, 29.4, 29.3, 29.1, 28.8, 26.8, 22.6, 18.7, 18.2, 14.1; IR (ATR): $\tilde{\upsilon}_{max}$ (cm^{-1})= 3379, 3147, 2924, 2855, 1679, 1186. MS (TOF MS ESI$^+$): m/z (%) = 701.4 (100) $[C_{71}H_{120}F_6N_{10}O_7S_2]^{2+}$, 374.3 (48) $[C_{69}H_{120}N_9O_3]^{3+}$, 1682.8 (20) $[C_{73}H_{120}F_{12}N_{11}O_{11}S_4]^+$. Anal. calcd for $C_{75}H_{120}N_{12}O_{15}F_{18}S_6{\cdot}H_2O$: C 45.5, H 6.2, N 8.5, S 9.7; found C 45.0, H 6.4, N 8.7, S 10.0.

6a-NTf$_2$. Prepared as described for compound **3a-NTf$_2$** from 0.070 g of 3,3',3''-(benzene-1,3,5-triyltris(methylene))tris(1-((*S*)-1-(benzylamino)-3-methyl-1-oxobutan-2-yl)-1H-imidazol-3-ium) bromide ($6.16{\cdot}10^{-2}$mmol, 1 equiv) and 0.059 g of lithium bis((trifluoromethyl)sulfonyl)amide (0.205 mmol, 3.3 equiv). The reaction gave a waxy product (0.0957 g, 90.0%): Tg 30 ºC; $[\alpha]_D^{25}$ = 17.9 deg cm^3 g^{-1} dm^{-1} (c = 0.032 g cm^{-3}, MeOH). ^{1}H NMR (400 MHz, ACN-*d*$_3$, δ ppm): 8.97 (s, 3H), 7.55 (s, 3H), 7.37 (m, 6H), 7.32-7.20 (m, 15H), 5.36 (s, 6H), 4.56 (d, *J* = 9.6 Hz, 3H), 4.40 (d, *J* = 14.9 Hz, 3H), 4.25 (d, *J* = 14.9 Hz, 3H), 2.31 (m, 3H), 0.92 (d, *J* = 6.6 Hz, 9H), 0.75 (d, *J* = 6.6 Hz, 9H); ^{13}C NMR (75 MHz, $CDCl_3$, δ ppm): 166.3, 137.0, 135.5, 135.1, 131.1, 128.7, 127.8, 127.7, 123.2, 121.6 (CF_3), 117.5 (CF_3), 68.8, 52.6, 43.9, 31.9, 18.6, 18.1; IR (ATR): $\tilde{\upsilon}_{max}$ (cm^{-1}) = 3373, 3146, 2972, 1679, 1181. MS (ESI$^+$): m/z (%) = 296.4 (100) $[C_{54}H_{66}N_9O_3]^{3+}$, 584.8 (55) $[C_{56}H_{66}F_6N_{10}O_7S_2]^{2+}$. Anal. calcd for $C_{60}H_{66}N_{12}O_{15}F_{18}S_6{\cdot}3H_2O$: C 40.4, H 4.1, N 9.4, S 10.8; found C 40.9, H 4.3, N 9.1, S 10.6.

7a-NTf$_2$. Prepared as described for compound **3a-NTf$_2$** from 0.097 g of 3,3',3''-(benzene-1,3,5-triyltris(methylene))tris(1-((*S*)-1-(dodecylamino)-1-oxo-3-phenylpropan-2-yl)-1H-imidazol-3-ium) bromide ($6.44{\cdot}10^{-2}$ mmol, 1 equiv) and 0.0616 g of lithium bis((trifluoromethyl)sulfonyl)amide (0.215 mmol, 3.3 equiv). The reaction gave a yellow waxy product (0.107 g, 79%): Tg 21 ºC; $[\alpha]_D^{25}$ = -1.3 deg cm^3 g^{-1} dm^{-1} (c = 0.011 g cm^{-3}, MeOH). ^{1}H NMR (400 MHz, $CDCl_3$, δ): 8.54 (s, 3H), 7.75 (s, 3H), 7.56 (s, 3H), 7.49 (s, 3H), 7.22-7.10 (m, 12H), 7.08-6.97 (m, 3H), 6.47 (m, NH), 5.13 (d, *J* = 9.7 Hz, 6H), 3.30 (dd, *J* = 13.6, 7.3 Hz, 3H), 3.16 (m, 6H), 2.91 (m, 3H), 1.17 (m, 64H), 0.81 (t, *J* = 6.7 Hz, 9H); ^{13}C NMR (101 MHz, $CDCl_3$, δ): 165.6, 135.4, 134.8, 133.7, 131.0, 129.0, 128.9, 127.8, 123.1, 121.5, 121.2 (CF_3), 118.0 (CF_3), 63.8, 52.3, 40.0, 39.9, 31.9, 29.6, 29.4, 29.3, 29.1, 28.7, 26.6, 22.7, 14.1; IR (ATR): $\tilde{\upsilon}_{max}$ (cm^{-1}) = 3378, 3148, 2925, 2856, 1678, 1551, 1457, 1346, 1187, 1137, 1054. MS (TOF MS ES$^+$): m/z (%) = 773.44 (100) $[C_{83}H_{120}F_6N_{10}O_7S_2]^{2+}$, 422.31 (20) $[C_{81}H_{120}N_9O_3]^{3+}$. Anal. calcd for $C_{87}H_{120}N_{12}O_{15}F_{18}S_6$: C 49.6, H 5.7, N 8.0, S 9.1; found C 49.4, H 6.0, N 7.5, S 9.7.

8a-NTf$_2$. Prepared as described for compound **3a-NTf$_2$** from 0.045 g of 3,3',3''-(benzene-1,3,5-triyltris(methylene))tris(1-((*S*)-1-(benzylamino)-1-oxo-3-phenylpropan-2-yl)-1H-imidazol-3-ium) bromide ($3.5{\cdot}10^{-2}$mmol, 1 equiv) and 0.0339 g of lithium bis((trifluoromethyl)sulfonyl)amide (0.118 mmol, 3.3 equiv). The reaction gave a waxy product (0.047 g, 70.2%): Tg 43ºC; $[\alpha]_D^{25}$ = -1.9 deg cm^3 g^{-1} dm^{-1} (c = 0.013 g cm^{-3}, MeOH). ^{1}H NMR (400 MHz, $CDCl_3$, δ ppm): 8.53 (s, 3H), 7.68 (s, 3H), 7.48 (s, 3H), 7.42 (s, 3H), 7.24-6.79 (m, 33H), 5.29-5.05 (m, 9H), 4.38 (dd, *J* = 14.7, 6.6 Hz, 3H), 4.05 (dt, *J* = 15.8, 5.8 Hz, 3H), 3.31 (dd, *J* = 13.5, 7.6 Hz, 3H), 3.14 (dd, *J* = 13.6, 8.0 Hz, 3H); ^{13}C NMR (126 MHz, $CDCl_3$, δ ppm): 165.8, 136.6, 135.4, 135.0, 133.6, 130.9, 129.1, 128.9, 128.6, 127.8, 127.6, 123.2, 121.6, 120.9 (CF_3), 118.3 (CF_3), 63.7, 52.4, 43.8, 39.7; IR (ATR): $\tilde{\upsilon}_{max}$ (cm^{-1}) = 3371, 3147, 2926, 1679, 1182. MS (ESI$^+$): m/z (%) = 344.5 (35) $[C_{66}H_{66}N_9O_3]^{3+}$, 656.4 (100) $[C_{68}H_{66}F_6N_{10}O_7S_2]^{2+}$, 1592.6 (10) $[C_{70}H_{66}F_{12}N_{11}O_{11}S_4]^+$. Anal. calcd for $C_{72}H_{66}N_{12}O_{15}F_{18}S_6$: C 46.2, H 3.6, N 9.0, S 10.3; found C 46.3, H 3.4, N 8.8, S 9.7.

Conflicts of interest

There are no conflicts to declare

Acknowledgements

This research was funded by FEDER/MINISTERIO DE CIENCIA, INNOVACIÓN Y UNIVERSIDADES, grant numbers RTI2018-098233-B-C22 and PID2020-117610RB-I00, Pla de Promoció de la Investigació de la Universitat Jaume I, grant UJI-B2019-40, Consellería de Innovació, Universitat Ciencia (AICO/2021/139) and Consejería de Educación de la Junta de Castilla y León (project BU067P20). A.V. work was funded by MICINN within the predoctoral fellowship program, grant FPU15/01191. Technical support from the SECIC of the UJI and Andrea Sancho-Medina's contributions to transmembrane anion transport experiments are gratefully acknowledged.

Notes and references

1 F. Bray, J. Ferlay, I. Soerjomataram, R. L. Siegel, L. A. Torre and A. Jemal, *CA Cancer J. Clin.*, 2018, **68**, 394-424.
2 World Health Organization, Implications of the SDGs for health monitoring-a challenge and an opportunity for all countries, World Health Statistics, 2016: Monitoring Health for the SDGs Sustainable Development Goals, WHO Press, Geneva, Switzerland, 2016.
3 D. E. Thurston, Chemistry and Pharmacology of Anticancer Drugs, 1st ed.; CRS Press; Taylor and Francis group: Abingdon, UK 2006.
4 I. Ali, A. Haque, K. Saleem and M. F. Hsieh, *Bioorg. Med. Chem.*, 2013, **21**, 3808-3820.
5 N. Sternberg, S. M. Donat, J. Bellmunt, R. E. Millikan, W. Stadler, P. De Mulder, A. Sherif, H. Von Der Maase, T. Tsukamoto and M. S. Soloway, *Urology*, 2007, **69**, 62-79.
6 F. Zagouri, S. Peroukidis, K. Tzannis, V. Kouloulias and A. Bamias, *Crit. Rev. Oncol. Hematol.,* 2015, **93**, 36-49.
7 I. M. Marrucho, L. C. Branco and L. P. N. Rebelo, *Annu. Rev. Chem. Biomol. Eng.,* 2014, **5**, 527-546.
8 X. Fan, H. Cheng, X. Wang, E. Ye, X. J. Loh, Y.-L. Wu and Z. Li, *Adv. Healthcare Mater.*, 2018, **7**, 1701143.
9 K. S. Egorova, E. G. Gordeev and V. P. Ananikov, *Chem. Rev.,* 2017, **117**, 7132-7189.
10 S. N. Pedro, C. S. R. Freire, A. J. D. Silvestre and M. G. Freire, *Int. J. Mol. Sci.*, 2020, **21**, 8298–8348.
11 J. Gravel and R. Schmitzer, *Org. Biomol. Chem*., 2017, **15**, 1051-1071.
12 J. L. Shamshina, S. P Kelley, G. Gurau and R. D. Rogers, *Nature*, 2015, **528**, 188-189.

 This journal is © The Royal Society of Chemistry 20xx

Please do not adjust margins

Please do not adjust margins

13 A. Hryniewicka, K. Niemirowicz-Laskowska, P. Wielgat, H. Car, T .Hauschild and J. W. Morzycki, *Bioorg. Chem.*, 2021, **108**, 104550.
14 N. Rezki, F. F. Al-blewi, S. A. Al-Sodies, A. K. Alnuzha, M. Messali, I. Ali and M. R. Aouad, *ACS Omega*, 2020, **5**, 4807−4815.
15 A. Miskiewicz, P. Ceranowicz, M. Szymczak, K. Bartus and P. Kowalczyk, *Int. J. Mol. Sci.,* 2018*,* **19**, 2779-2803.
16 N. Rezki, S. A. Al-Sodies, M. R Aouad, S. K. Bardaweel, M. Messali and S. H. El Ashry, *Inter. J. Mol. Sci.,* 2016, **17**, 766-786.
17 N. Rezki and M. R. Aouad, *Acta pharmaceutica,* 2017, **67**, 309-324.
18 A. Aljuhani, W. S. El-Sayed, P. K. Sahu, N. Rezki, M. R. Aouad, R. Salghi and M. Messali, *J. Mol. Liq.*, 2018, **249**, 747-753.
19 X.-L. Xu, C.-L. Yu, W. Chen, Y.-C. Li, L.-J. Yang, Y. Li, H.-B. Zhang and X.-D. Yang, *Org. Biomol. Chem*., 2015, **3**, 1550-1557.
20 M. H. Fernandes, R. Ferraz and C. Prudencio, *Chem. Med. Chem.*, 2017, **12**, 11-18.
21 P. Cancemi, M. Buttacavoli, F. D'Anna, S. Feo, R. M. Fontana, R. Noto, A. Sutera, P. Vitaleb and G. Gallo, *New J. Chem*., 2017, **41**, 3574–3585.
22 S. V. Malhotra, V. Kumar, C. Velez and B. Zayas, *MedChemComm,* 2014, **5**, 1404-1409.
23 S. N. Riduan and Y. Zhang, *Chem. Soc. Rev.*, 2013, **42**, 9055-9070.
24 D. Wang, C. Richter, A. Rühling, S. Hüwel, F. Glorius and H. J. Galla, *Biochem. Biophys. Res. Commun.,* 2015, **467**, 1033–1038.
25 N. Rezki, M. Messali, S. A. Al-Sodies, A. Naqvi, A. S. K. Bardaweel, F. F. Al-blewi, M. R. Aouad and E. S. H. El Ashry, *J. Mol. Liq.,* 2018, **265**, 428–444.
26 S. V. Malhotra and V. Kumar, *Bioorg. Med. Chem. Lett.,* 2010, **20**, 581-585.
27 B. D. Wright, M. C. Deblock, P. O. Wagers, E. Duah, N. K. Robishaw, K. L. Shelton, M. R. Southerland, M. A. DeBord, K. M. Kersten, L. J. McDonald, J. A. Stiel, M. J. Panzner, C. A. Tessier, S. Paruchuri and W. J. Youngs, *Med. Chem. Res.*, 2015, **24**, 2838-2861.
28 R. Rondla, *Inorg. Chim. Acta,* 2018, **477**, 183-191.
29 W. Youngs, M. Panzner, C. Tessier, M. Deblock, B. Wright, P. Wagers and N. Robishaw, Azolium and purinium salt anticancer and antimicrobial agents US 2014, 0142307 A1.
30 B. Altava, D. S. Barbosa, M. I. Burguete, J. Escorihuela, S. V. Luis, *Tetrahedron:Asymmetry*, 2009, **20**, 999-1003.
31 L. González-Mendoza, J. Escorihuela, B. Altava, M. I. Burguete and S. V. Luis, *Org. Biomol. Chem.*, 2015, **13**, 5450-5459.
32 L. Gonzalez-Mendoza, B. Altava, M. I. Burguete, J. Escorihuela, E. Hernando, S. V. Luis, R. Quesada and C. Vicent, *RSC Adv.,* 2015, **5**, 34415-34423.
33 L. Gonzalez-Mendoza, B. Altava, M. Bolte, M. I. Burguete, E. García-Verdugo and S. V. Luis, *Eur. J. Org. Chem.,* 2012, 4996-5009.
34 A. Valls, B. Altava, M. I. Burguete, J. Escorihuela, V. Martí Centelles and S. V. Luis, *Org. Chem. Front.,* 2019, **62**, 1214-1225.
35 A. Valls, J. J. Andreu, E. Falomir, S. V. Luis, E. Atrián-Blasco, S. G. Mitchell and B. Altava, *Pharmaceuticals*, 2020, **13**, 482.
36 P. A. Gale, R. Pérez-Tomás and R. Quesada, *Acc. Chem. Res.*, 2013, **46**, 2801-2813.
37 N. Busschaert and P. A. Gale, *Angew. Chem. Int. Ed.,* 2013, **52**, 1374-1382.
38 S.-K. Ko, S. K. Kim, A. Share, V. M. Lynch, J. Park, W. Namkung, W. V. Rossom, N. Busschaert, P. A. Gale, J. L. Sessler and I. Shin, *Nat. Chem.,* 2014, **6**, 885-892.
39 J. T. Davis, in Topics in Heterocyclic Chemistry, ed. P. A. Gale and W. Dehaen, Springer, Berlin, Heidelberg, 2010, **24**, 145-176.
40 L. González, J. Escorihuela, B. Altava, M. I. Burguete and S. V. Luis, *Eur. J. Org. Chem.*, 2014, 5356-5363.
41 B. A. Webb, M. Chimenti, M. P. Jacobson and D. L. Barber, *Nat. Rev. Cancer,* 2011, **11**, 671-677.
42 L. Tapia, Y. Pérez, M. Bolte, J. Casas, J. Sol, R. Quesada and I. Alfonso, *Angew. Chem. Int. Ed.*, 2019, **131**, 12595-12598.
43 S. V. Shinde and P. Talukdar, *Angew. Chem. Int. Ed.*, 2017, **129**, 4302-4306.
44 A. Roy, O. Biswas and P. Talukdar, *Chem. Commun.,* 2017, **53**, 3122-3125.
45 E. N. W. Howe, N. Busschaert, X. Wu, S. N. Berry, J. Ho, M. E. Light, D. D. Czech, H. A. Klein, J. A. Kitchen and P. A. Gale, *J. Am. Chem. Soc.,* 2016, **138**, 8301-8308.
46 R. B. P. Elmes, N. Busschaert, D. D. Czech, P. A. Gale and K. A. Jolliffe, *Chem. Commun.,* 2015, **51**, 10107-10110.
47 N. Busschaert, R. B. P. Elmes, D. D. Czech, X. Wu, I. L. Kirby, E. M. Peck, K. D. Hendzel, S. K. Shaw, B. Chan, B. D. Smith, K. A. Jolliffe and P. A. Gale, *Chem. Sci.,* 2014, **5**, 3617-3626.
48 S. Rodríguez-Nieto, M. A. Medina and A. R. Quesada, *Anticancer Res.,* 2001, **21**, 3457−3460,
49 J. C. Stockert, R. W. Horobin, L. L. Colombo and A. Blázquez-Castro, *Acta Histochem.,* 2018, **120**, 159-167.
50 Biophysical Chemistry, Advance applications. M. Khalid Ed. (Chapter 6) S. H. Alotaibi, A. A. Momen, Anticancer Drugs' Deoxyribonucleic Acid (DNA) Interactions. 2019.
51 M. Goftar, N. Kor and Z. Kor. *Int. J. Adv. Biol. Biomed. Res.*, 2014, **2**, 811-822.
52 K. Cook, K. Tarnawsky, A. J. Swinton, D. D. Yang, A. S. Senetra, G. A. Caputo, B. R. Carone and T. D. Vaden, *Biomolecules*, 2019, **9**, 251–261.
53 M. Galluzzi, C. Schulte, P. Milani and A. Podesta, *Langmuir*, 2018, **34**, 12452–12462.
54 R. F. M. Frade, A. Matias, L. C. Branco, C. A. M. Afonso and C. M. M. Duarte, *Green Chem.,* 2007, **9**, 873–877.
55 K. Kalyanasundaram and J. K. Thomas, *J. Am. Chem. Soc.,* 1977, **99**, 2039-2044.
56 K. Kalyanasundaram, Photochemistry in Microheterogeneous Systems, Academic Press, New York, 1987.
57 J. Aguiar, P. Carpena, J. A. Molina-Bolívar and C. Carnero Ruiz, *J. Colloid Interface Sci.,* 2003, **258**, 116–122.
58 H. Xu, N. Du, Y. Song, S. Song and W. Hou, *J. Colloid Interface Sci.,* 2018, **509**, 265-274.
59 M. Frindi, B. Michels and R. Zana, *J. Phys. Chem.,* 1991, **95**, 4832-4837.
60 O. Regev and R. Zana*, J. Colloid Interface Sci.,* 1999, **210**, 8-17.
61 E. D. Goddard, N. J. Turro and P. L. Kuo, *Langmuir*, 1985, **2**, 352-355.
62 C. G. Liu, K. G. H. Desai, X. G. Chen and H. J. Park, *J. Agric. Food Chem.,* 2005, **53**, 437-441.
63 X. Dong and C. Liu, *J. Nanomat.,* 2010, Article ID 906936.
64 T. Yoshimura, T. Ichinokawa, M. Kaji and K. Esumi, *Colloids Surf. A: Physicochem. Eng. Aspects,* 2006, **273**, 208-212.
65 T. Sakai, R. Ikoshi, N. Toshida and M. Kagaya, *J. Phys. Chem. B,* 2013, **117**, 5081-5089.
66 Y. You, J. Zhao, R. Jiang and J. Cao, *Colloid Polym. Sci.,* 2009, **287**, 839-846.
67 L. Piñeiro, M. Novo and W. Al-Souf, *Adv. Colloid Interface Sci.*, 2015, **205**, 1-12.
68 P. Drücker, A. Rühling, D. Grill, D. Wang, A. Draeger, V. Gerke, F. Glorius and H. J. Galla, *Langmuir*, 2017, **33**, 1333−1342.

Please do not adjust margins

Structure−Antitumor Activity Relationships of Tripodal Imidazolium-amino acid based ionic liquids. Effect of the Nature of the Amino Acid, Amide Substitution and Anion

Adriana Valls,[a] Belén Altava,[a] Laura Conesa,[a] Eva Falomir,[a] Eduardo García-Verdugo,[a] Santiago Vicente Luis,[a] Roberto Quesada,[b] Israel Carreira-Barral,[b] Vladimir Aseyev[c]

[a] Department of Inorganic and Organic Chemistry, ESTCE, University Jaume I, Av. Sos Baynat, s/n, 12004, Castellón, Spain. E-mail: altava@uji.es, luiss@uji.es
[b] Department of Chemistry, Faculty of Science, Burgos University, 09001 Burgos, Spain
[c] Department of Chemistry, University of Helsinki, P.O. Box 55 (A413, A. I. Virtasen aukio 1), FIN-00014 HY Helsinki, Finland

Index.

1) Microscopic appearance of A549 cell line

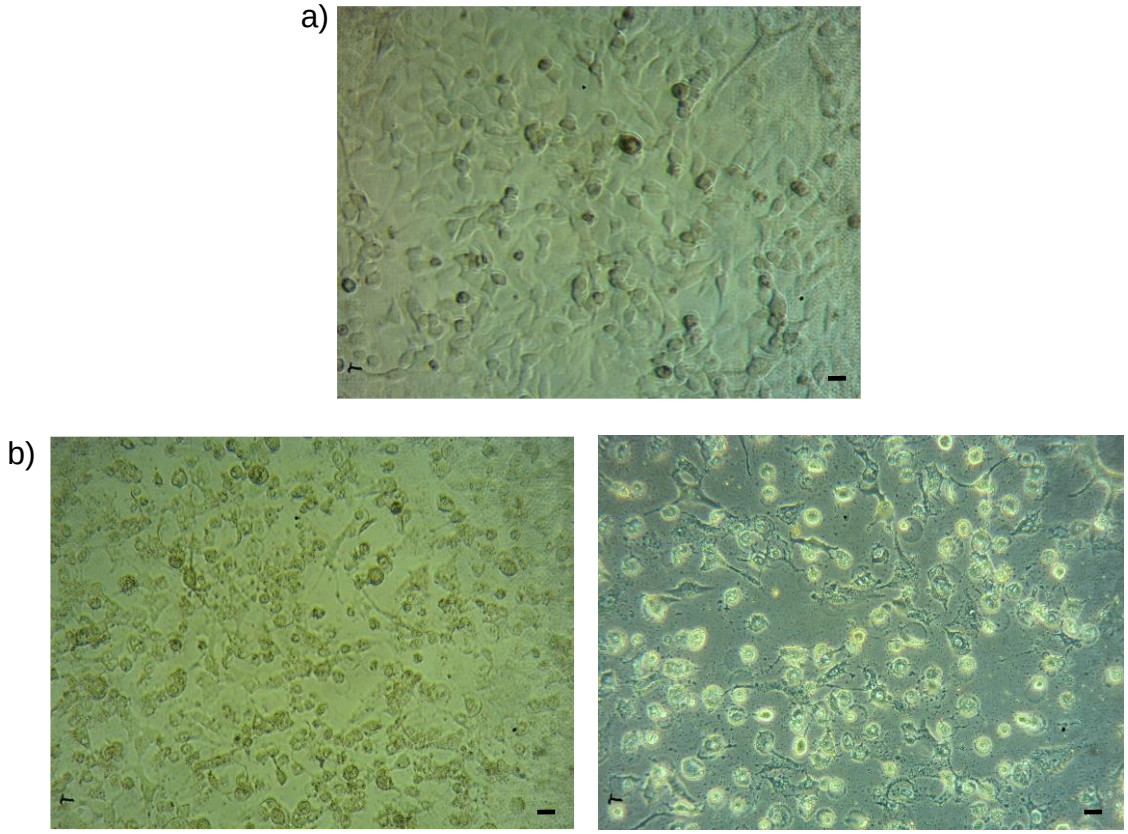

Figure S1. Microscopic appearance of A549 cell line in DMEM medium a) control; b) incubated with **7a-Br** (5 μM) at physiologic external pH, after 2 days under white and phase contrast (scale bar 10 μm).

2) Fluorescence experiments

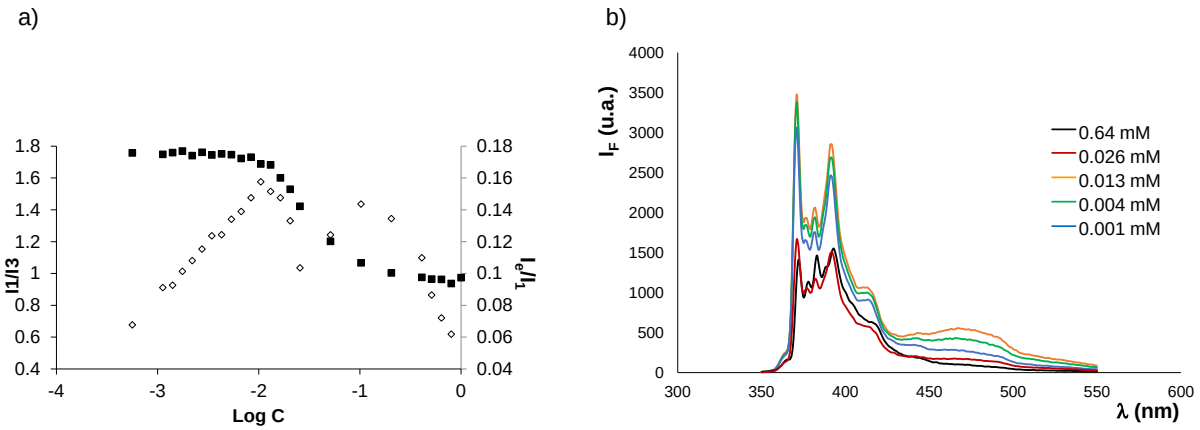

Figure S2. a) Plot of polarity ratio I_1/I_3 (orange, left axes) and Ie/I_1 (blue, right axes) *vs* log C (mM) for **3b-Br** in H_2O at 25 ºC, b) Emission spectra of pyrene in H_2O in the presence of different amounts of **3b-Br**.

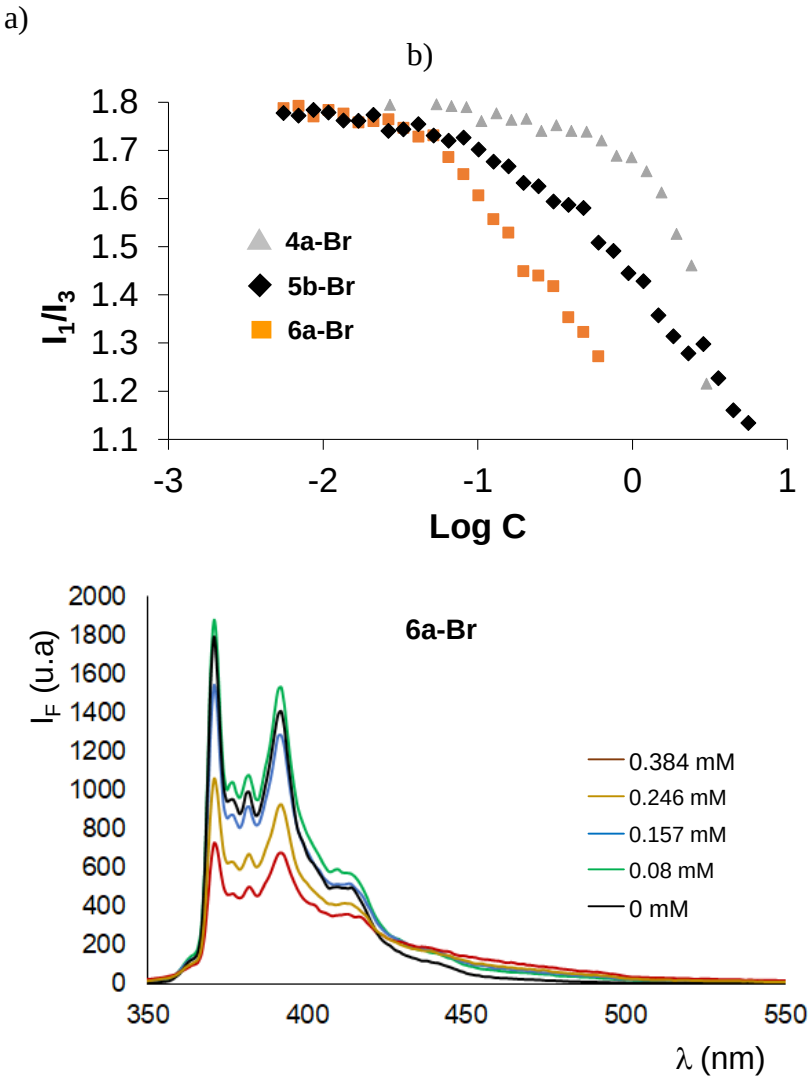

Figure S3. a) Plot of polarity ratio I_1/I_3 *vs* log C (C mM) in H_2O at 25ºC for: **4a-Br**, **6a-Br** and **5b-Br.** b) Emission spectra of pyrene in H_2O in the presence of different amounts of **6a-Br**.

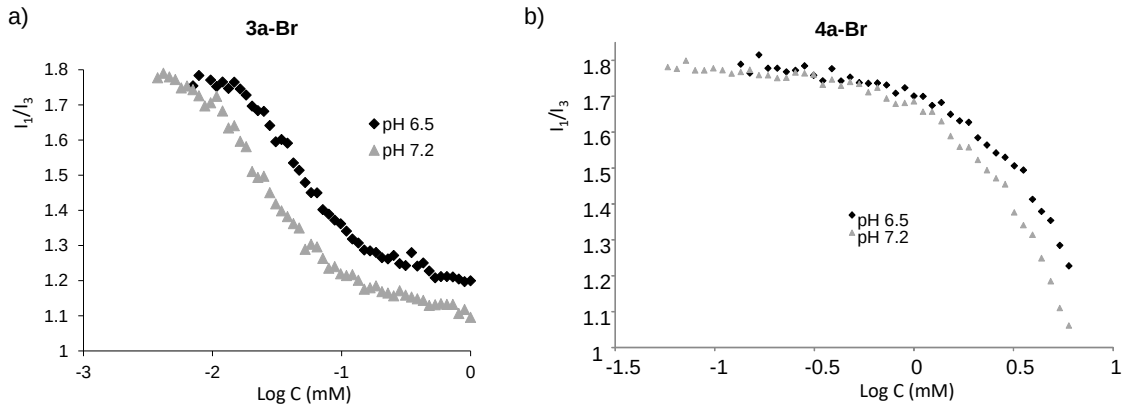

Figure S4. Plot of polarity ratio I_1/I_3 *vs* log C (C mM) in buffer at different pHs at 25 ºC for: a) **3a-Br** and b) **4a-Br**

3) ^{1}H NMR experiments for aggregation studies

a)

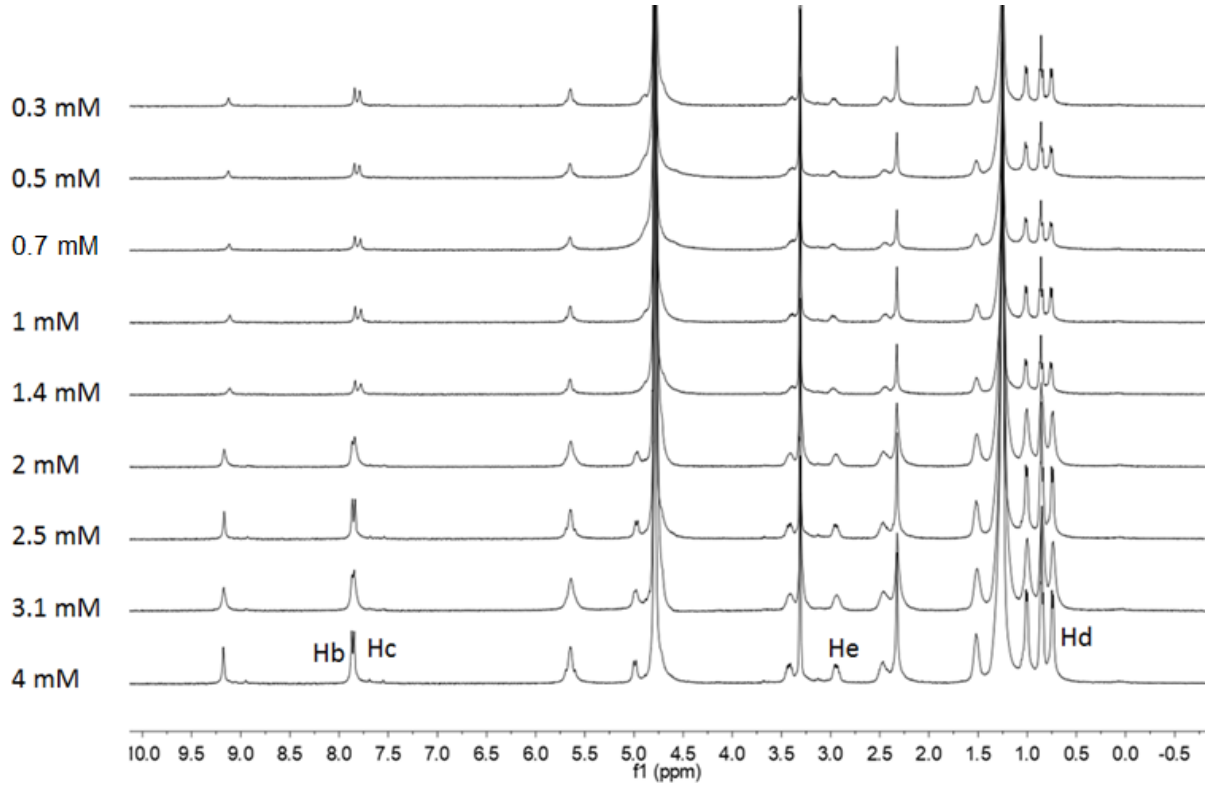

b)

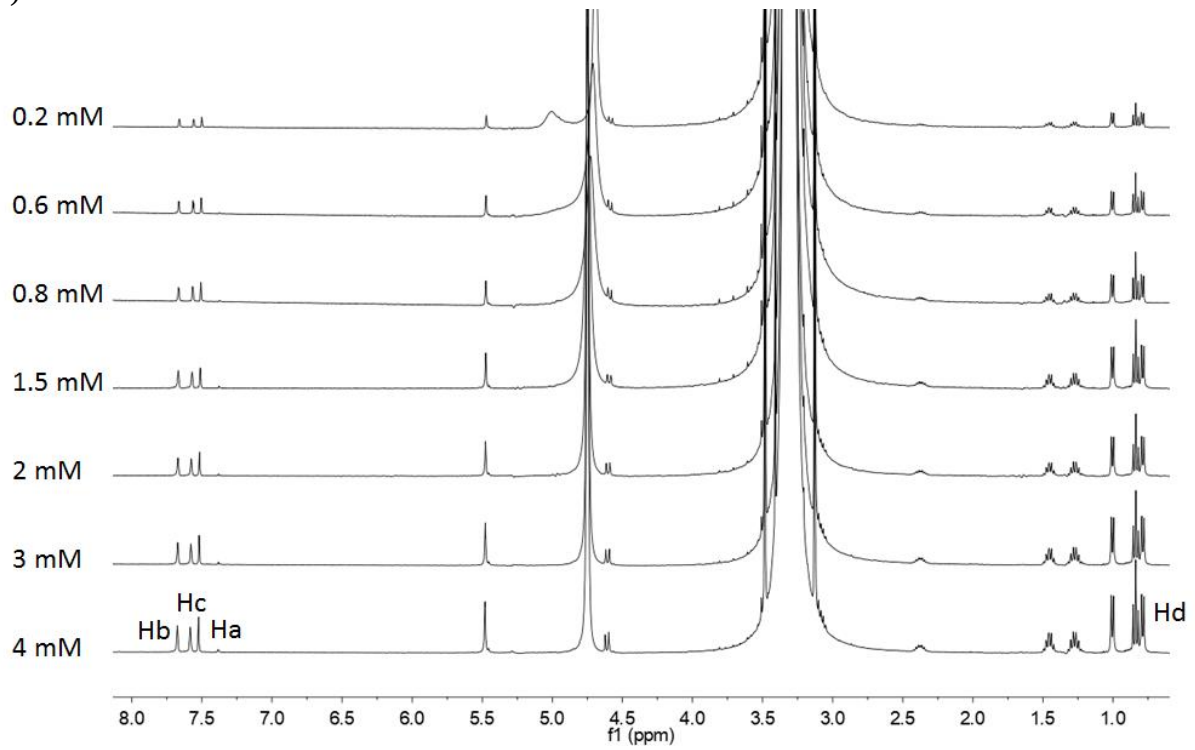

Figure S5 Partial 1H NMR of tripodal compounds at different concentrations in CD_3OD/D_2O 1/1 v/v (400 MHz): a) **3b-Br** b) **4a-Br**

4) **LS experiments**

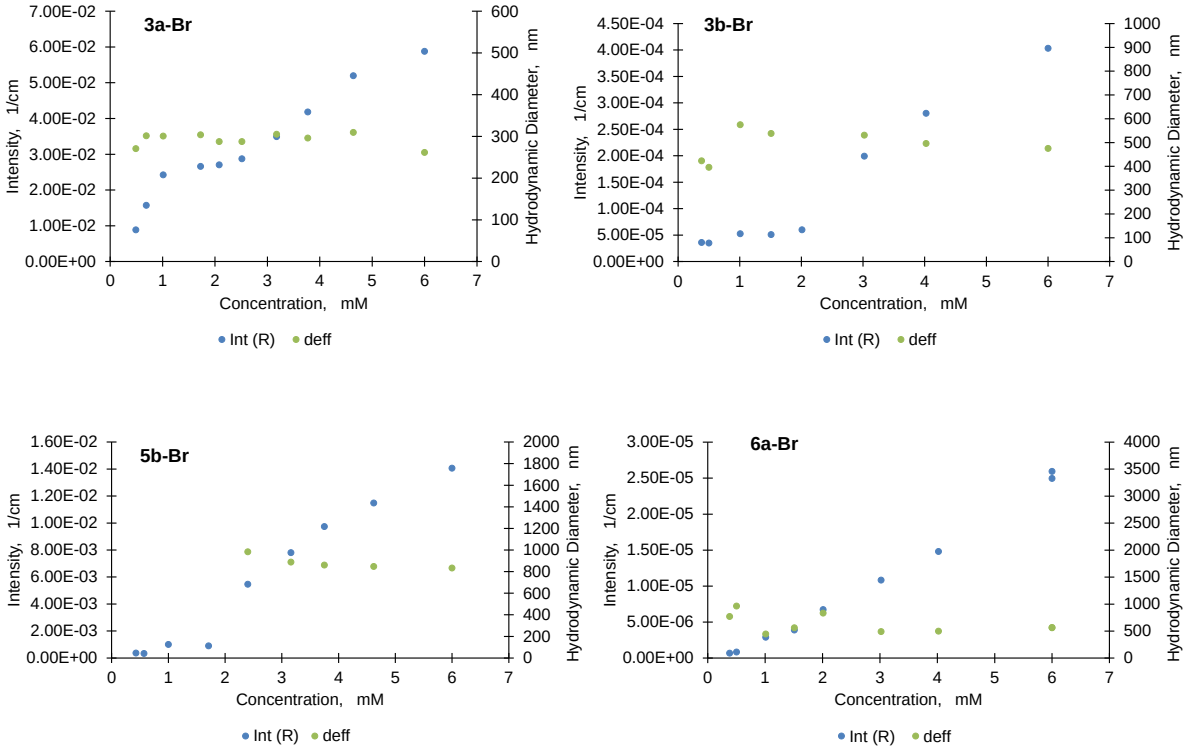

Figure S6. Hydrodynamic diameter (green circles, right axes) and intensity of the scattered light in absolute units ($1/cm^{-1}$) (blue circles, left axes) obtained with DLS for **3a-Br**, **3b-Br**, **5b-Br** and **6a-Br** in CH_3OH/H_2O (1/1 v/v) and presented as a function of the surfactant concentration.

5) Optical microcopy and SEM images

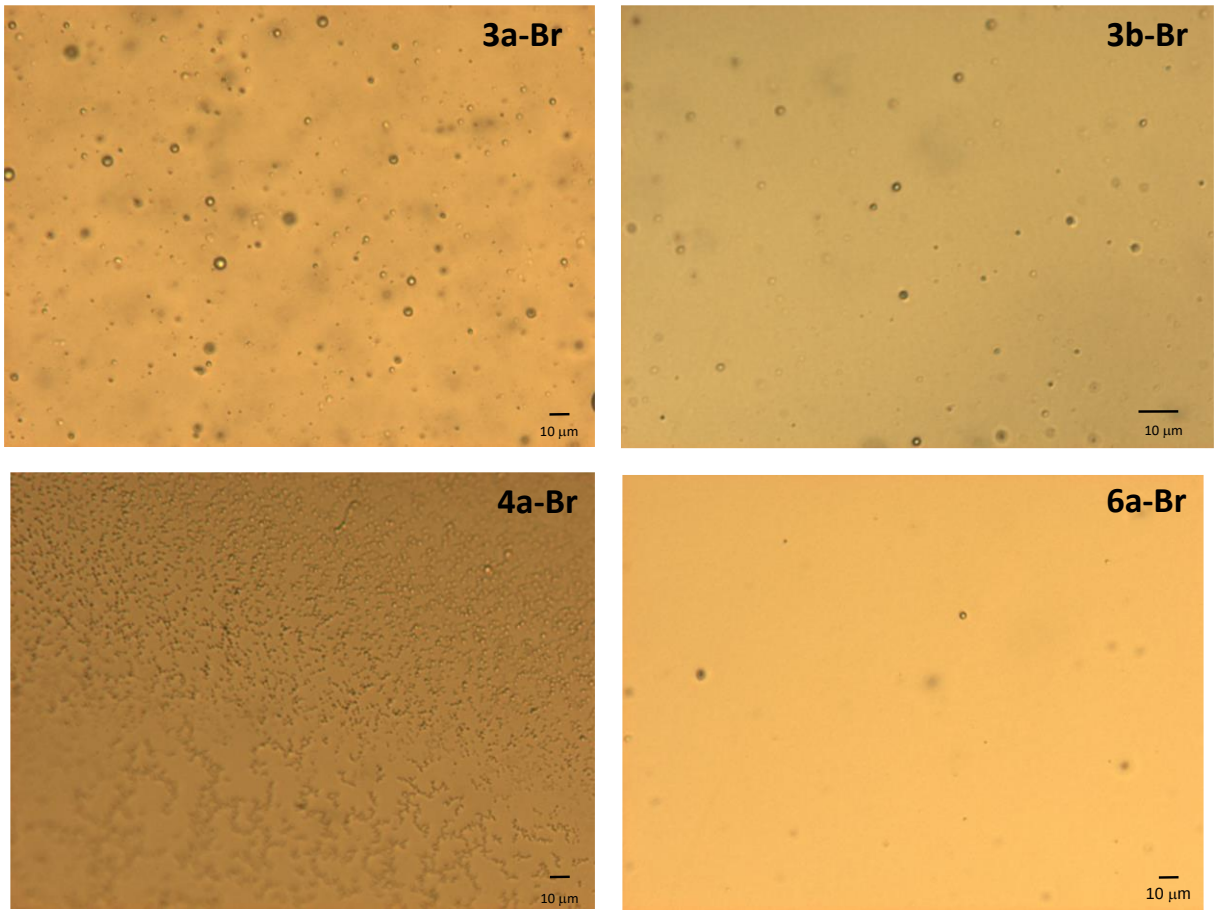

Figure S7. Optical microscopy images for some tripodal compounds (6 mM in H_2O/CH_3OH 1/1)

a)

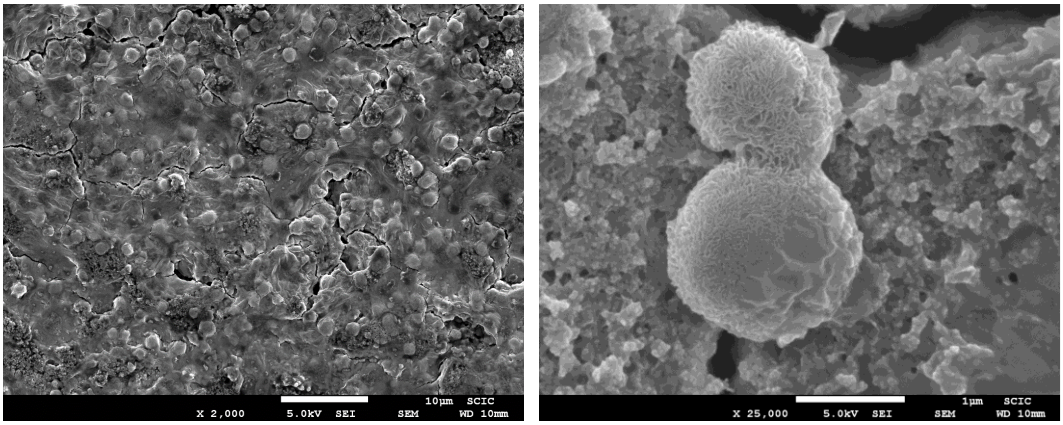

b)

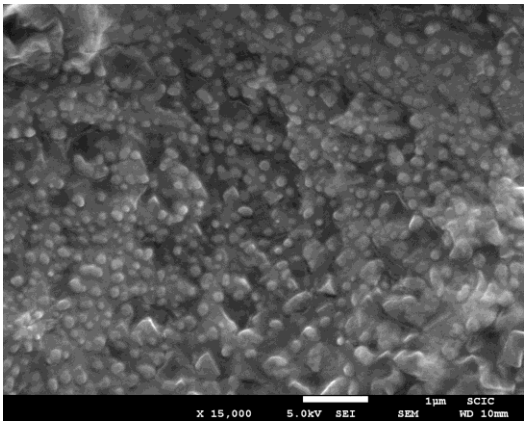

Figure S8. SEM images for some tripodal compounds in H_2O/CH_3OH 1/1: a) **3a-Br** and b) **6a-Br**

6) Chloride transport studies

Nitrate outside the vesicles

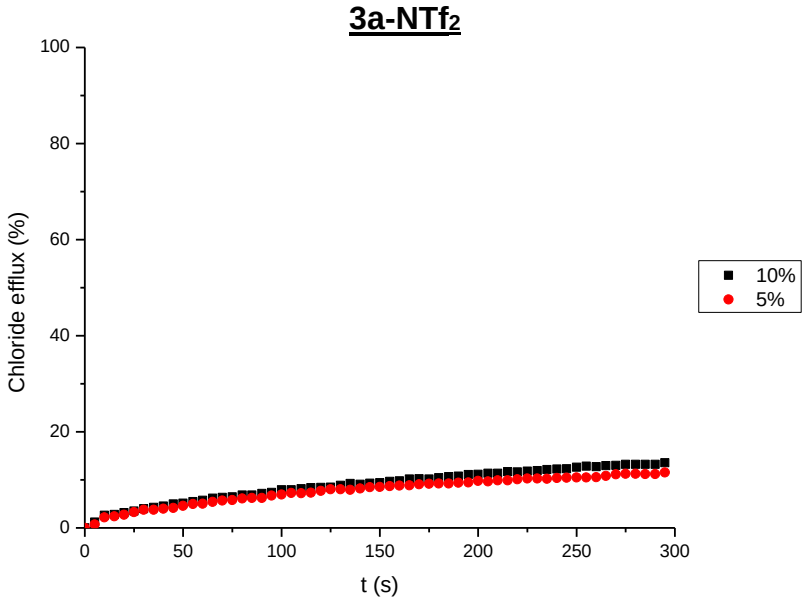

Figure S9. Chloride efflux promoted by **3a-NTf$_2$** (50 µM - 10%; 25 µM - 5% mol carrier to lipid concentration) in unilamellar POPC vesicles. Vesicles loaded with 489 mM NaCl were buffered at pH 7.2 with 5 mM phosphate and dispersed in 489 mM $NaNO_3$ buffered at pH 7.2. Each trace represents the average of at least three trials.

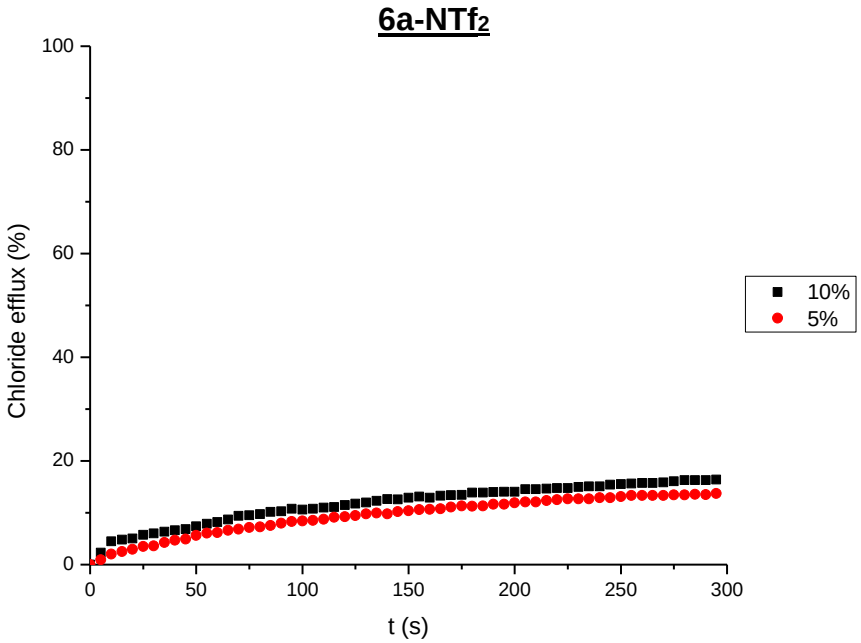

Figure S10. Chloride efflux promoted by **6a-NTf$_2$** (50 µM - 10%; 25 µM - 5% mol carrier to lipid concentration) in unilamellar POPC vesicles. Vesicles loaded with 489 mM NaCl were buffered at pH 7.2 with 5 mM phosphate and dispersed in 489 mM $NaNO_3$ buffered at pH 7.2. Each trace represents the average of at least three trials.

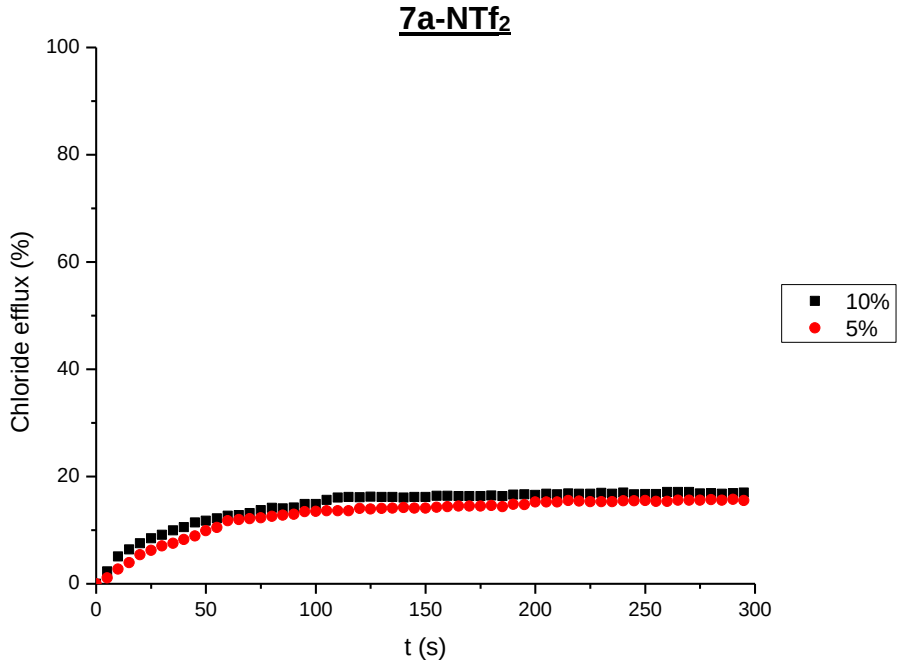

Figure S11. Chloride efflux promoted by **7a-NTf$_2$** (50 µM - 10%; 25 µM - 5% mol carrier to lipid concentration) in unilamellar POPC vesicles. Vesicles loaded with 489 mM NaCl were buffered at pH 7.2 with 5 mM phosphate and dispersed in 489 mM $NaNO_3$ buffered at pH 7.2. Each trace represents the average of at least three trials.

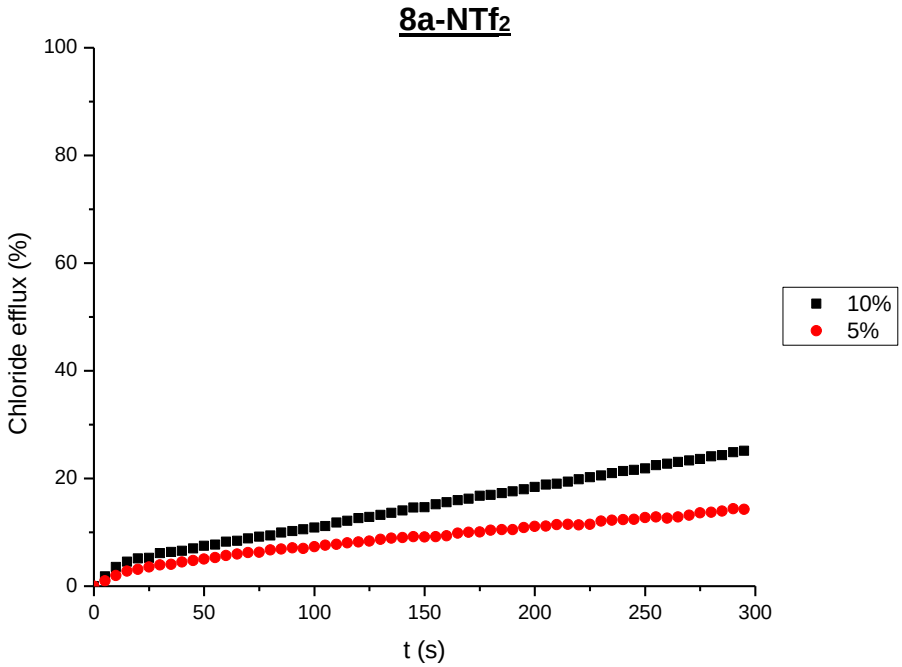

Figure S12. Chloride efflux promoted by **8a-NTf$_2$** (50 µM - 10%; 25 µM - 5% mol carrier to lipid concentration) in unilamellar POPC vesicles. Vesicles loaded with 489 mM NaCl were buffered at pH 7.2 with 5 mM phosphate and dispersed in 489 mM $NaNO_3$ buffered at pH 7.2. Each trace represents the average of at least three trials.

Sulfate and bicarbonate outside the vesicles

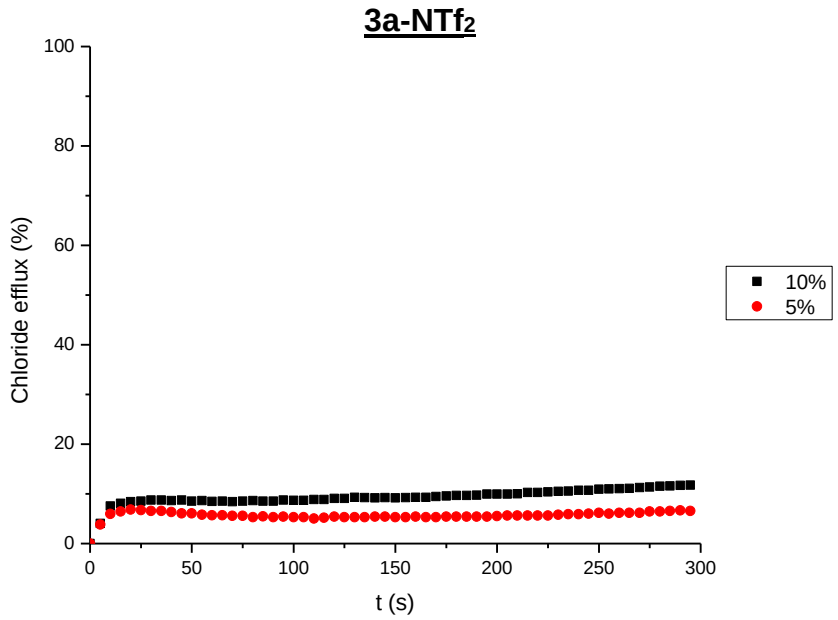

Figure S13. Chloride efflux promoted by **3a-NTf$_2$** (50 µM - 10%; 25 µM - 5% mol carrier to lipid concentration) in unilamellar POPC vesicles. The vesicles, which contained NaCl (451 mM NaCl and 20 mM phosphate buffer, pH 7.2), were immersed in Na_2SO_4 (150 mM Na_2SO_4, 40 mM HCO_3^- and 20 mM phosphate buffer, pH 7.2). Each trace represents an average of at least three different experiments.

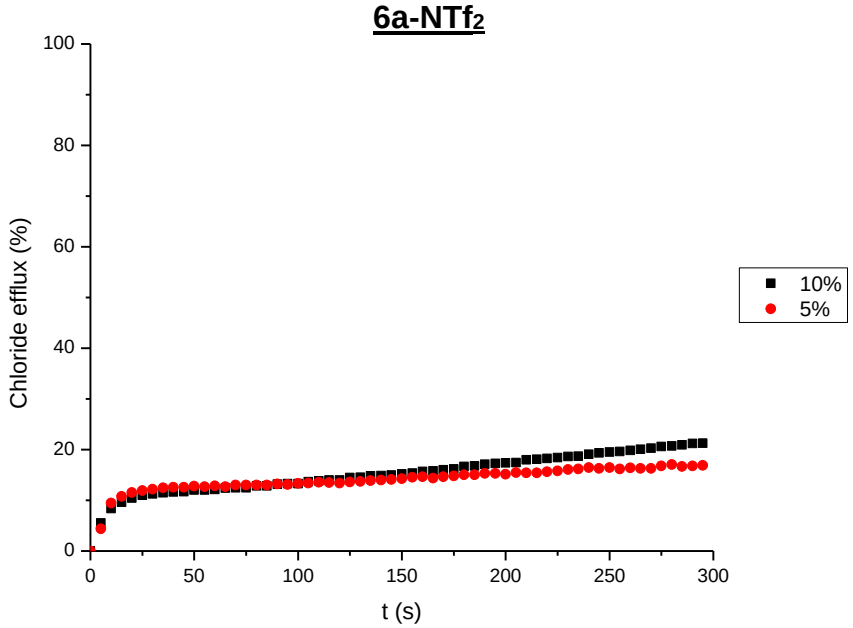

Figure S14. Chloride efflux promoted by **6a-NTf$_2$** (50 µM - 10%; 25 µM - 5% mol carrier to lipid concentration) in unilamellar POPC vesicles. The vesicles, which contained NaCl (451 mM NaCl and 20 mM phosphate buffer, pH 7.2), were immersed in Na_2SO_4 (150 mM Na_2SO_4, 40 mM HCO_3^- and 20 mM phosphate buffer, pH 7.2). Each trace represents an average of at least three different experiments.

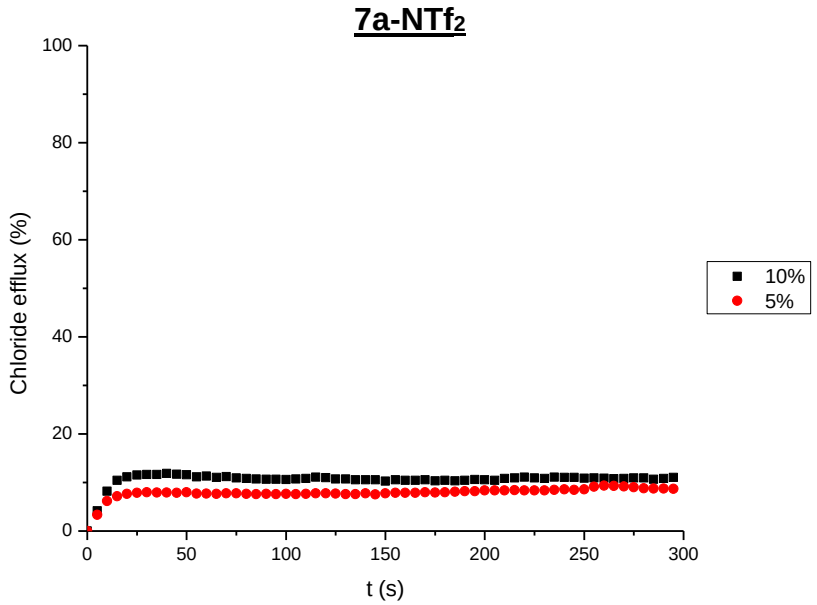

Figure S15. Chloride efflux promoted by **7a-NTf$_2$** (50 µM - 10%; 25 µM - 5% mol carrier to lipid concentration) in unilamellar POPC vesicles. The vesicles, which contained NaCl (451 mM NaCl and 20 mM phosphate buffer, pH 7.2), were immersed in Na_2SO_4 (150 mM Na_2SO_4, 40 mM HCO_3^- and 20 mM phosphate buffer, pH 7.2). Each trace represents an average of at least three different experiments.

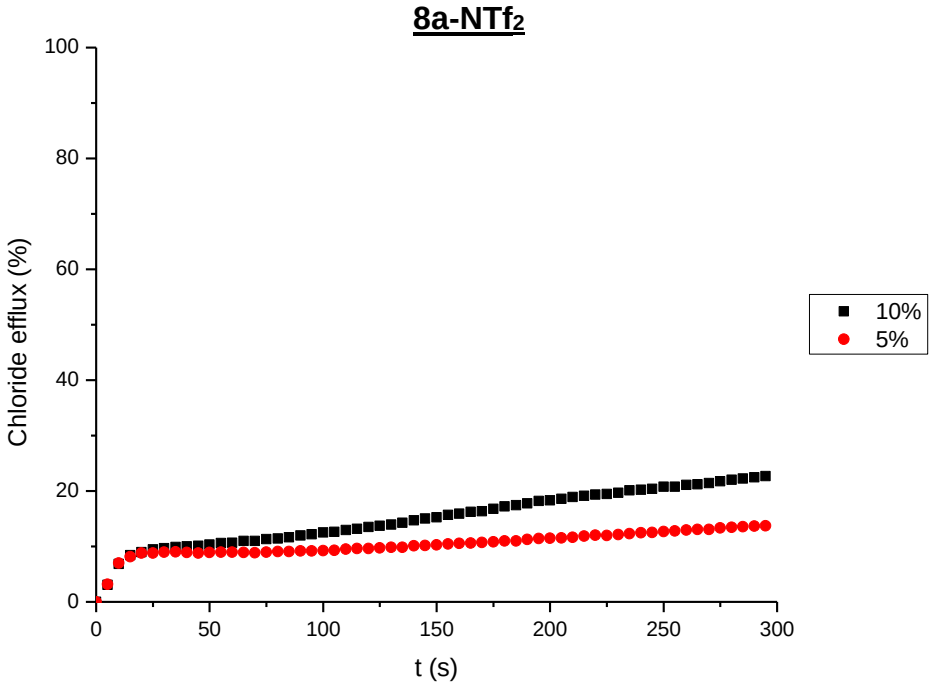

Figure S16. Chloride efflux promoted by **8a-NTf$_2$** (50 µM - 10%; 25 µM - 5% mol carrier to lipid concentration) in unilamellar POPC vesicles. The vesicles, which contained NaCl (451 mM NaCl and 20 mM phosphate buffer, pH 7.2), were immersed in Na_2SO_4 (150 mM Na_2SO_4, 40 mM HCO_3^- and 20 mM phosphate buffer, pH 7.2). Each trace represents an average of at least three different experiments.

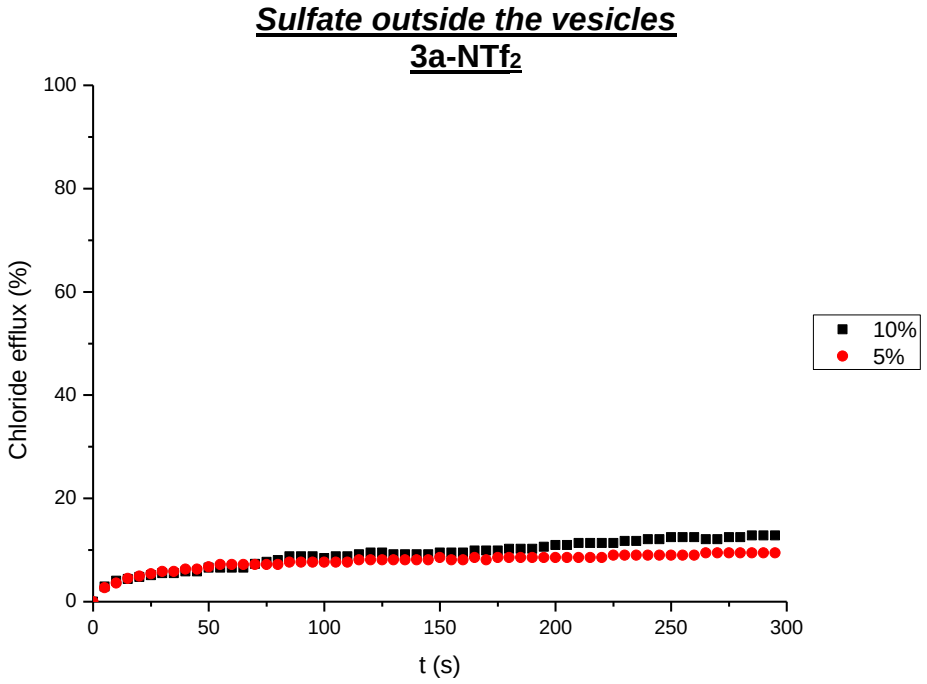

Figure S17. Chloride efflux promoted by **3a-NTf$_2$** (50 µM - 10%; 25 µM - 5% mol carrier to lipid concentration) in unilamellar POPC vesicles. The vesicles, which contained NaCl (451 mM NaCl and 20 mM phosphate buffer, pH 7.2), were immersed in Na_2SO_4 (150 mM Na_2SO_4 and 20 mM phosphate buffer, pH 7.2). Each trace corresponds to one experiment.

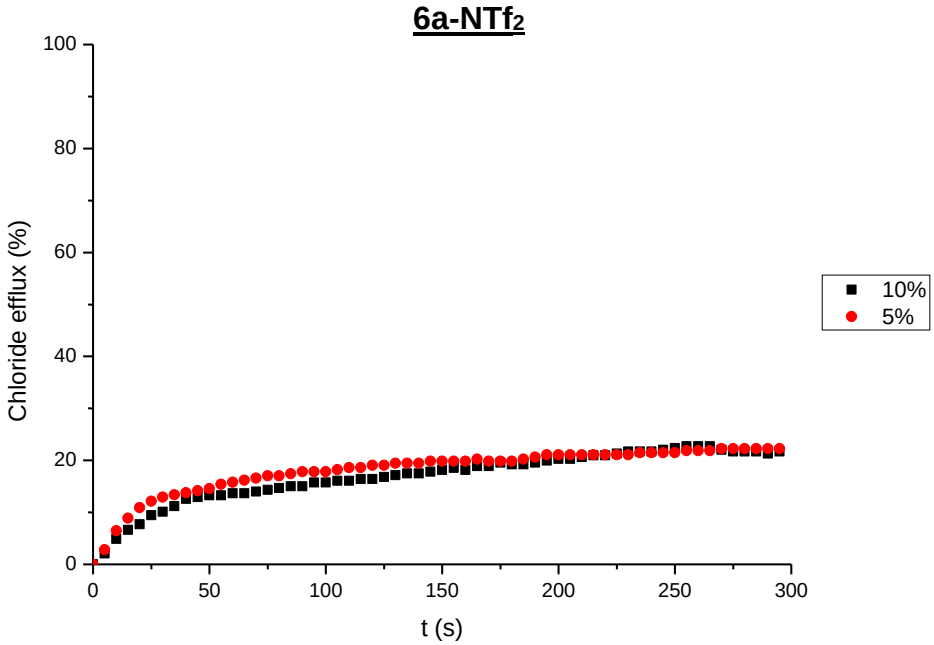

Figure S18. Chloride efflux promoted by **6a-NTf$_2$** (50 µM - 10%; 25 µM - 5% mol carrier to lipid concentration) in unilamellar POPC vesicles. The vesicles, which contained NaCl (451 mM NaCl and 20 mM phosphate buffer, pH 7.2), were immersed in Na_2SO_4 (150 mM Na_2SO_4 and 20 mM phosphate buffer, pH 7.2). Each trace corresponds to one experiment.

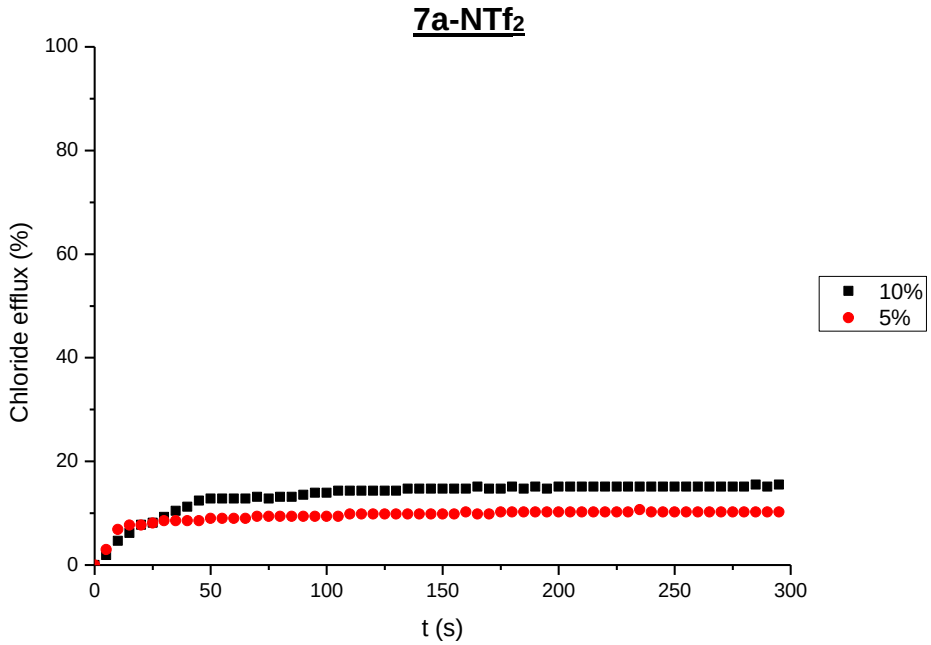

Figure S19. Chloride efflux promoted by **7a-NTf$_2$** (50 µM - 10%; 25 µM - 5% mol carrier to lipid concentration) in unilamellar POPC vesicles. The vesicles, which contained NaCl (451 mM NaCl and 20 mM phosphate buffer, pH 7.2), were immersed in Na_2SO_4 (150 mM Na_2SO_4 and 20 mM phosphate buffer, pH 7.2). Each trace corresponds to one experiment.

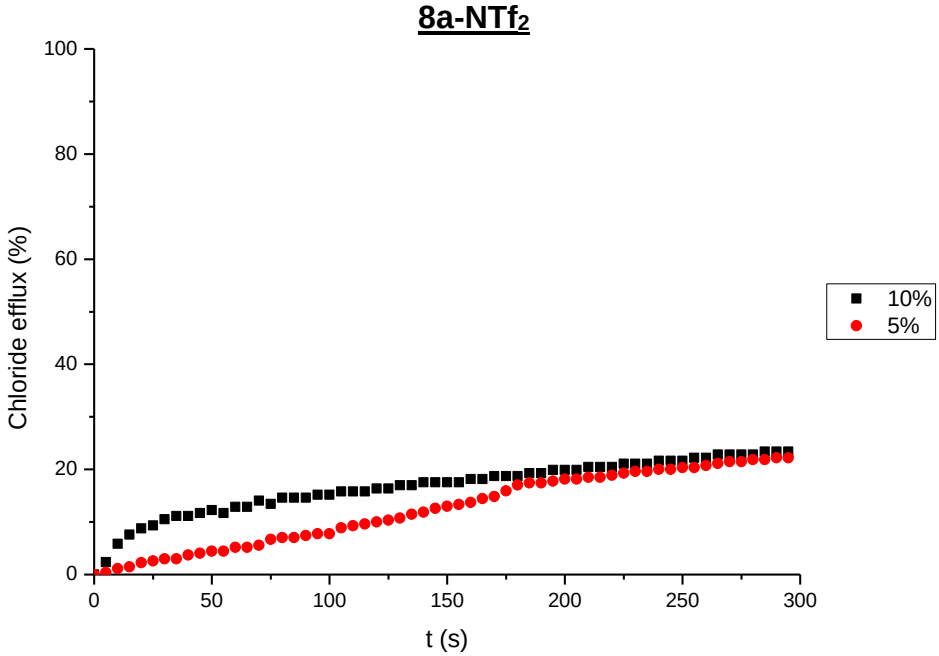

Figure S20. Chloride efflux promoted by **8a-NTf$_2$** (50 µM - 10%; 25 µM - 5% mol carrier to lipid concentration) in unilamellar POPC vesicles. The vesicles, which contained NaCl (451 mM NaCl and 20 mM phosphate buffer, pH 7.2), were immersed in Na_2SO_4 (150 mM Na_2SO_4 and 20 mM phosphate buffer, pH 7.2). Each trace corresponds to one experiment.

7) Chloride ^{1}H NMR titration experiments

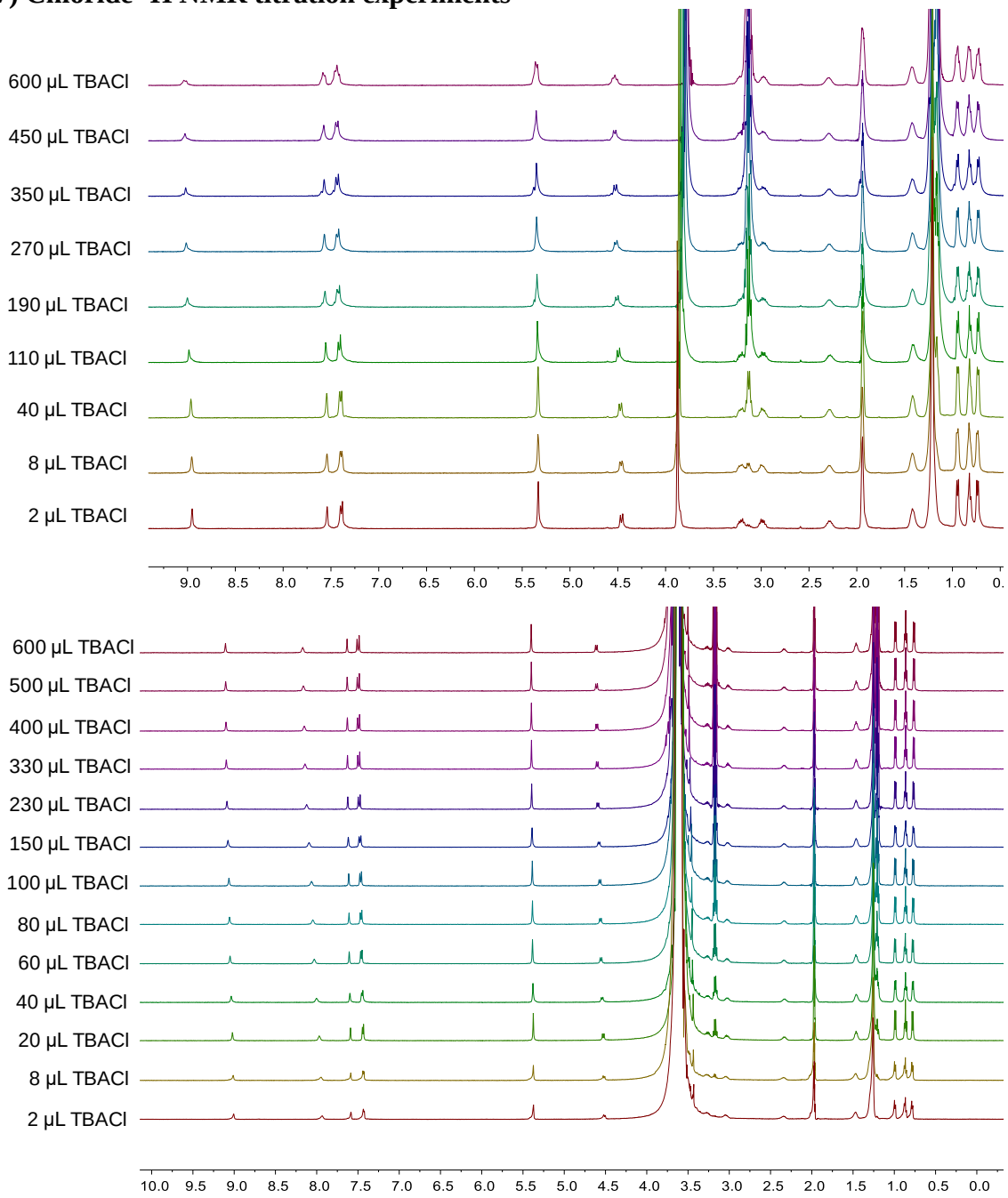

Figure S21. Partial ^{1}H NMR spectra (400 MHz, CD_3CN/D_2O 8/2) for **3a-NTf$_2$** (6 mM) obtained upon addition of different aliquots of a 60 mM solution of TBACl

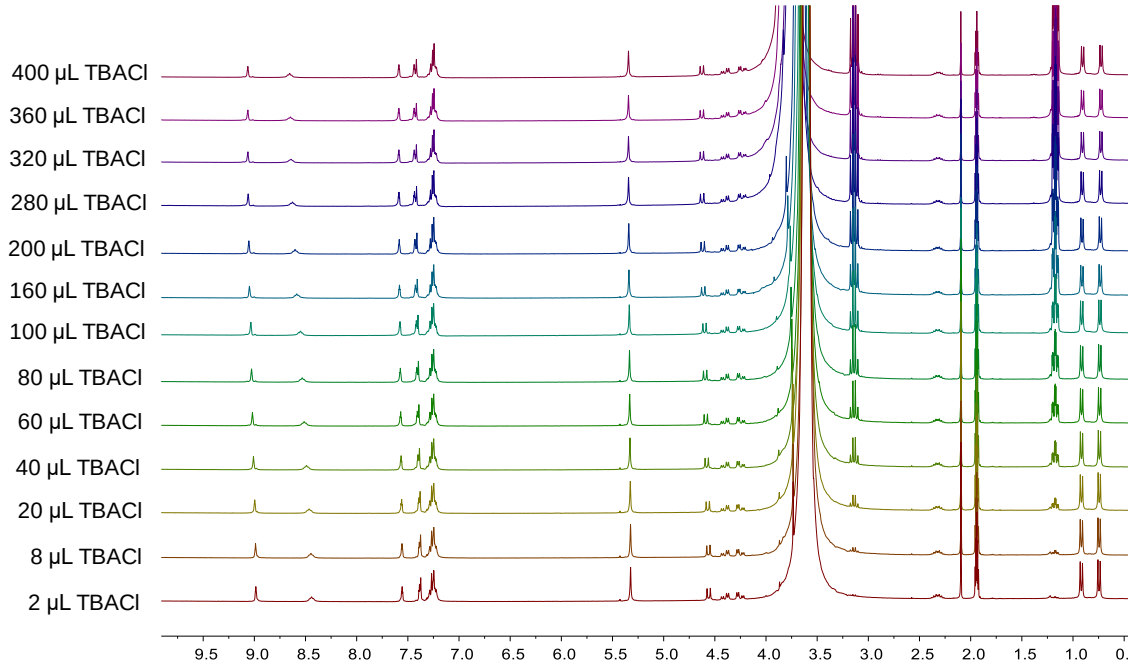

Figure S22. Partial ^{1}H NMR spectra (300 MHz, CD_3CN/D_2O 8/2) for **6a-NTf$_2$** (6 mM) obtained upon addition of different aliquots of a 60 mM solution of TBACl

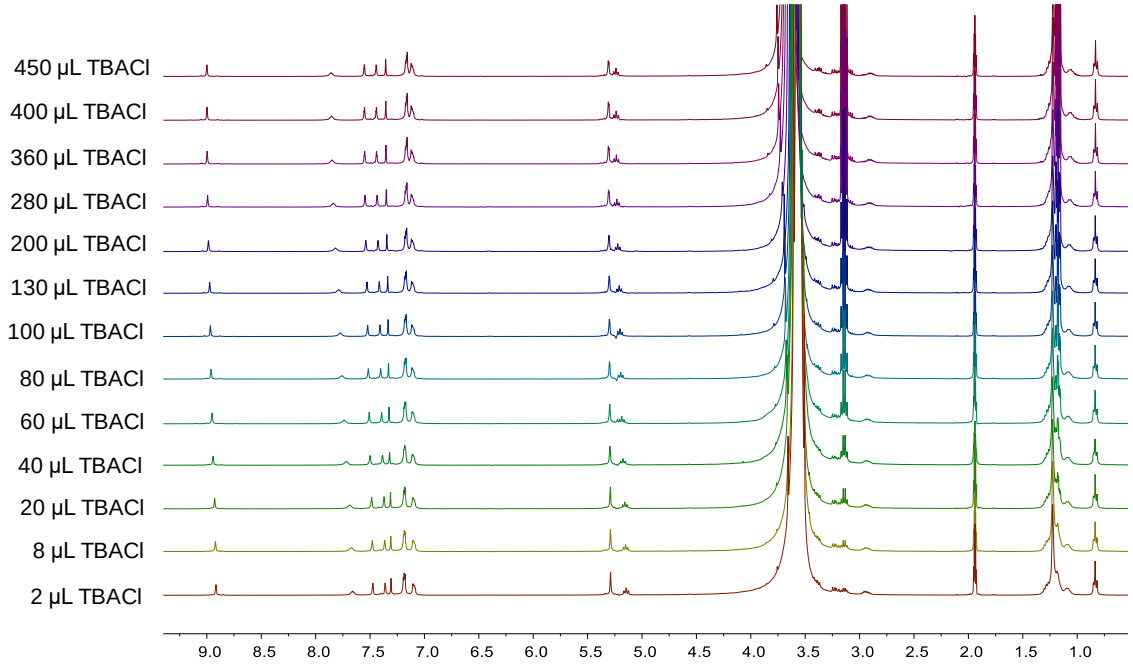

Figure S23. Partial ^{1}H NMR spectra (400 MHz, CD_3CN/D_2O 8/2) for **7a-NTf$_2$** (6 mM) obtained upon addition of different aliquots of a 60 mM solution of TBACl

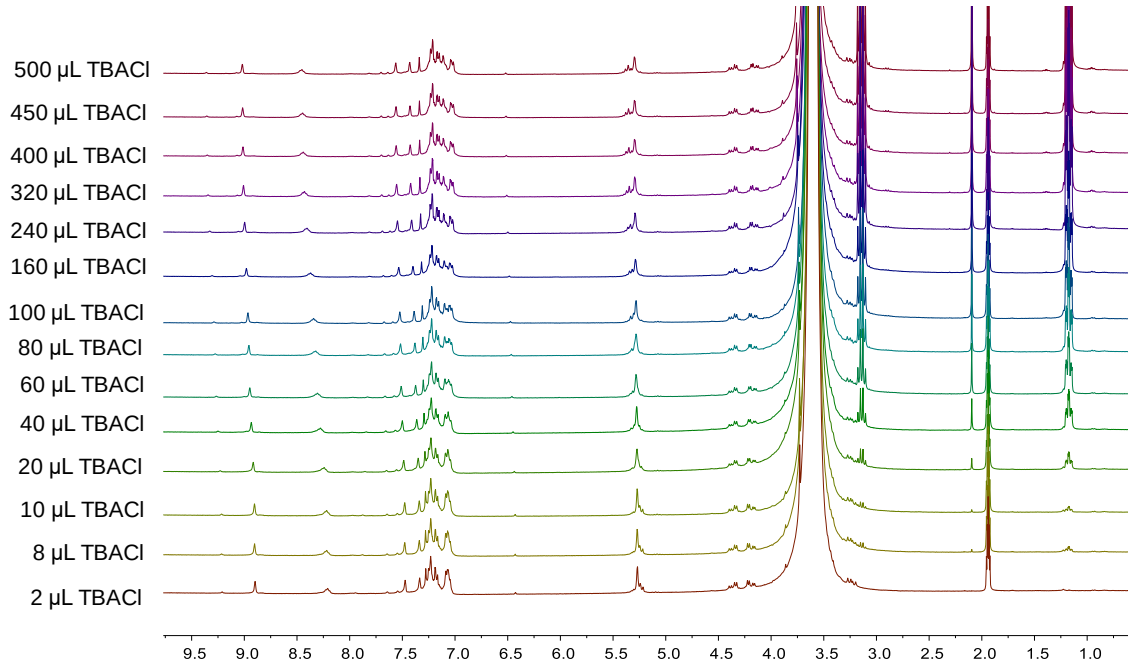

Figure S24. Partial ^{1}H NMR spectra (300 MHz, CD_3CN/D_2O 8/2) for **8a-NTf$_2$** (6 mM) obtained upon addition of different aliquots of a 60 mM solution of TBACl

8) Fitted binding isotherms

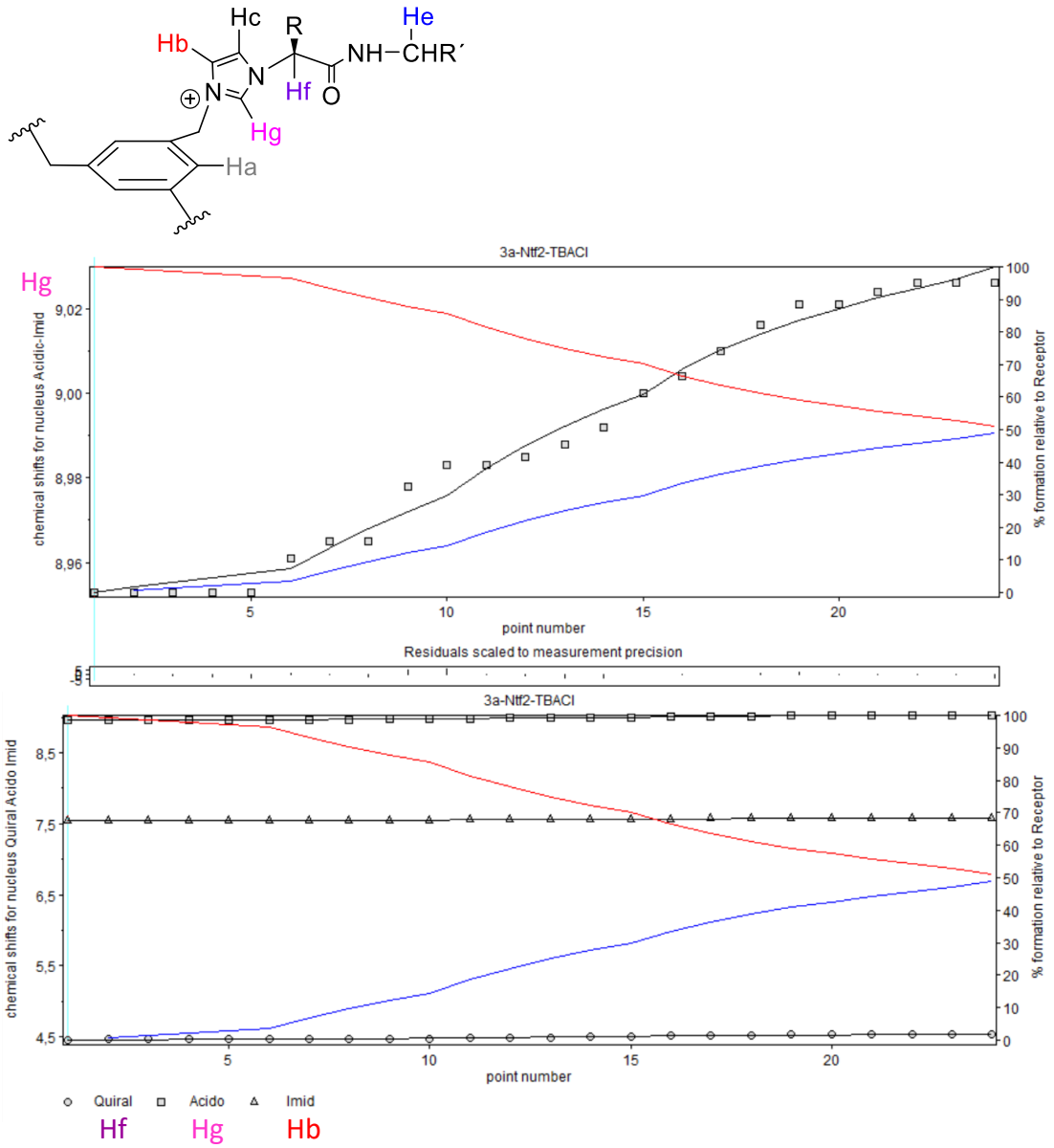

Figure S25. Fitted binding isotherms obtained for the titration of a 6 mM solution of compound **3a-NTf$_2$** with a 60 mM solution of TBACl (CD_3CN/D_2O 8/2). In order to avoid the dilution effect, the latter was prepared with the former. The graph shows the change in chemical shift of the signals corresponding to imidazolium H_g, H_f, H_b protons of the molecule, fitted to the 1:1 binding model.

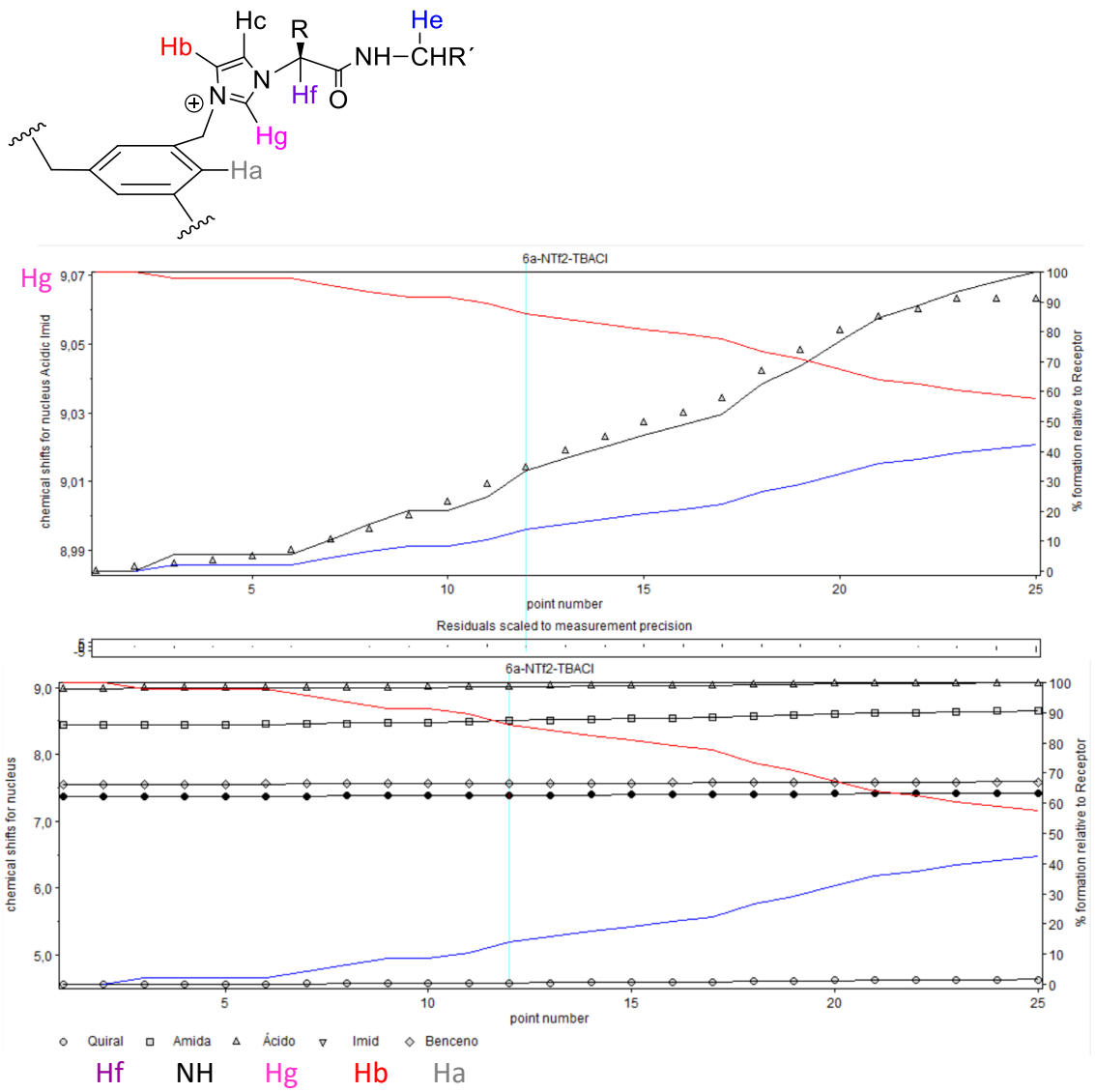

Figure S26. Fitted binding isotherms obtained for the titration of a 6 mM solution of compound **6a-NTf$_2$** with a 60 mM solution of TBACl (CD_3CN/D_2O 8/2). In order to avoid the dilution effect, the latter was prepared with the former. The graph shows the change in chemical shift of the signals corresponding to H_g, H_f, NH, H_b, H_a protons of the molecule, fitted to the 1:1 binding model.

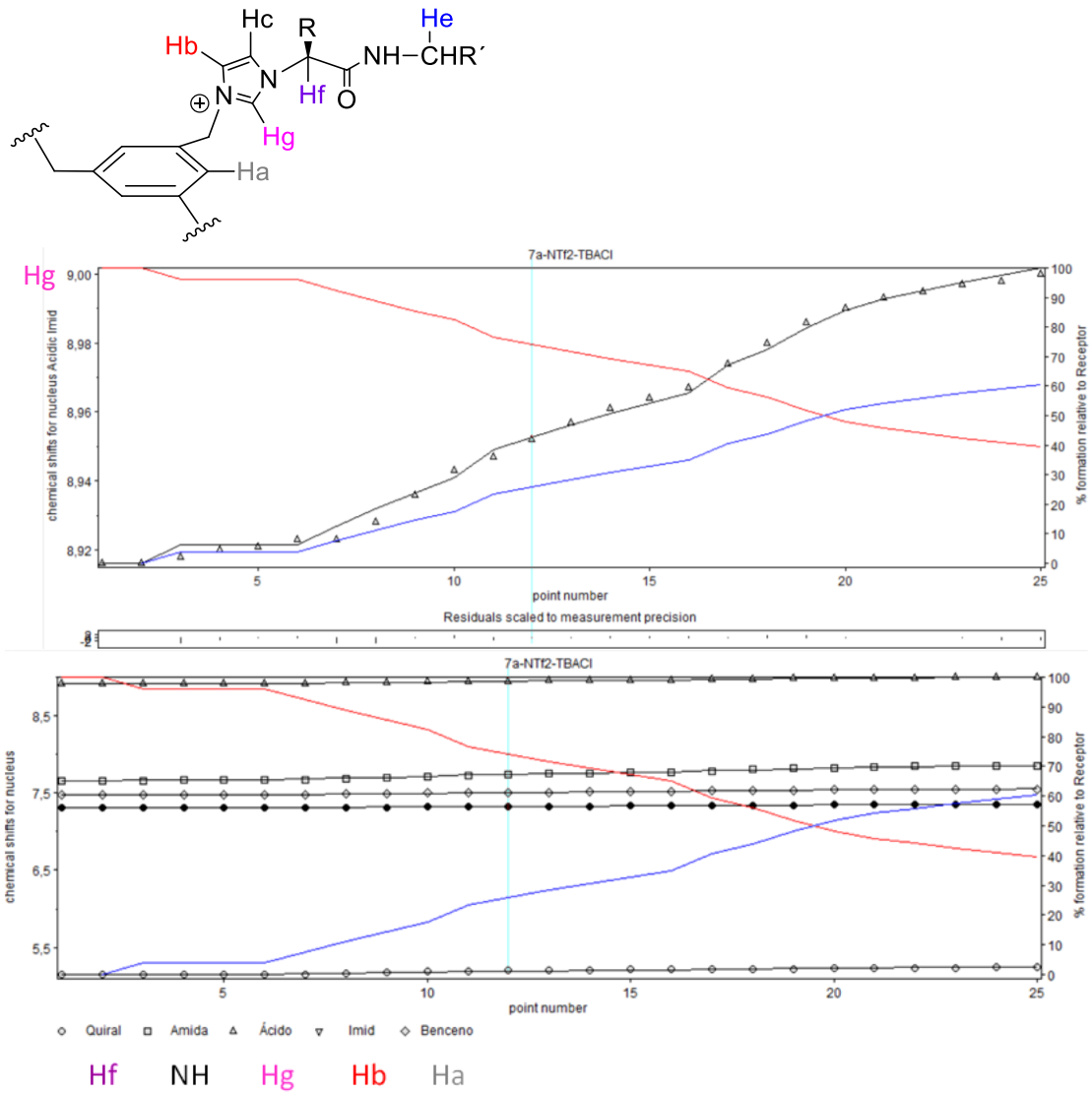

Figure S27. Fitted binding isotherms obtained for the titration of a 6 mM solution of compound **7a-NTf$_2$** with a 60 mM solution of TBACl (CD_3CN/D_2O 8/2). In order to avoid the dilution effect, the latter was prepared with the former. The graph shows the change in chemical shift of the signals corresponding to H_g, H_f, NH, H_b, H_a protons of the molecule, fitted to the 1:1 binding model.

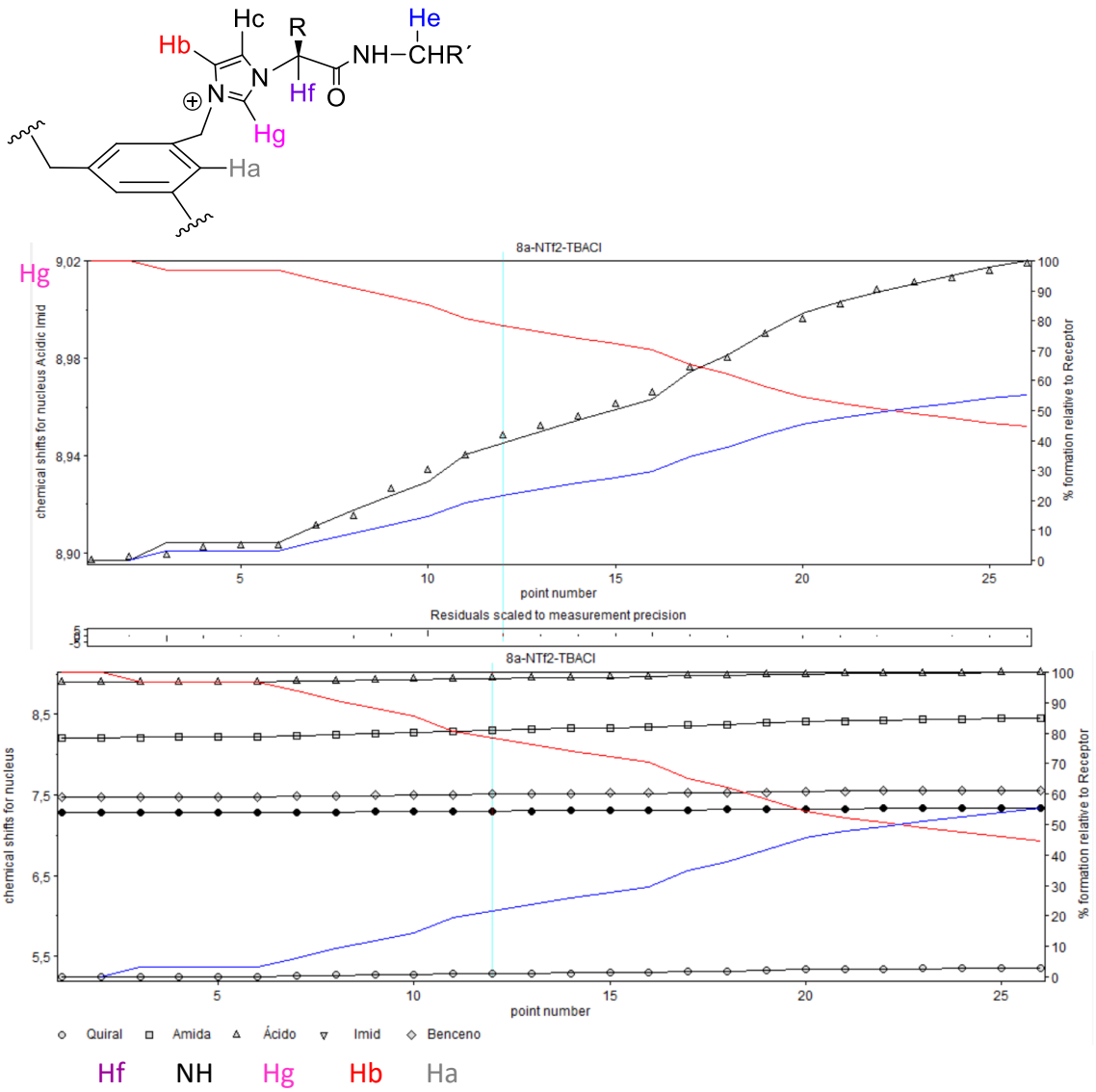

Figure S28. Fitted binding isotherms obtained for the titration of a 6 mM solution of compound **8a-NTf$_2$** with a 60 mM solution of TBACl (CD_3CN/D_2O 8/2). In order to avoid the dilution effect, the latter was prepared with the former. The graph shows the change in chemical shift of the signals corresponding to H_g, H_f, NH, H_b, H_a protons of the molecule, fitted to the 1:1 binding model.

9) Carboxyfluorescein transport studies

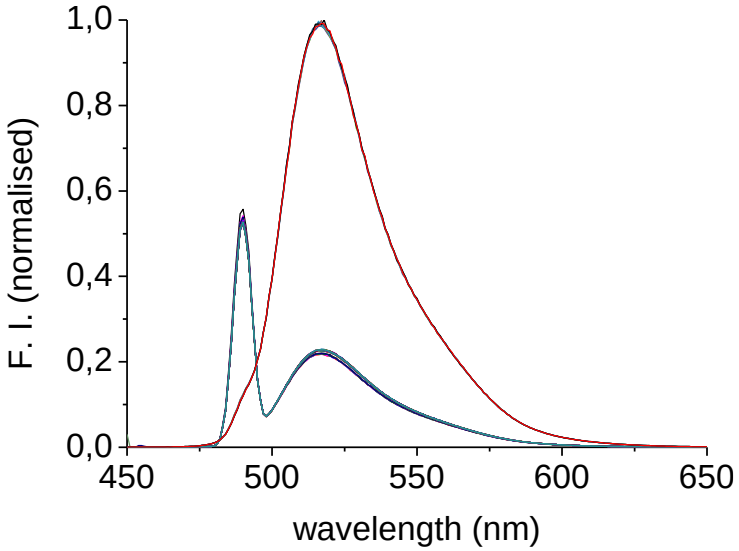

Figure S29. Carboxyfluorescein normalized fluorescence intensity recorded upon addition of **DMSO**, the blank, to POPC vesicles (0.05 mM). Vesicles (loaded with 451 mM NaCl buffered at pH 7.2 with 20 mM phosphate and containing 50 mM CF; I.S. 500 mM) were suspended in Na_2SO_4 (150 mM, buffered at pH 7.2 with 20 mM phosphate; I.S. 500 mM). At t = 60 s DMSO was added (10 μL), while at t = 360 s the detergent (20 μL) was added. Each spectrum represents the average of six trials, carried out with three different batches of vesicles.

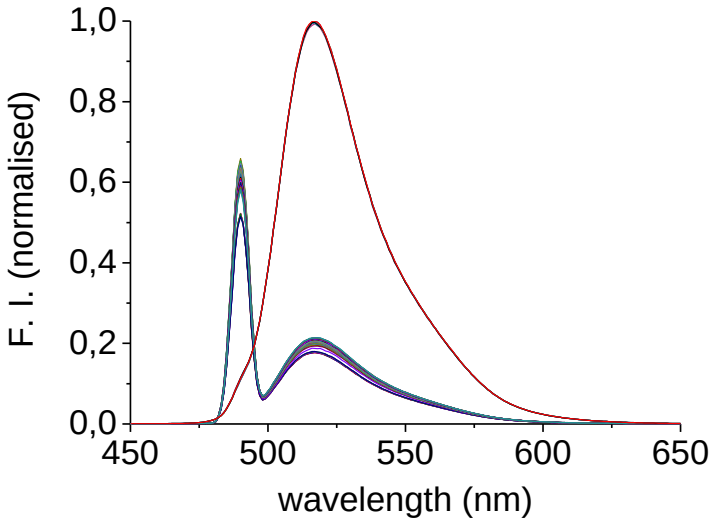

Figure S30. Carboxyfluorescein normalized fluorescence intensity recorded upon addition of **3a-NTf_2** to POPC vesicles (0.05 mM). Vesicles (loaded with 451 mM NaCl buffered at pH 7.2 with 20 mM phosphate, and containing 50 mM CF; I.S. 500 mM) were suspended in Na_2SO_4 (150 mM, buffered at pH 7.2 with 20 mM phosphate; I.S. 500 mM). At t = 60 s the compound was added (10% mol carrier to lipid), while at t = 360 s the detergent (20 μL) was added. Each spectrum represents the average of three trials.

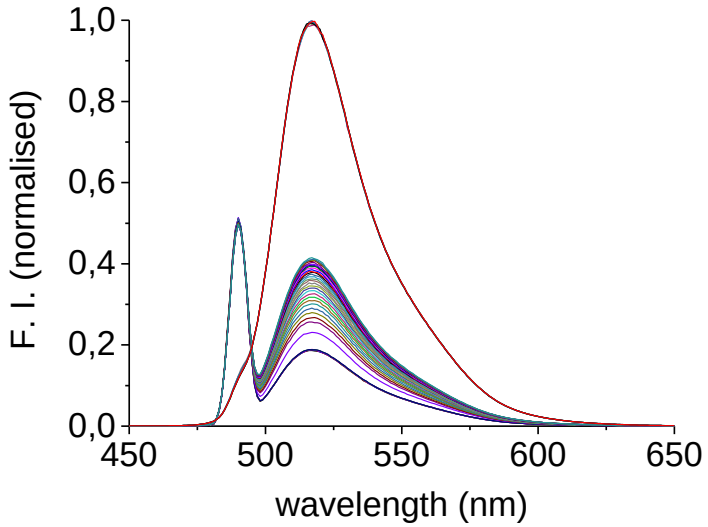

Figure S31. Carboxyfluorescein normalized fluorescence intensity recorded upon addition of **6a-NTf$_2$** to POPC vesicles (0.05 mM). Vesicles (loaded with 451 mM NaCl buffered at pH 7.2 with 20 mM phosphate, and containing 50 mM CF; I.S. 500 mM) were suspended in Na_2SO_4 (150 mM, buffered at pH 7.2 with 20 mM phosphate; I.S. 500 mM). At t = 60 s the compound was added (10% mol carrier to lipid), while at t = 360 s the detergent (20 μL) was added. Each spectrum represents the average of three trials.

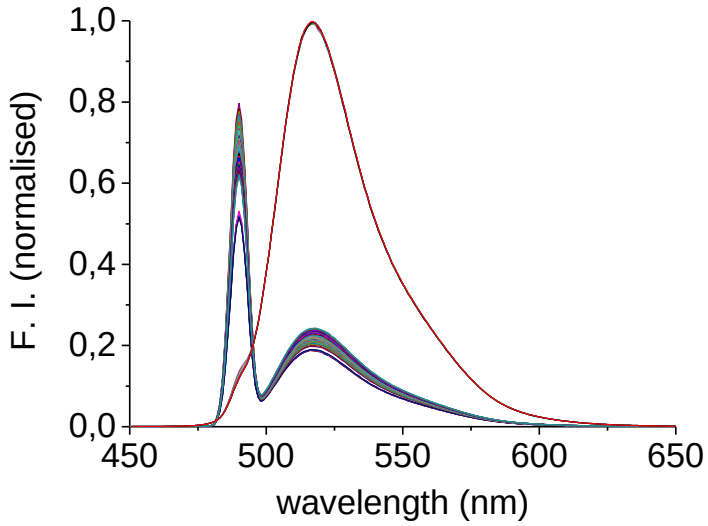

Figure S32. Carboxyfluorescein normalized fluorescence intensity recorded upon addition of **7a-NTf$_2$** to POPC vesicles (0.05 mM). Vesicles (loaded with 451 mM NaCl buffered at pH 7.2 with 20 mM phosphate, and containing 50 mM CF; I.S. 500 mM) were suspended in Na_2SO_4 (150 mM, buffered at pH 7.2 with 20 mM phosphate; I.S. 500 mM). At t = 60 s the compound was added (10% mol carrier to lipid), while at t = 360 s the detergent (20 μL) was added. Each spectrum represents the average of three trials.

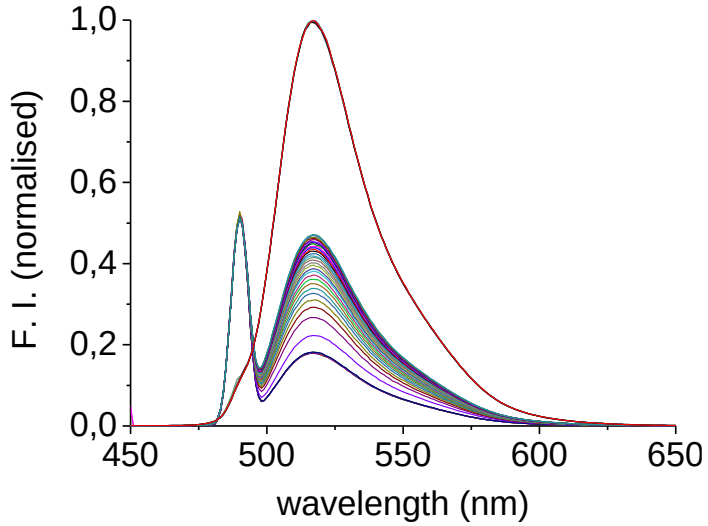

Figure S33. Carboxyfluorescein normalized fluorescence intensity recorded upon addition of **8a-NTf$_2$** to POPC vesicles (0.05 mM). Vesicles (loaded with 451 mM NaCl buffered at pH 7.2 with 20 mM phosphate, and containing 50 mM CF; I.S. 500 mM) were suspended in Na_2SO_4 (150 mM, buffered at pH 7.2 with 20 mM phosphate; I.S. 500 mM). At t = 60 s the compound was added (10% mol carrier to lipid), while at t = 360 s the detergent (20 μL) was added. Each spectrum represents the average of three trials.

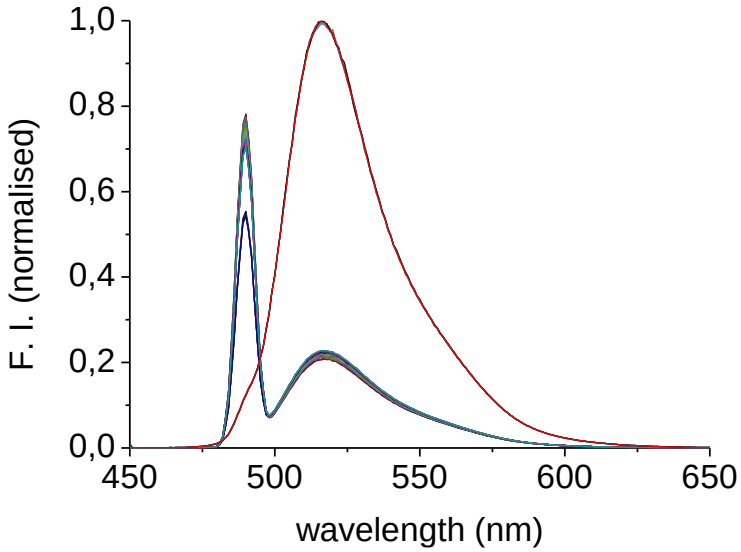

Figure S34. Carboxyfluorescein normalized fluorescence intensity recorded upon addition of **3a-Br** to POPC vesicles (0.05 mM). Vesicles (loaded with 451 mM NaCl buffered at pH 7.2 with 20 mM phosphate and containing 50 mM CF; I.S. 500 mM) were suspended in Na_2SO_4 (150 mM, buffered at pH 7.2 with 20 mM phosphate; I.S. 500 mM). At t = 60 s the compound was added (10% mol carrier to lipid), while at t = 360 s the detergent (20 μL) was added. Each spectrum represents the average of six trials, carried out with three different batches of vesicles.

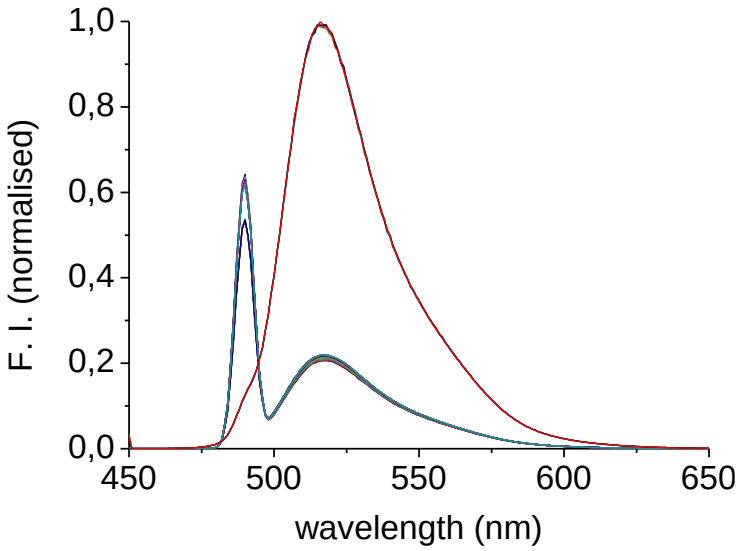

Figure S35. Carboxyfluorescein normalized fluorescence intensity recorded upon addition of **3b-Br** to POPC vesicles (0.05 mM). Vesicles (loaded with 451 mM NaCl buffered at pH 7.2 with 20 mM phosphate and containing 50 mM CF; I.S. 500 mM) were suspended in Na_2SO_4 (150 mM, buffered at pH 7.2 with 20 mM phosphate; I.S. 500 mM). At t = 60 s the compound was added (10% mol carrier to lipid), while at t = 360 s the detergent (20 μL) was added. Each spectrum represents the average of six trials, carried out with three different batches of vesicles.

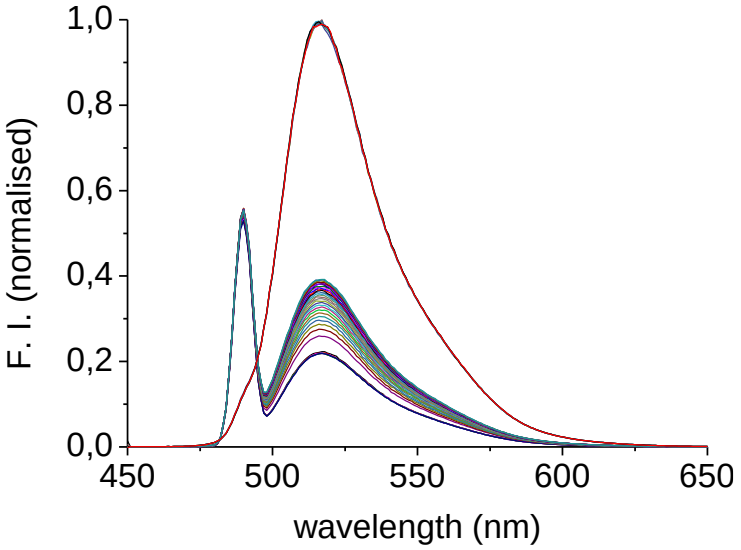

Figure S36. Carboxyfluorescein normalized fluorescence intensity recorded upon addition of **4a-Br** to POPC vesicles (0.05 mM). Vesicles (loaded with 451 mM NaCl buffered at pH 7.2 with 20 mM phosphate and containing 50 mM CF; I.S. 500 mM) were suspended in Na_2SO_4 (150 mM, buffered at pH 7.2 with 20 mM phosphate; I.S. 500 mM). At t = 60 s the compound was added (10% mol carrier to lipid), while at t = 360 s the detergent (20 μL) was added. Each spectrum represents the average of six trials, carried out with three different batches of vesicles.

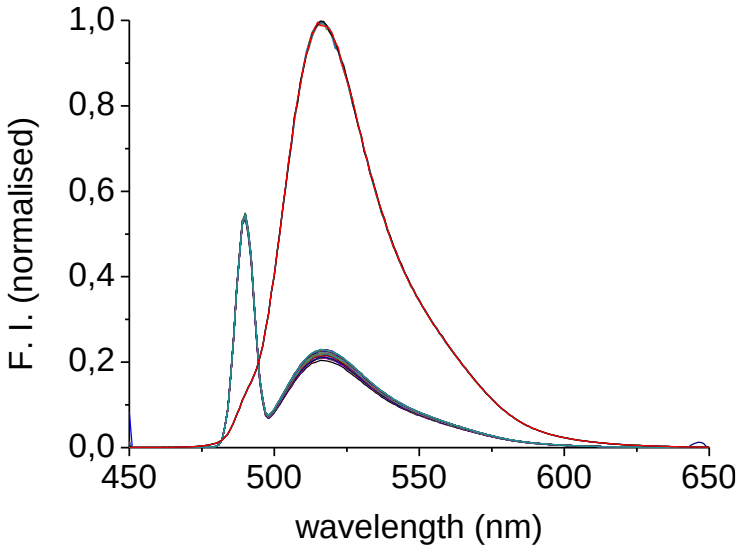

Figure S37. Carboxyfluorescein normalized fluorescence intensity recorded upon addition of **5a-Br** to POPC vesicles (0.05 mM). Vesicles (loaded with 451 mM NaCl buffered at pH 7.2 with 20 mM phosphate and containing 50 mM CF; I.S. 500 mM) were suspended in Na_2SO_4 (150 mM, buffered at pH 7.2 with 20 mM phosphate; I.S. 500 mM). At t = 60 s the compound was added (10% mol carrier to lipid), while at t = 360 s the detergent (20 μL) was added. Each spectrum represents the average of six trials, carried out with three different batches of vesicles.

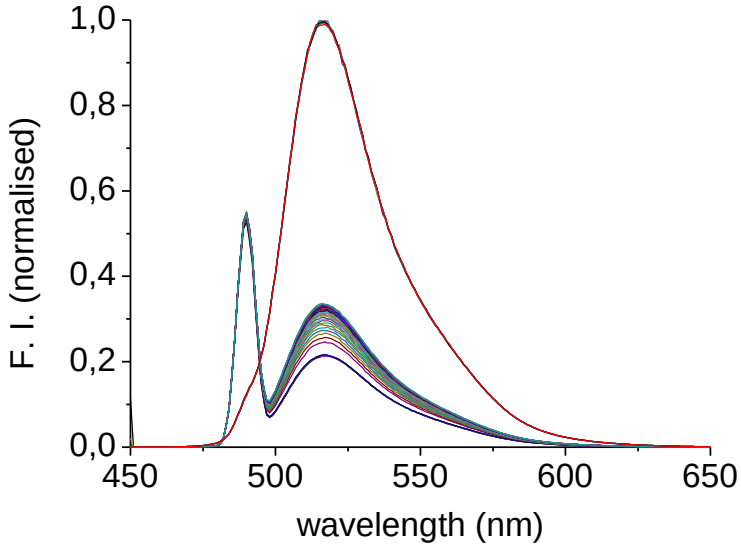

Figure S38. Carboxyfluorescein normalized fluorescence intensity recorded upon addition of **6a-Br** to POPC vesicles (0.05 mM). Vesicles (loaded with 451 mM NaCl buffered at pH 7.2 with 20 mM phosphate and containing 50 mM CF; I.S. 500 mM) were suspended in Na_2SO_4 (150 mM, buffered at pH 7.2 with 20 mM phosphate; I.S. 500 mM). At t = 60 s the compound was added (10% mol carrier to lipid), while at t = 360 s the detergent (20 μL) was added. Each spectrum represents the average of six trials, carried out with three different batches of vesicles.

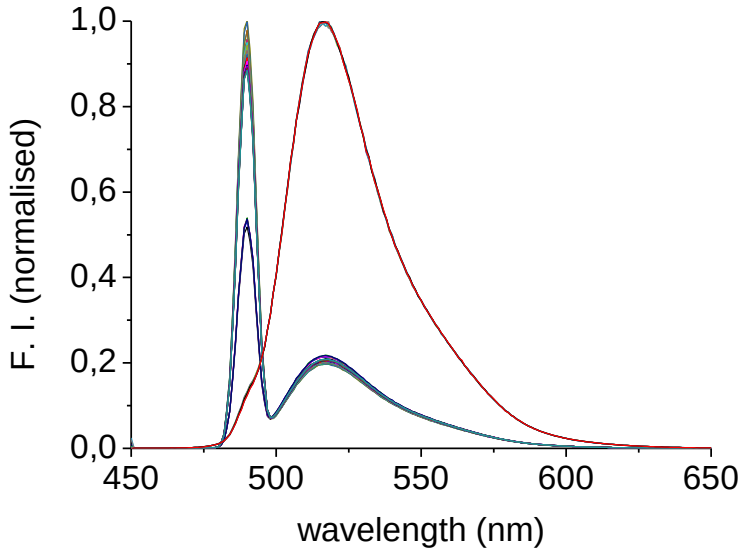

Figure S39. Carboxyfluorescein normalized fluorescence intensity recorded upon addition of **7a-Br** to POPC vesicles (0.05 mM). Vesicles (loaded with 451 mM NaCl buffered at pH 7.2 with 20 mM phosphate and containing 50 mM CF; I.S. 500 mM) were suspended in Na_2SO_4 (150 mM, buffered at pH 7.2 with 20 mM phosphate; I.S. 500 mM). At t = 60 s the compound was added (10% mol carrier to lipid), while at t = 360 s the detergent (20 μL) was added. Each spectrum represents the average of six trials, carried out with three different batches of vesicles.

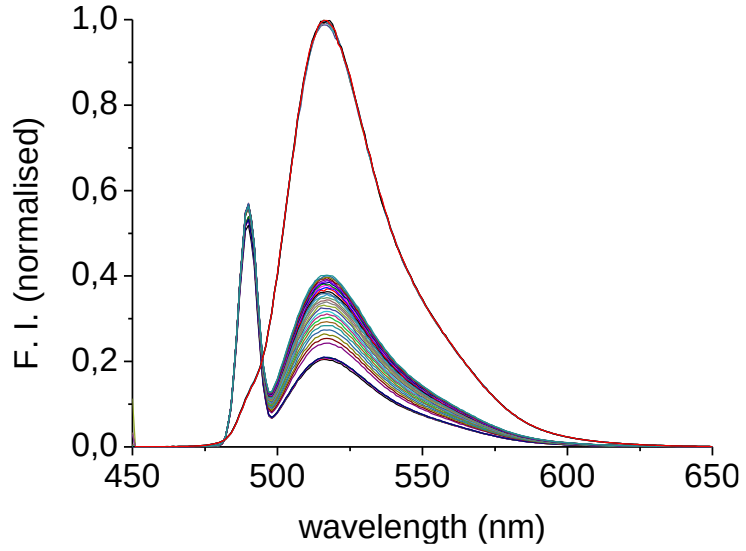

Figure S40. Carboxyfluorescein normalized fluorescence intensity recorded upon addition of **8a-Br** to POPC vesicles (0.05 mM). Vesicles (loaded with 451 mM NaCl buffered at pH 7.2 with 20 mM phosphate and containing 50 mM CF; I.S. 500 mM) were suspended in Na_2SO_4 (150 mM, buffered at pH 7.2 with 20 mM phosphate; I.S. 500 mM). At t = 60 s the compound was added (10% mol carrier to lipid), while at t = 360 s the detergent (20 μL) was added. Each spectrum represents the average of six trials, carried out with three different batches of vesicles.

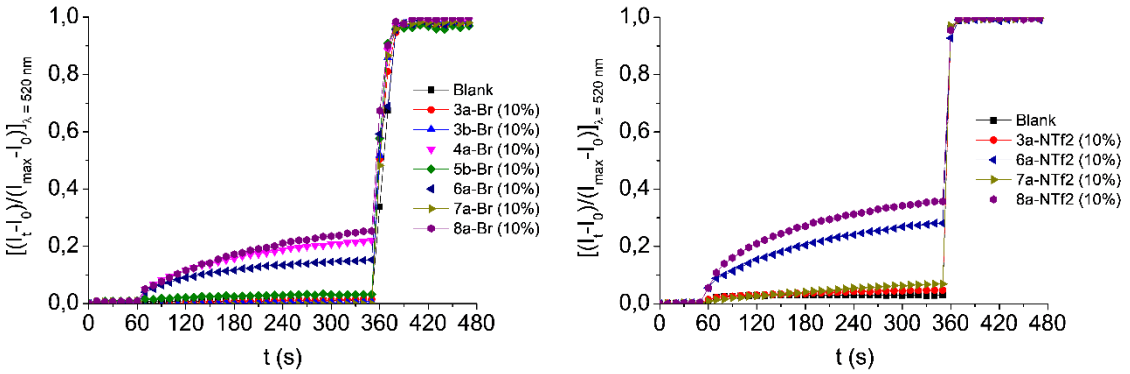

Figure S41. Carboxyfluorescein leakage observed upon addition of the studied compounds to POPC vesicles (0.05 mM). Vesicles (loaded with 451 mM NaCl buffered at pH 7.2 with 20 mM phosphate and containing 50 mM CF; I.S. 500 mM) were suspended in Na_2SO_4 (150 mM, buffered at pH 7.2 with 20 mM phosphate; I.S. 500 mM). At t = 60 s the compound was added (10% mol carrier to lipid), while at t = 360 s the detergent (20 μL) was added. The blank is DMSO (10 μL). Each trace represents the average of six trials, carried out with three different batches of vesicles

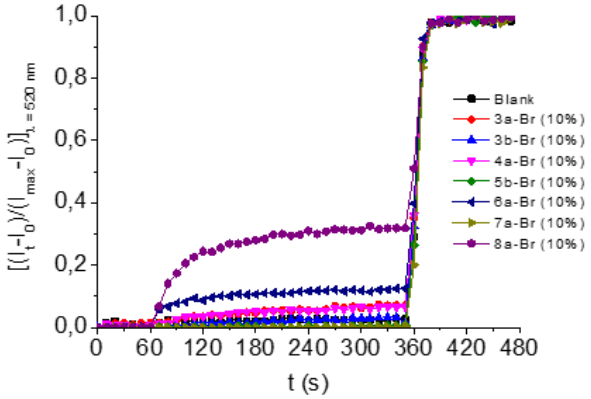

Figure S42. Carboxyfluorescein leakage observed upon addition of **3a-Br** (red trace), **3b-Br** (light blue trace), **4a-Br** (pink trace), **5b-Br** (green trace), **6a-Br** (dark blue trace), **7a-Br** (gold trace) and **8a-Br** (purple trace) to POPC vesicles (0.05 mM). Vesicles (loaded with 451 mM NaCl buffered at pH 7.2 with 20 mM phosphate and containing 50 mM CF; I.S. 500 mM) were suspended in Na_2SO_4 (150 mM, buffered at pH 6.2 with 20 mM phosphate; I.S. 500 mM). At t = 60 s the compound was added (10% mol carrier to lipid), while at t = 360 s the detergent (20 μL) was added. The blank is DMSO (10 μL). Each trace represents the average of six trials, carried out with three different batches of vesicles.

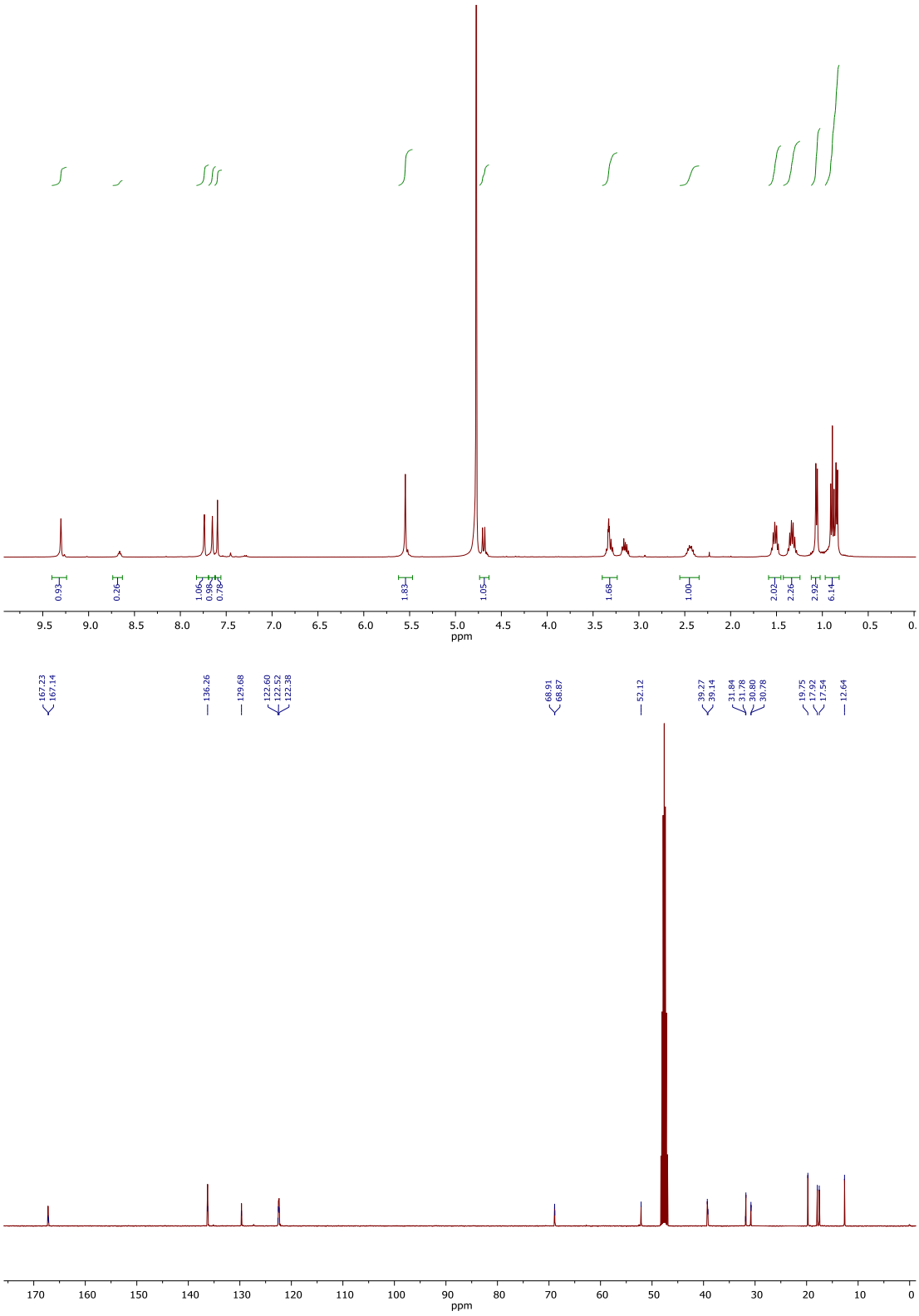

Figure S43. ^{1}H NMR (400 MHz, Methanol-d_4,) and ^{13}C-NMR (101 MHz, Methanol-d_4) of compound **4a-Br**

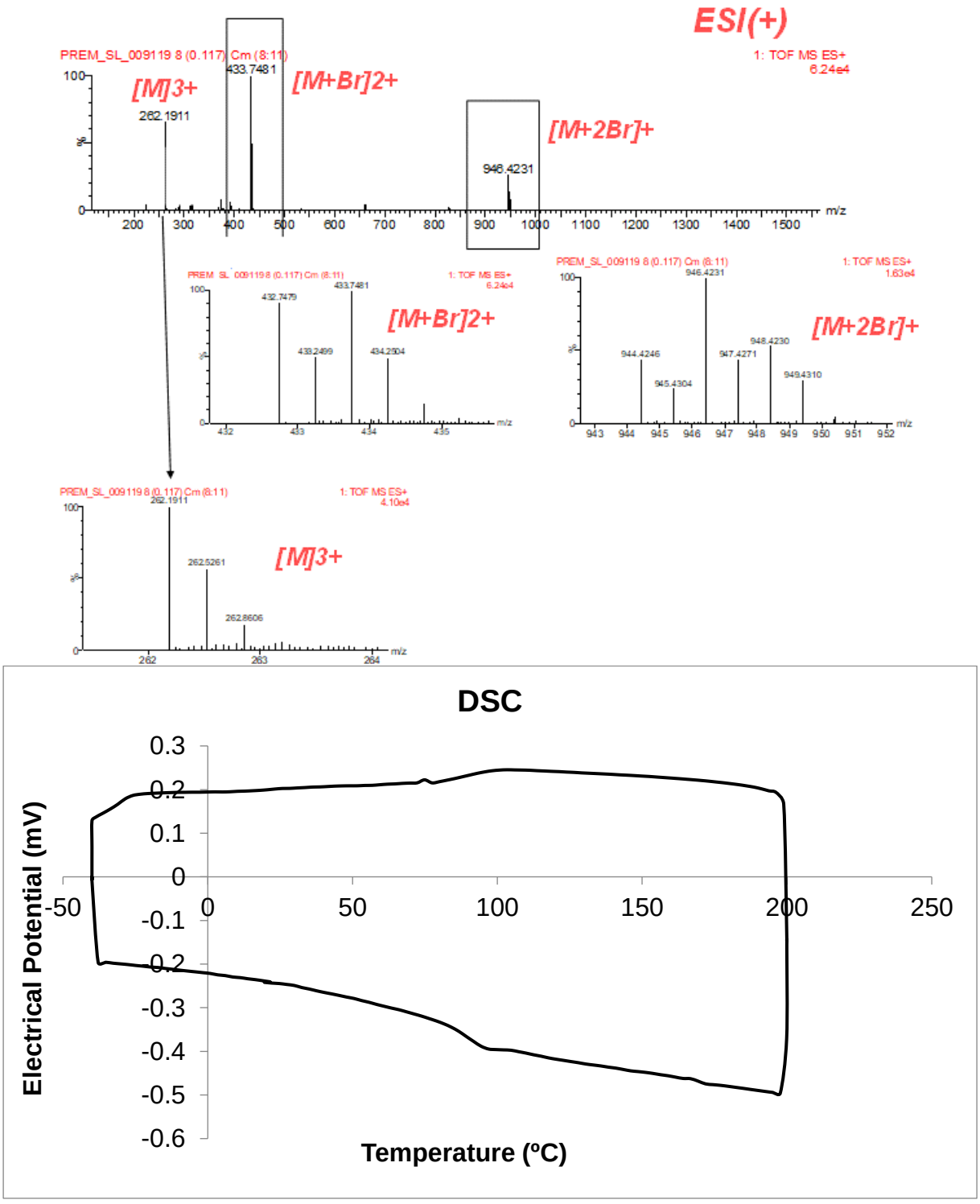

Figure S44. ESI-MS (+) and DSC (second heating and cooling cycle) of compound **4a-Br.**

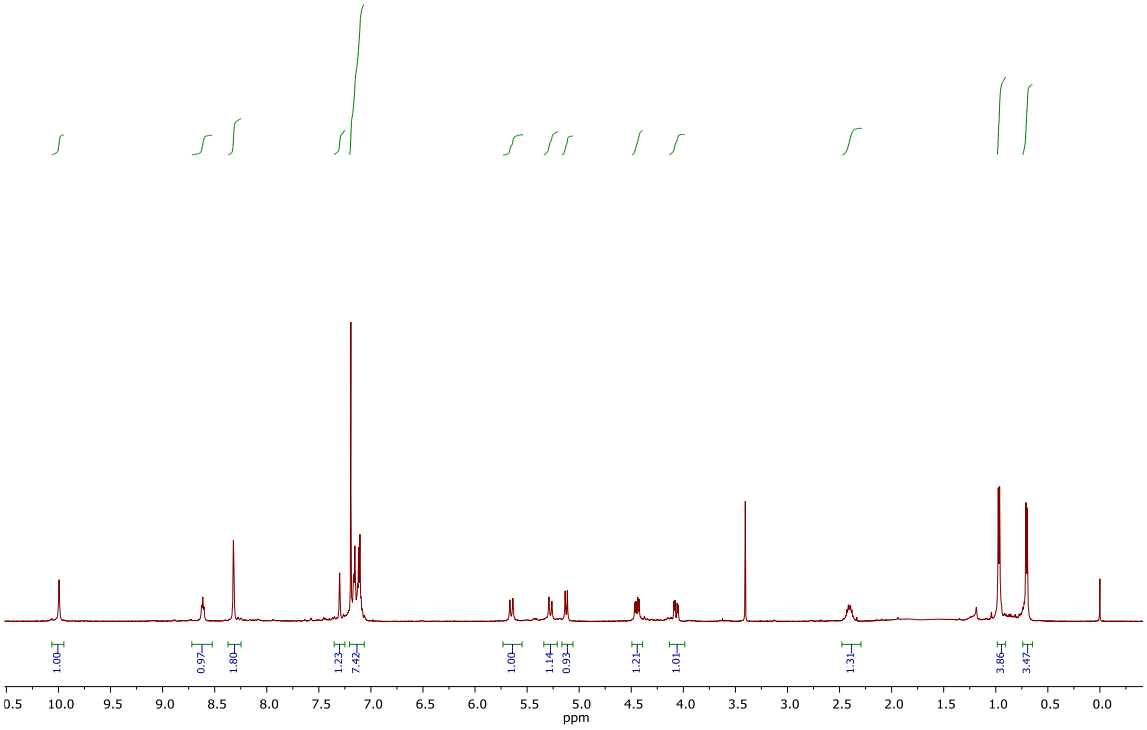

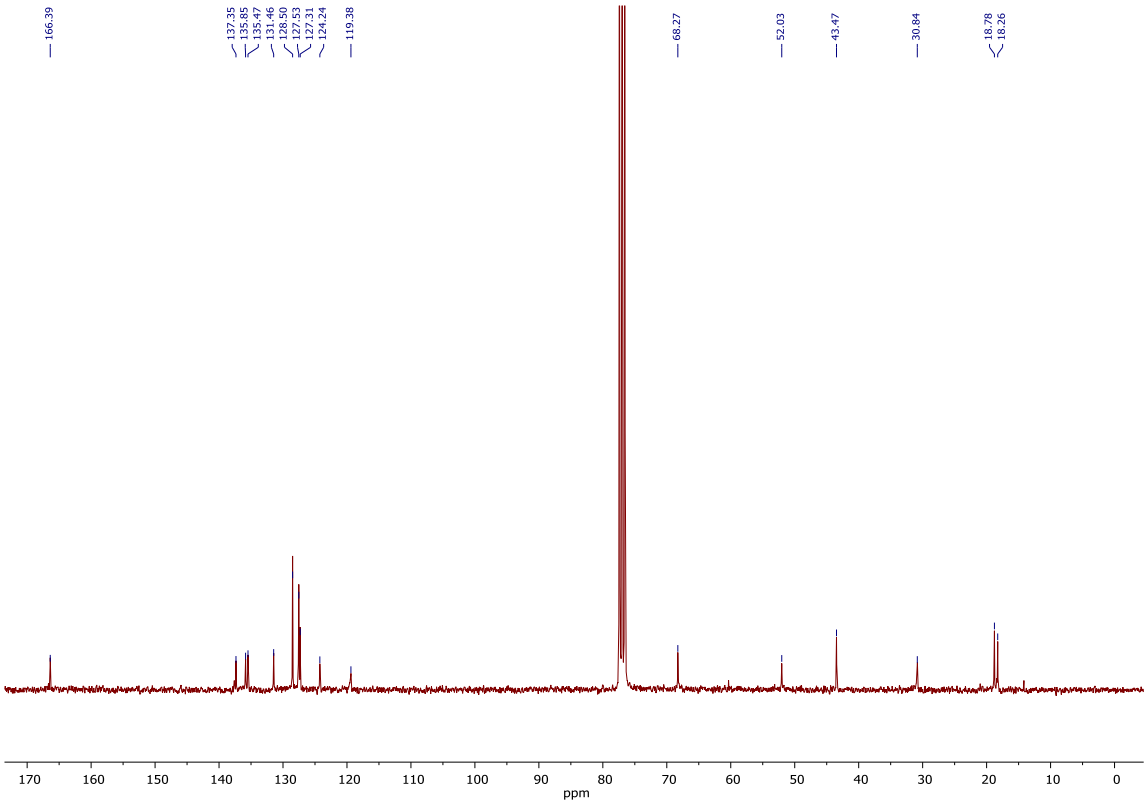

Figure S45. ^{1}H NMR (500 MHz, $CDCl_3$) and ^{13}C-NMR (75 MHz, $CDCl_3$) of compound **6a-Br**

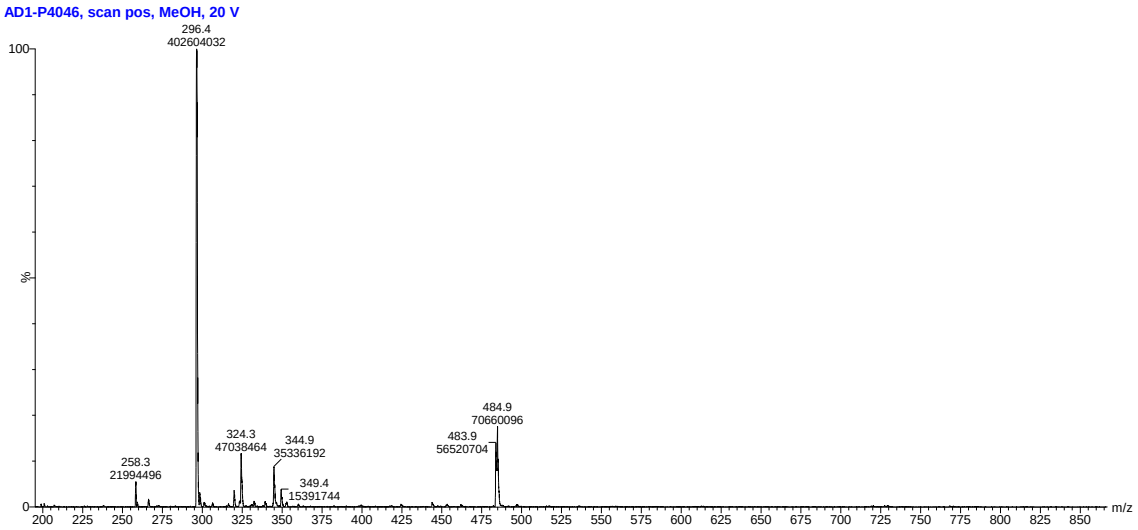

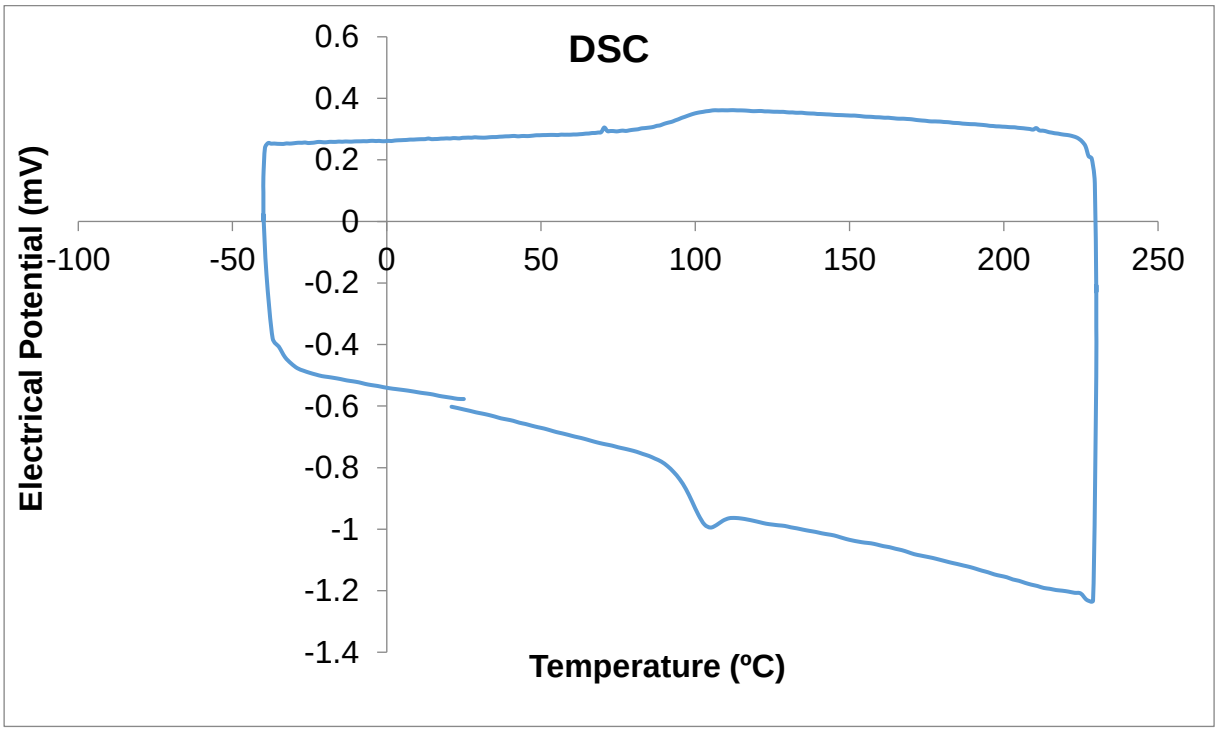

Figure S46. ESI-MS (+) and DSC (second heating and cooling cycle) of compound **6a-Br.**

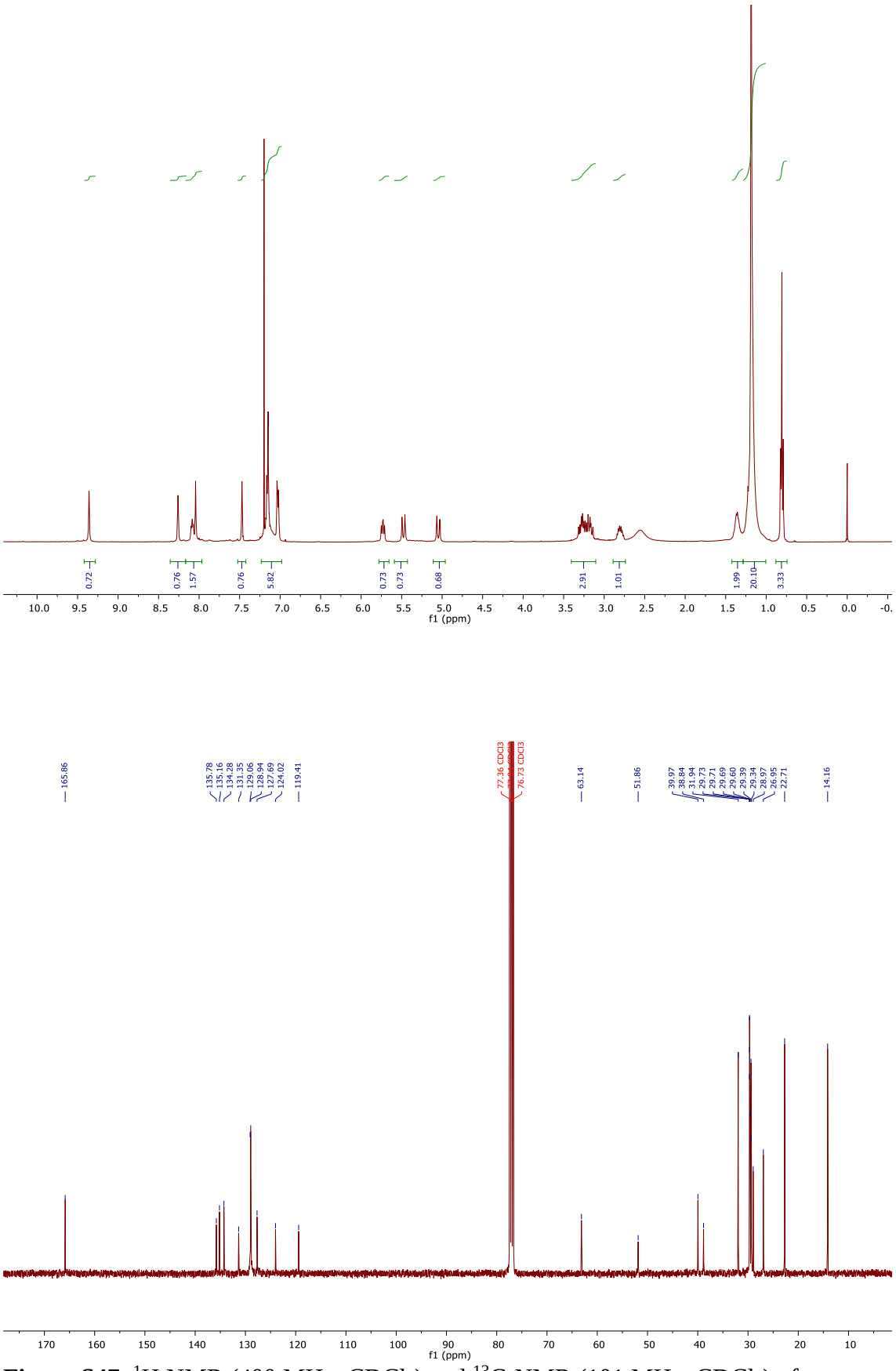

Figure S47. ^{1}H NMR (400 MHz, $CDCl_3$) and ^{13}C-NMR (101 MHz, $CDCl_3$) of compound **7a-Br**

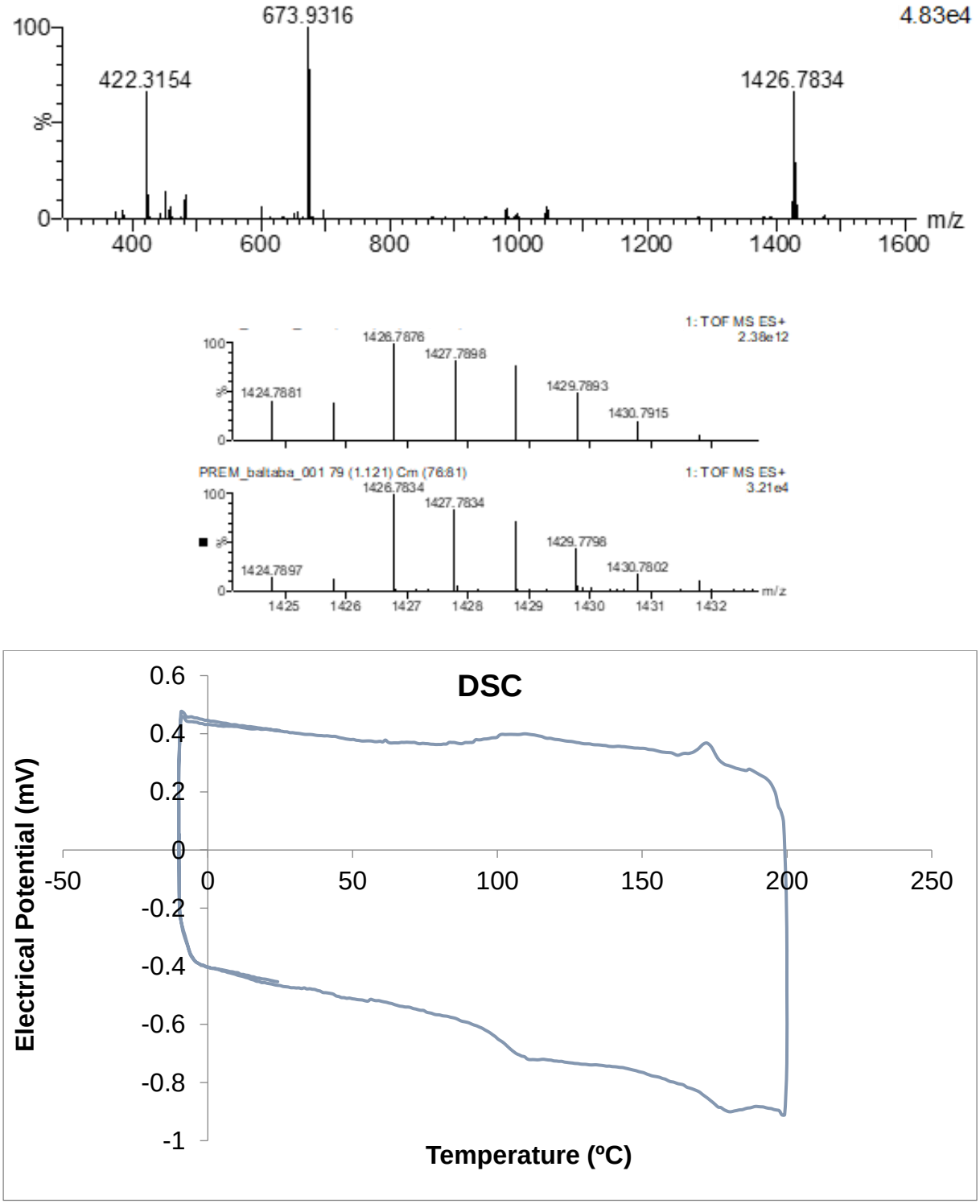

Figure S48. ESI-MS (+) and DSC (second heating and cooling cycle) of compound **7a-Br.**

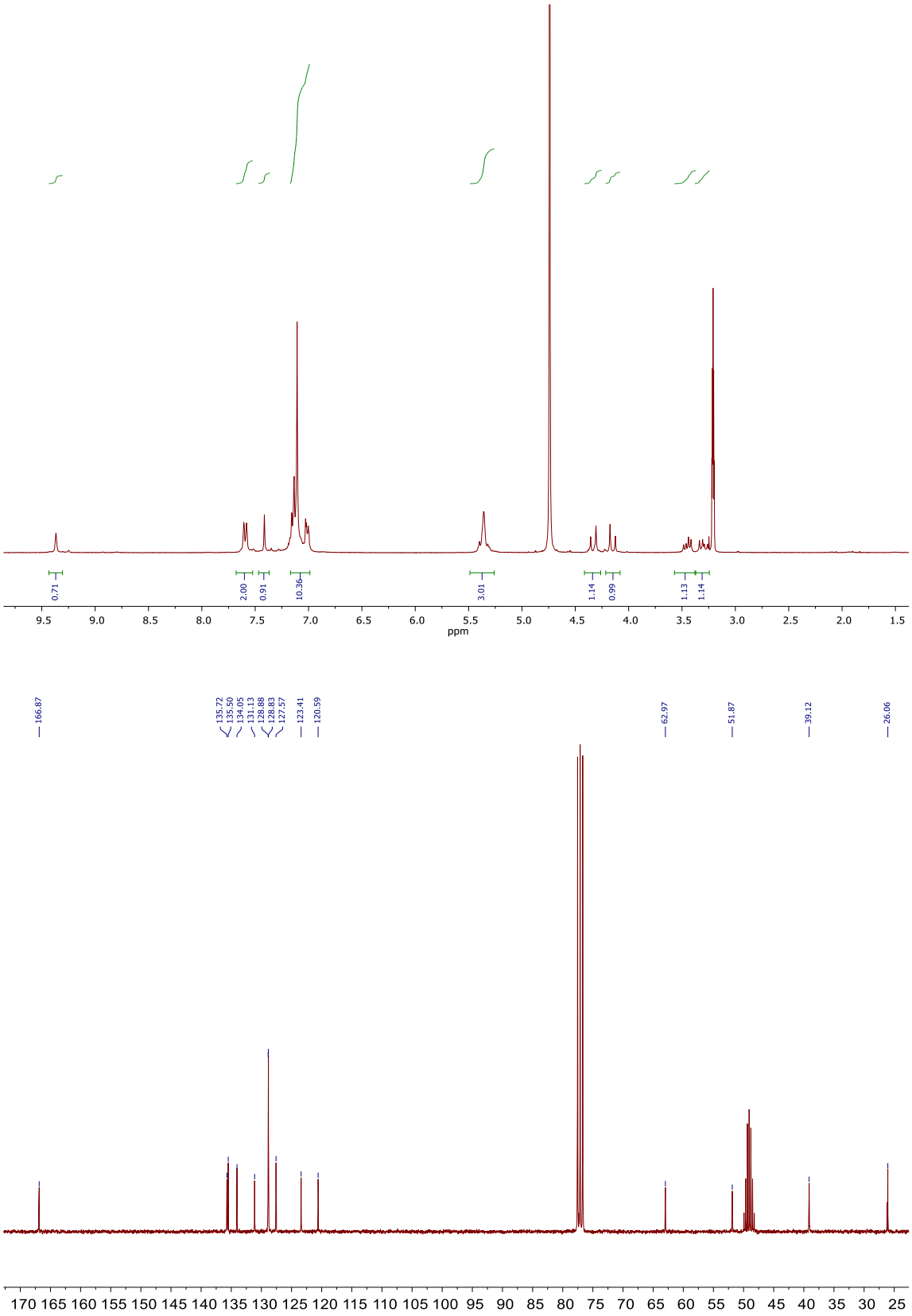

Figure S49. ^{1}H NMR (400 MHz, methanol-d_4/$CDCl_3$) and ^{13}C-NMR (75 MHz, methanol-d_4/$CDCl_3$) of compound **8a-Br.**

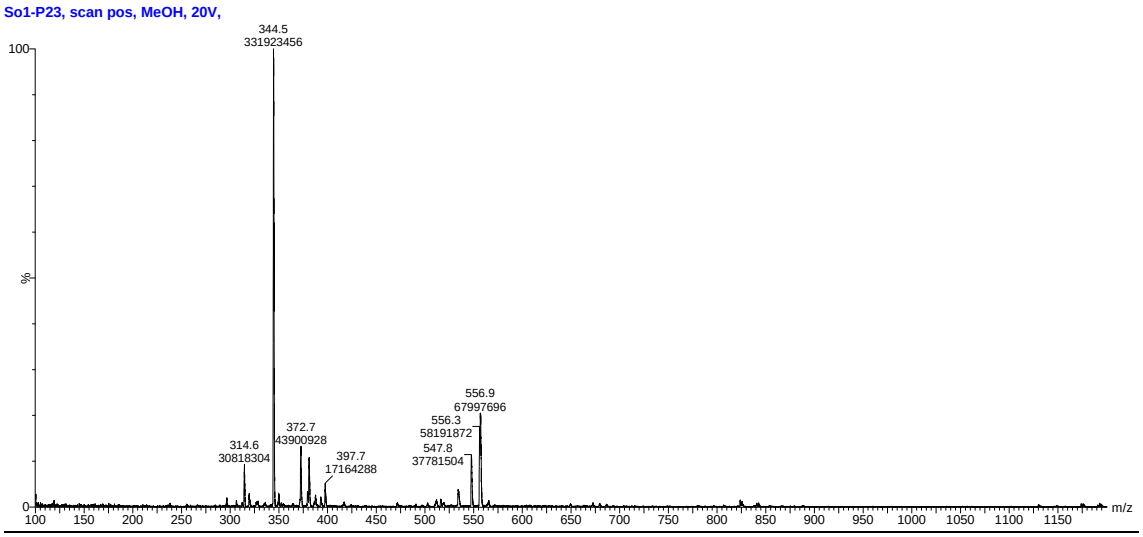

Figure S50. ESI-MS (+) of compound **8a-Br.**

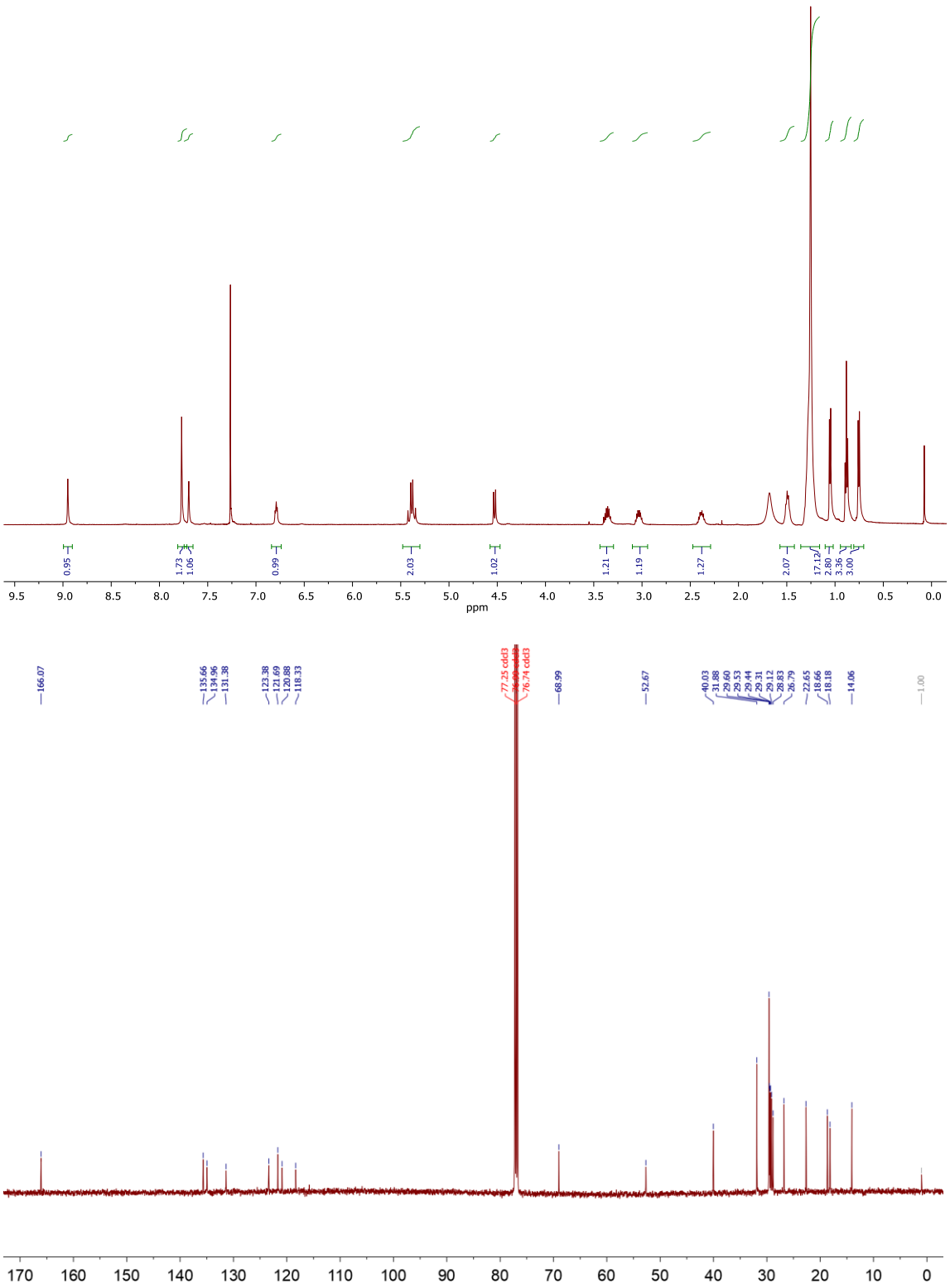

Figure S51. ^{1}H NMR (500 MHz, $CDCl_3$) and ^{13}C-NMR (126 MHz, $CDCl_3$) of compound **3a-NTf$_2$.**

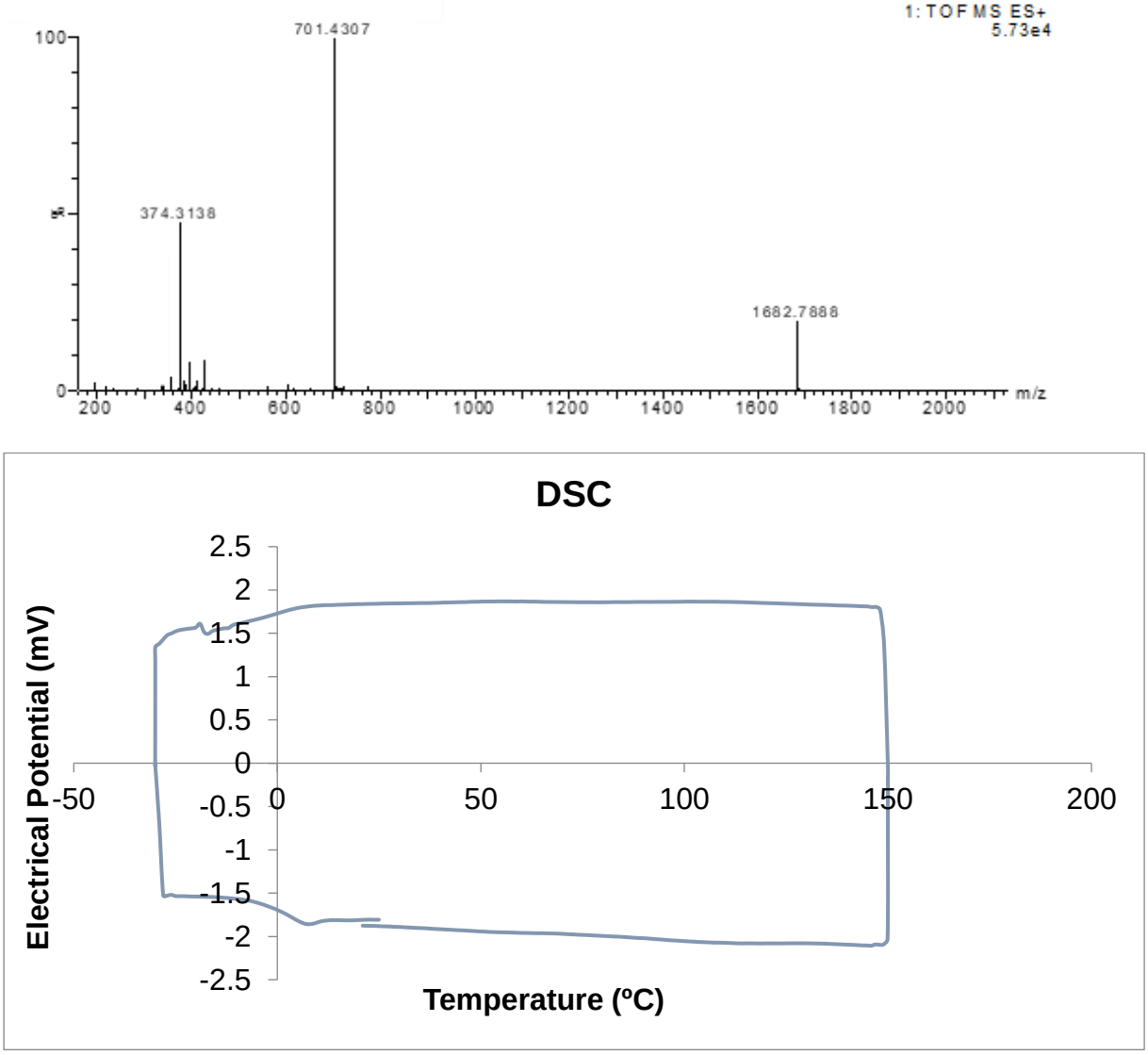

Figure S52. ESI-MS (+) and DSC (second heating and cooling cycle) of compound **3a-NTf$_2$.**

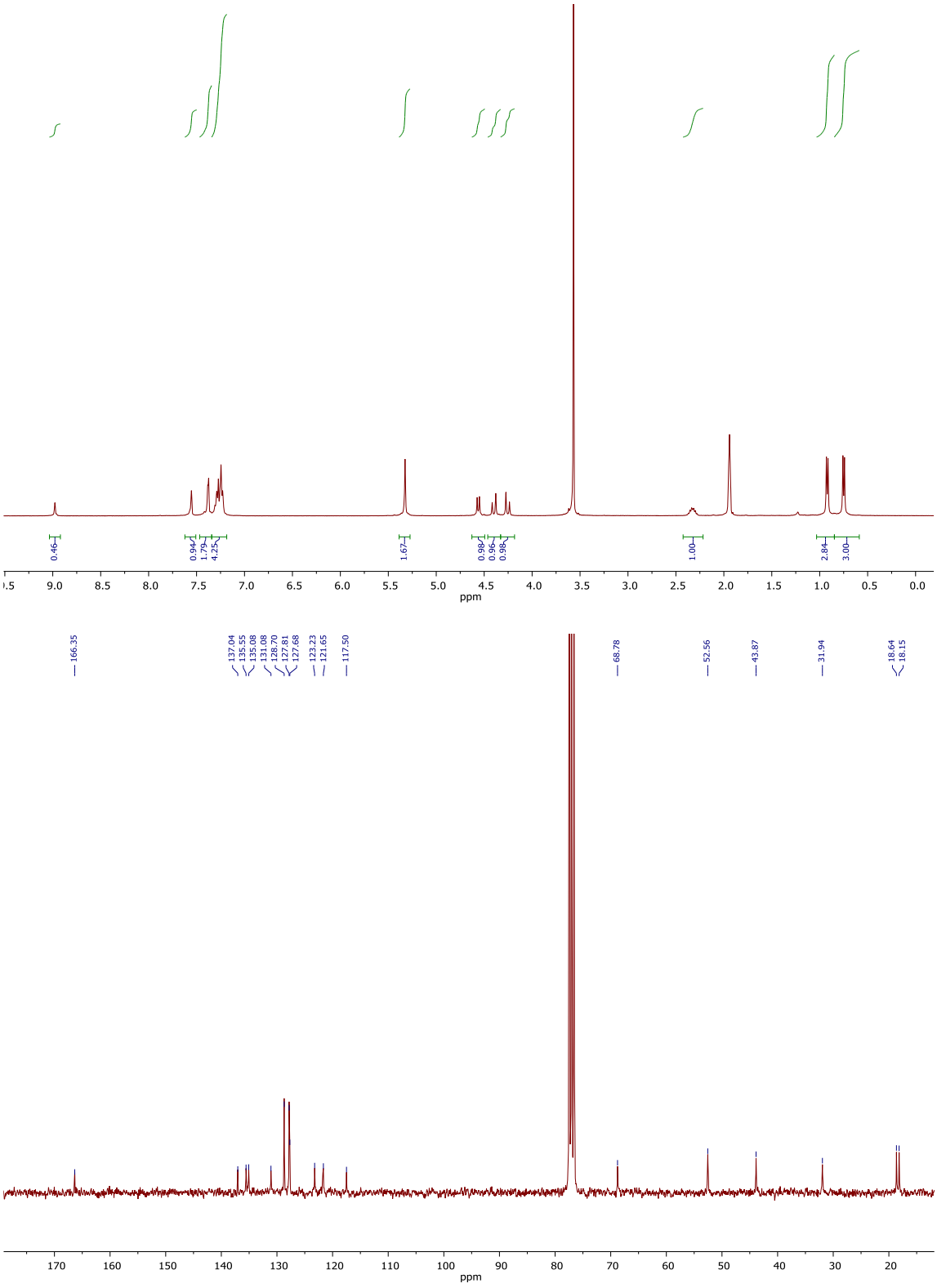

Figure S53. ^{1}H NMR (400 MHz, ACN-d_3) and ^{13}C-NMR (75 MHz, $CDCl_3$) of compound **6a-NTf$_2$.**

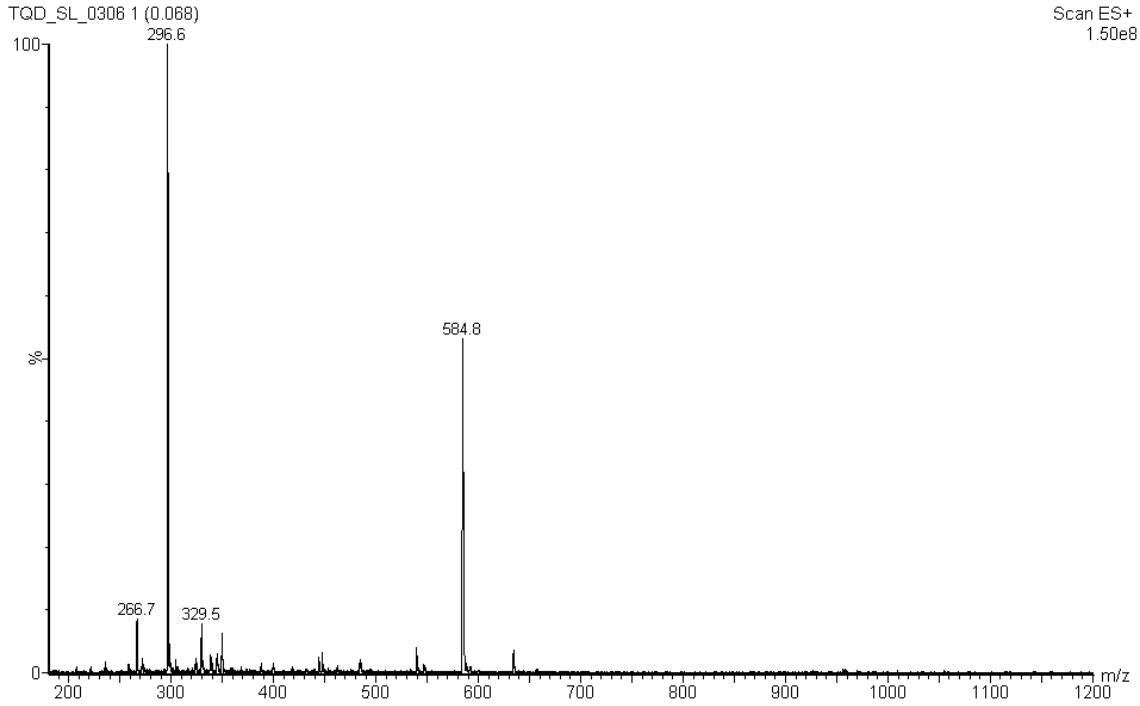

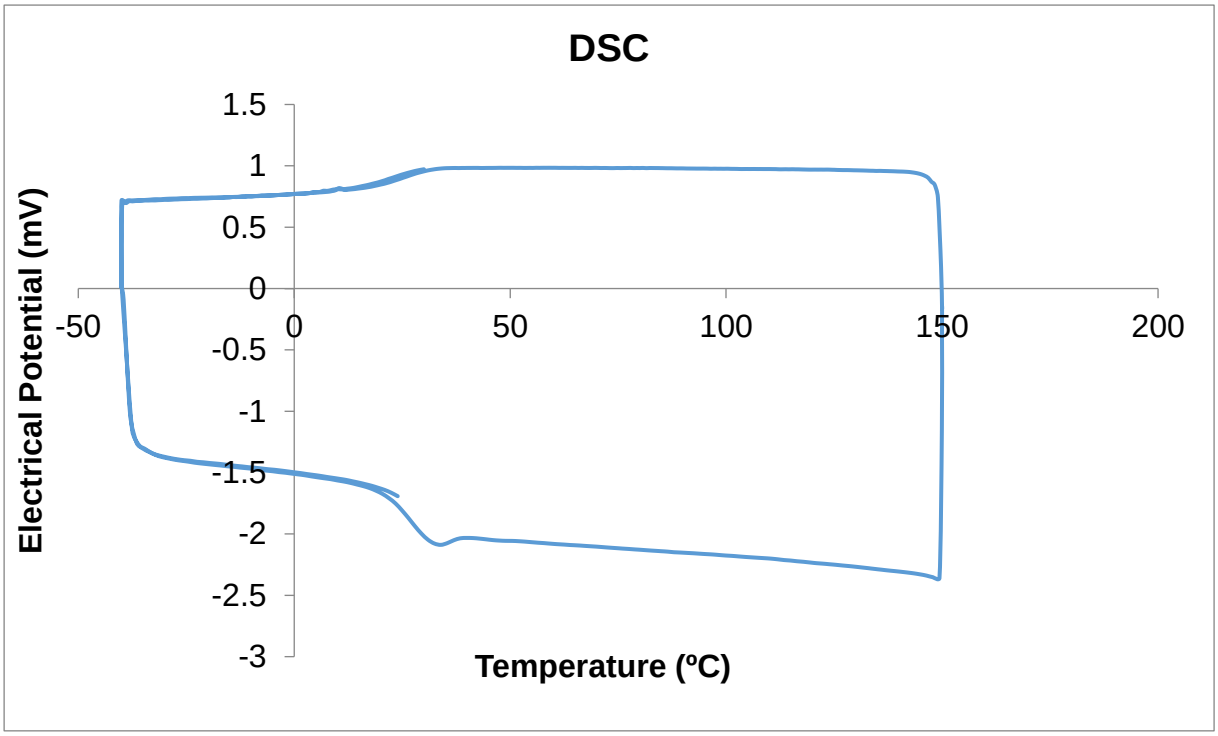

Figure S54. ESI-MS (+) and DSC (second heating and cooling cycle) of compound **6a-NTf$_2$.**

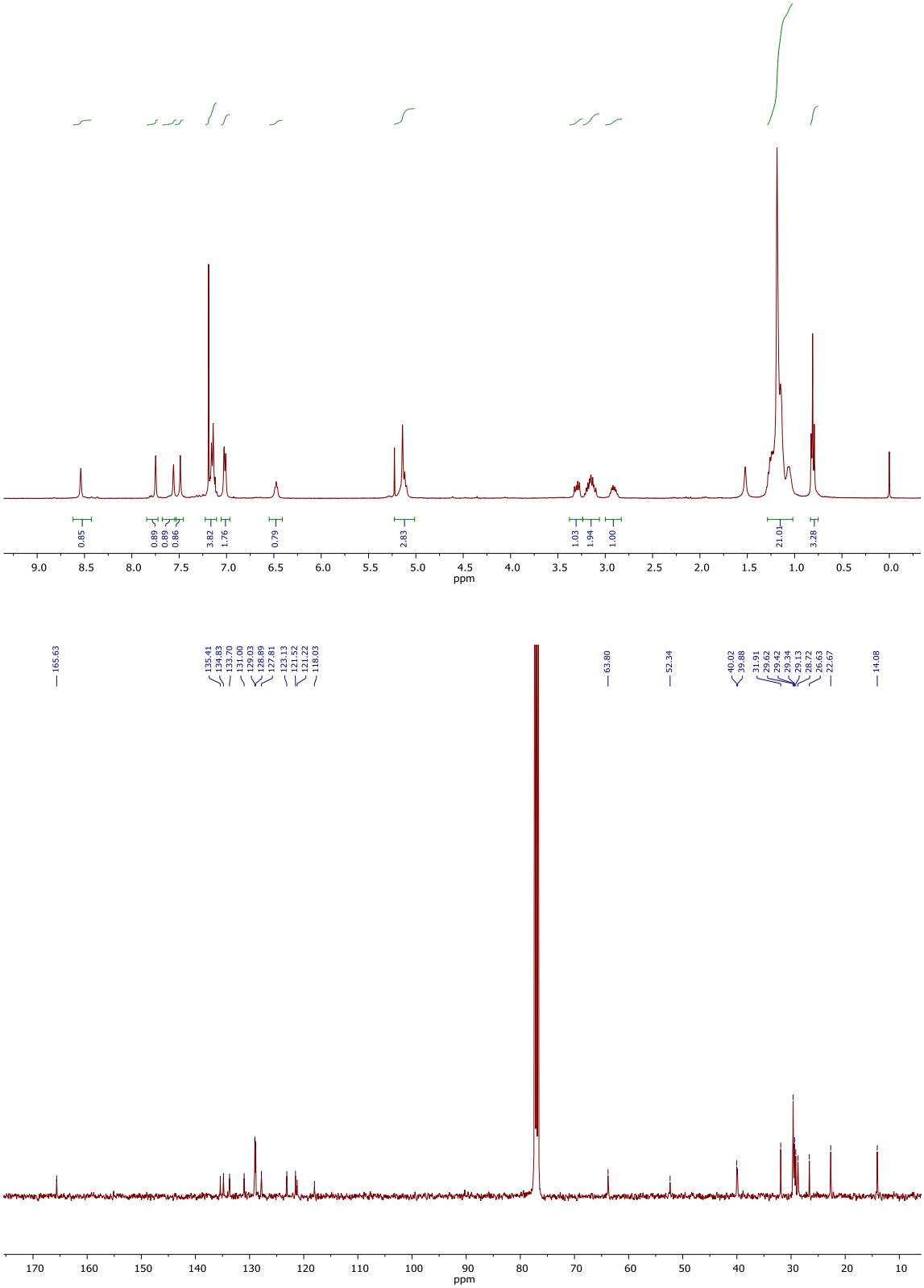

Figure S55. ^{1}H NMR (400 MHz, $CDCl_3$) and ^{13}C-NMR (101 MHz, $CDCl_3$) of compound **7a-NTf$_2$.**

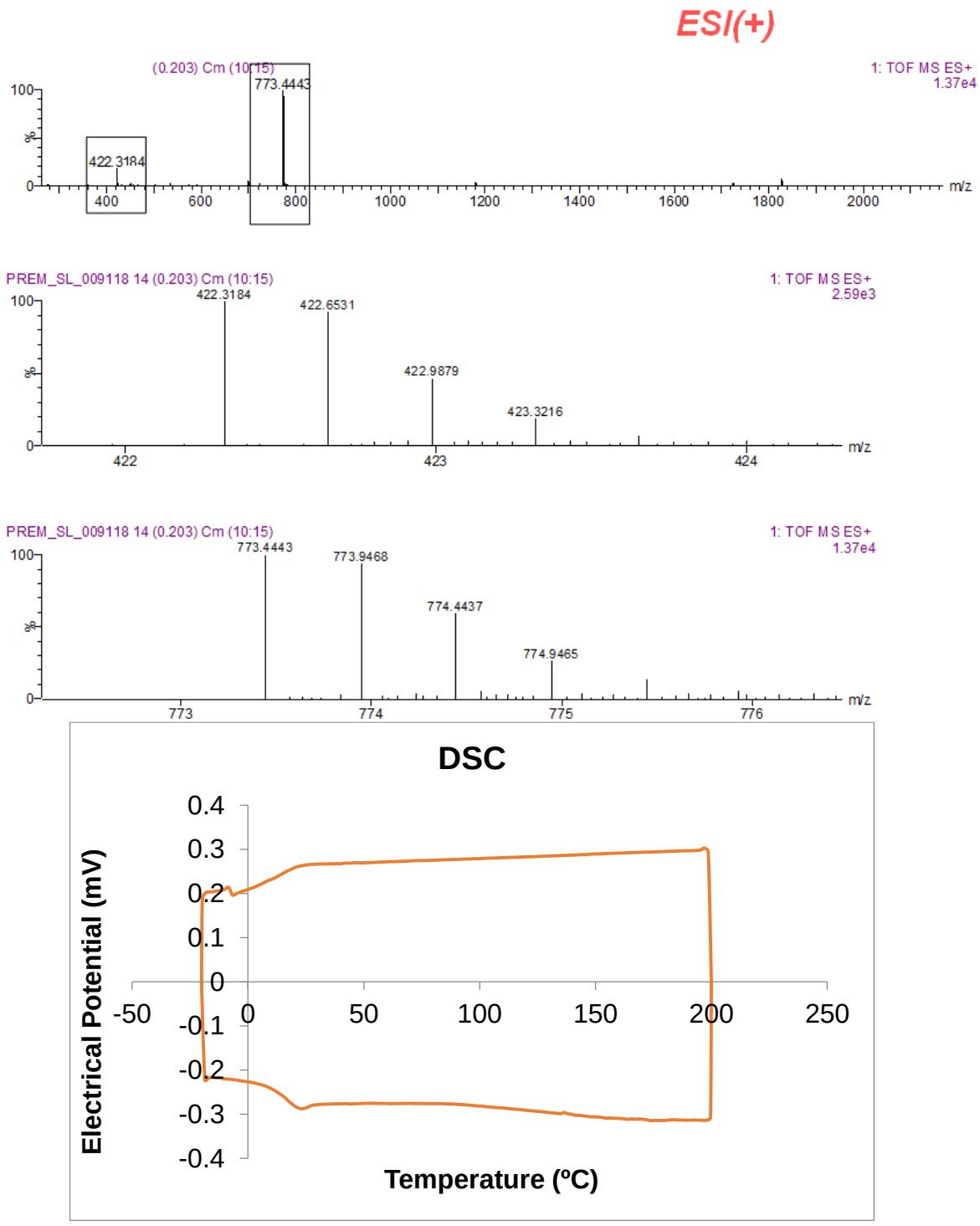

Figure S56. ESI-MS (+) and DSC (second heating and cooling cycle) of compound **7a-NTf$_2$.**

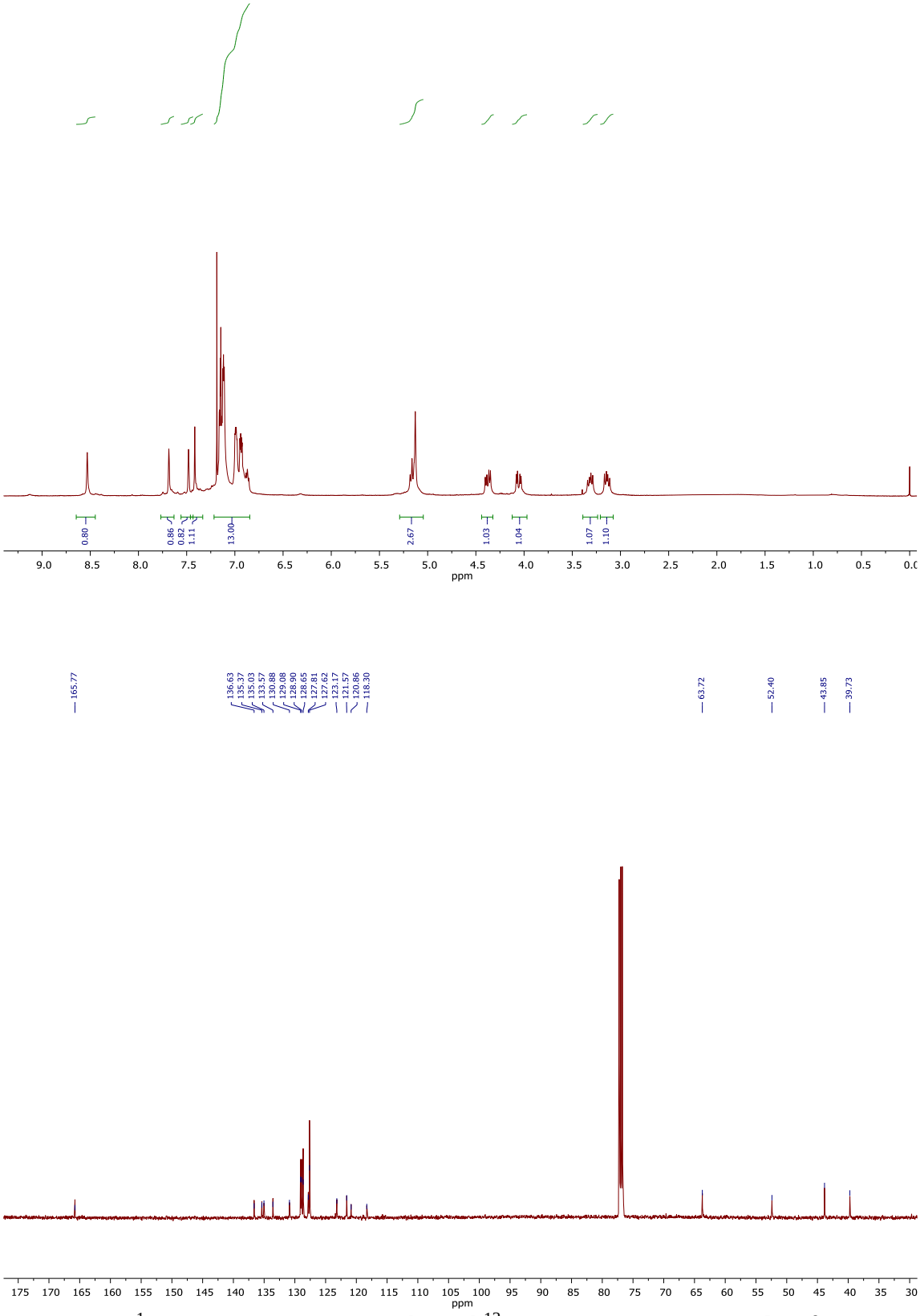

Figure S57. ^{1}H NMR (400 MHz, $CDCl_3$) and ^{13}C-NMR (126 MHz, $CDCl_3$) of compound **8a-NTf$_2$.**

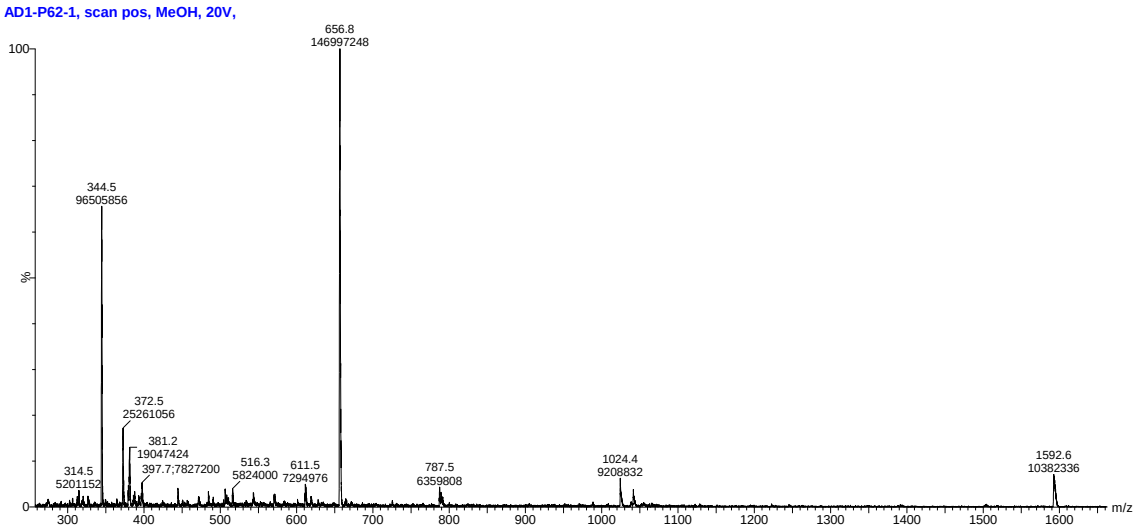

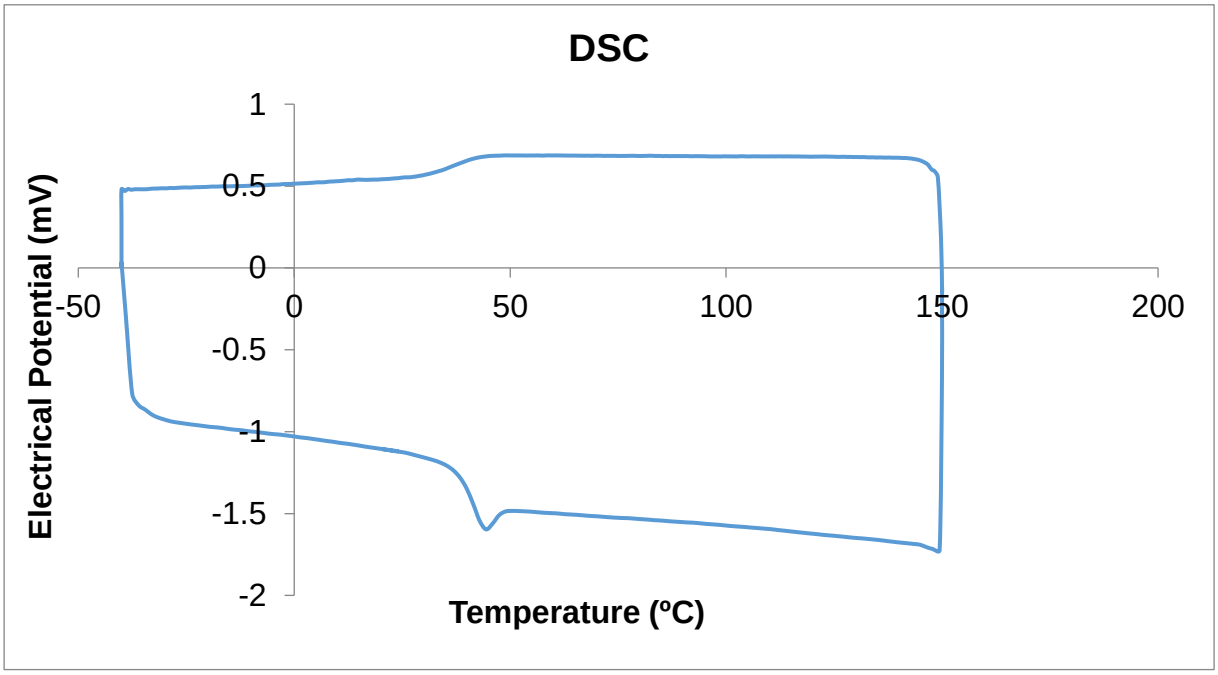

Figure S56. ESI-MS (+) and DSC (second heating and cooling cycle) of compound **8a-NTf$_2$.**